Development of a Wireless Sensor Used to Monitor Corrosion in Reinforced Concrete Structures

by

Kristi Michelle Grizzle, B.S.C.E.

Thesis

Presented to the Faculty of the Graduate School of

The University of Texas at Austin

in Partial Fulfillment

of the Requirements

for the Degree of

Master of Science in Engineering

The University of Texas at Austin

May 2003

Development of a Wireless Sensor Used to Monitor Corrosion in Reinforced Concrete Structures

Approved by
Supervising Committee:

Sharon L. Wood

Dean P. Neikirk

Dedication

To my supportive and loving parents, who have never once doubted me.

Acknowledgements

I gratefully acknowledge the Texas Higher Education Coordinating Board for funding this project (#003658-0201-2001) and providing me with an opportunity to learn.

I give my sincerest thanks to my advisor, Dr. Sharon L. Wood, for her tremendous amount of patience and kind words of encouragement. She is dedicated to furthering women in the field of engineering, and I have benefited from that. Also, it was her undergraduate reinforced concrete design class that encouraged me to attend graduate school.

I give a special thanks to Dr. Dean Neikirk and Dr. Harovel Wheat for the technical expertise in their respective fields. Dr. Neikirk's electrical engineering knowledge and creativity made this research a success. Dr. Wheat's knowledge and excitement about corrosion and willingness to help are unmatched.

I wish to thank the staffs and students at both the Ferguson Structural Engineering Lab and our rivals, the Construction Materials Research Group, especially: Chris Bilich, Tammer Botros, Francisco Brenes, John Eggers, Andrea Kotys, Jennifer Nicolas, Ruben Salas, Chris Shoemaker, and Jarkko Simonen.

I also want to thank Matt Andringa for helping me understand electrical engineering, and Jennifer Steele, a great mentee, for helping me with my work.

Last but not least, I wish to thank my family (Mom, Dad, Jenn, and Josh) and friends for loving and supporting me.

May 2003

Abstract

Development of a Wireless Sensor Used to Monitor Corrosion in Reinforced Concrete Structures

Kristi Michelle Grizzle, M.S.E.

The University of Texas at Austin, 2003

Supervisor: Sharon L. Wood

The objective of this thesis is to discuss the development of a prototype wireless sensor to detect corrosion in reinforced concrete structures. These sensors are intended to be embedded inside the concrete near the reinforcement when the concrete is placed. Unlike existing monitoring systems for corrosion, there is no electrical connection between the prototype sensor and the reinforcement. Rather, the sensor contains a steel wire state switch which corrodes. Because the sensor is embedded in the concrete near the reinforcement, the sensor is exposed to the same environment as the reinforcement and corrodes at the same rate. Prototype sensors have been designed and are currently being tested in accelerated corrosion tests. The prototype sensor has proven to be rugged and is not damaged during placement of the concrete.

Table of Contents

List of Tables

List of Figures

CHAPTER 1
Introduction

1.1 Corrosion of Civil Engineering Infrastructure

Corrosion of reinforcing and prestressing steels in concrete is a major problem throughout the world. Not only does corrosion degrade the integrity of the steel, but it also causes extensive damage to the concrete. Structures near the coast are vulnerable to corrosion because of salt in the air, and bridges that are exposed to deicing salts are also susceptible to corrosion. As of 1999, 15% of highway bridges in the United States were deemed structurally deficient due to corrosion attack (Koch, et. al., 1999). For remediation and replacement of these bridges, a direct cost of $8.3 billion is being spent annually (Koch, et. al., 1999). Indirect costs experienced by the user of these bridges, such as traffic delays and loss of productivity, are estimated to be ten times that of the direct costs (Koch, et. al., 1999). In addition to the enormous cost that corrosion incurs, loss of life is also an eminent danger.

Early detection of the corrosion significantly decreases the costs of repair and possibly eliminates the need to replace a structure. The wireless sensor developed in this thesis would detect the early signs of corrosion far before visible damage occurs.

1.2 Corrosion in Reinforced Concrete

Corrosion of reinforcement is the electrochemical degradation of steel in concrete. A passive layer naturally forms around steel inside concrete. This passive layer is created by calcium hydroxide (CaOH) which constitutes 20-25%

of the cement paste (Kitowski, 1993). This passive layer protects the steel from corrosion under normal conditions. Two things can cause this passive layer to break down, thereby allowing corrosion to occur: carbonation of the concrete and the presence of chloride ions near the steel. Carbonation of concrete is not the major cause of corrosion in bridges and other structures; however, the presence of chloride ions inside the concrete is the primary cause of corrosion (Manning, 1988).

Chloride ions infiltrate through the concrete to the surface of the steel when the concrete is exposed to deicing salts or salt air in marine environments. The presence of chloride ions on the steel surface causes an electrochemical cell to form. An electrochemical cell consists of an anode, a cathode, an electrolytic solution, and a conductor (Figure 1.1). The anode is where the corrosion takes place, and the cathode is where corrosion does not occur but the ionic balance of the reactions is maintained. The electrolytic solution allows ionic flow through an electric current. The conductor electrically connects the anode and cathode. In the case of corrosion in reinforced concrete, the anode and cathode occur directly on the steel's surface, so the steel itself is the conductor. The electrolytic solution is moist concrete or grout (Manning, 1988).

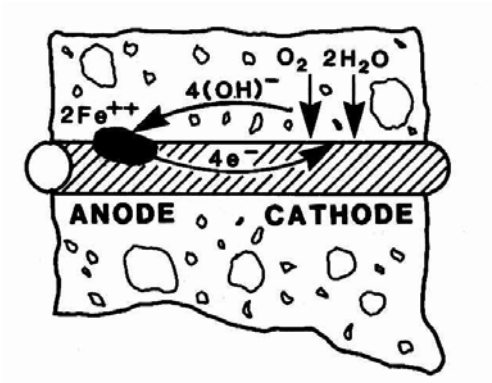

Figure 1.1 Model of Electrochemical Cell in Reinforced Concrete

(From Manning, 1998)

The electrochemical reaction that occurs in the cell is composed of an anodic half-cell reaction and a cathodic half-cell reaction. Equation 1.1 is the anodic reaction, where oxidation takes place, and Equation 1.2 is the cathodic reaction where reduction takes place (Jones, 1996).

$$Fe \rightarrow Fe^{2+} + 2e^{-} \tag{1.1}$$

$$2H_2O + O_2 + 4e^{-} \rightarrow 4OH^{-} \tag{1.2}$$

As the corrosion process occurs, the corrosion products formed from the electrochemical reactions cause a volumetric increase around the steel. This increase in volume causes internal stresses in the concrete, initiating delaminating, cracking, and eventually spalling (Figure 1.2).

Figure 1.2 Concrete Spalling from Bridge Bent in Lubbock, Texas

1.3 CURRENT METHODS FOR DETECTING CORROSION IN REINFORCED CONCRETE

Several methods are currently available for detecting corrosion in reinforced concrete structures, but each has at least one disadvantage. The

proposed wireless sensor attempts to avoid these disadvantages. The current methods are described briefly in this section (Manning, 1988).

One method is visual inspection. This involves inspecting the structure for extensive cracking, spalling, or rust staining. Unfortunately, when these signs are visible, the corrosion damage is severe and requires extensive, costly repairs and possibly replacement. The proposed sensor would detect signs of corrosion long before they were visible.

A way to detect corrosion before the damage is visible is the acoustic hammer method. This method involves striking the surface of the concrete with a hammer and listening for a hollow sound. The hollow sound indicates that cracks have formed within the concrete. This method can detect cracks that initiate around the steel before they reach the surface of the concrete. The primary advantages of this method are the low cost and ability to detect the early signs of corrosion, but it provides no information about rate or extent of corrosion that has occurred. The prototype sensor will provide this information.

Inspecting the reinforcing or prestressing steel is another way to detect corrosion. Concrete or grout can be removed from the area in question, and the steel can be inspected. This method is very expensive. Also, if the hole, where the concrete was removed, is not properly patched, corrosion could be accelerated in that area.

One electrical method for detecting corrosion involves determining the resistivity, or permeability, of the concrete. This test has been standardized (ASTM D 3633) and involves measuring the resistance between the steel and a sponge on the concrete surface. This test cannot be used with epoxy-coated reinforcement. Another disadvantage is that surface effects often dominate the reading, whereas the area closest to the steel is of primary interest. Also, the resistivity reading that is associated with corrosion is uncertain.

Another electrical method that is frequently used involves monitoring half-cell potentials. When corrosion occurs, there is a potential difference between the anodic half-cell reaction and the cathodic half-cell reaction, which can be measured by comparison with a reference cell, which has a known value. The potential difference is determined by connecting the steel and the reference cell through a voltmeter and moving the reference cell to the portion of concrete of interest. This test is also standardized (ASTM C 876). Problems associated with this method include that it only gives a probability of corrosion and it cannot be used with epoxy-coated reinforcement. Also, a direct connection must be made between the voltmeter and the steel. The prototype sensor is wireless and requires no connection to the reinforcing steel.

The galvanostatic pulse method, similar to the half-cell potential test, provides information on both probabilities of corrosion and corrosion rates (Mietz, 1995). In this method, an anodic current pulse is galvanostatically impressed onto the reinforcement, which causes a change in potential. The amount of the current required to make this potential change determines the corrosion rate. The disadvantage with this method is that an electrical connection to reinforcing steel must be available.

1.4 RECOMMENDATIONS FROM WIRELESS CRACK DETECTION SENSOR

Much of the motivation for this project came from a previous project conducted at the University of Texas at Austin. A wireless sensor used was developed to detect cracks in welded steel moment resisting connections (Novak, 2002). Novak believed that sensors for civil engineering structures should possess the following four attributes:

- Passive – The sensor should be passive so that it has an infinite life. Internal batteries would eventually run out, and external batteries would

require wires running through the concrete, which could be damaged during construction.

- Durable – Because the sensor will be embedded during placement of the concrete, it must be able to survive the construction process. The sensor must also be able to withstand the environmental conditions it will experience inside the concrete.
- Reliable – The sensor must provide reliable information about the level of reinforcement corrosion occurring inside the concrete. If a sensor provides a false reading, time and money could be wasted with unneeded repairs, or damage may go undetected.
- Economical – The sensor should have a low cost compared to the cost of repairing or replacing the structure. If the cost becomes too high, owners of structures would have to rely on the less advantageous, current detection methods previously discussed in this chapter.

Radio frequency (RF) technology was used as a means of powering this new class of sensor. An RF transmitter used for ham radios was modified for use on the project. A photograph of the portable transmitter is shown in Figure 1.3.

Figure 1.3 Portable RF Transmitter

The basic electrical components used in the crack detector sensor are implemented into the corrosion sensor. Each sensor comprises an inductor coil, a capacitor, and combinations of a capacitor and state switch (Figure 1.4). The inductor and capacitor alone form an L-C circuit which resonates at a characteristic frequency. When a combination of capacitor and state switch are added to the circuit, the characteristic frequency changes. Ideally, an infinite number of combinations can be added to the original circuit. For the corrosion sensor, different gauges of steel wire were used as the state switches. As each gauge of wire corrodes and fractures, the corresponding circuit will be broken and the sensor will resonate at a different frequency, thereby transmitting information to the inspector about the extent of corrosion damage.

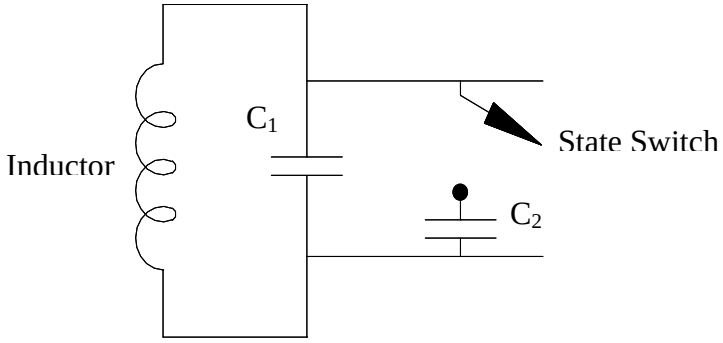

Figure 1.4 Electrical Components of Wireless Sensor

1.5 SCOPE OF RESEARCH WORK

The objective of this thesis is to develop a prototype wireless sensor to detect corrosion in reinforced concrete structures. These sensors are intended to be embedded inside the concrete at the same level as the reinforcement at the time of concrete placement. When interrogated, they will give a direct indication of the level of corrosion occurring in the steel.

The feasibility of using RF technology in concrete is explored in Chapter 2. The requirement for the proposed sensor to be durable is also addressed in this chapter. Several different ways of protecting the sensors are investigated.

The design of the state switch is discussed in Chapter 3. Steel wires, reinforcing steel, and prestressing strands were exposed to accelerated corrosion tests in simulated concrete solutions. This test provided a relatively quick way to determine corrosion rates of the steel wire state switches and compare with corrosion rates in the reinforcing steel and prestressing strands.

The fabrication and testing of the prototype sensor are discussed in Chapter 4. The components used to fabricate the sensor are presented and tests of the prototype sensor embedded in concrete prisms are discussed. The prisms are currently being subjected to wet and dry cycles using a sodium chloride solution, but preliminary data are presented. The durability of the prototype sensors are also demonstrated in Chapter 4 by embedding them in a full-scale concrete member.

Chapter 5 provides a summary of the results and recommendations for future work related to this project.

CHAPTER 2
Feasibility Study of Passive RF Sensors in Concrete

2.1 INTRODUCTION

The purpose of this initial series of tests was to determine if the fully passive RF sensor technology would operate in a concrete environment. This series of tests was performed to investigate the three objectives listed below:

- The RF sensors were tested for durability by casting them in concrete.
- Assuming that the RF sensors survived the construction process, they would be interrogated through concrete to verify that the signal could be read through such a medium.
- Assuming that the RF sensors could be interrogated through concrete, the amplitude of the sensor output received by the transmitter was analyzed to determine how the depth of embedment within the concrete affected the measured response.

Two types of passive RF sensors were tested: Electronic Article Surveillance (EAS) tags and 3M™ disc markers. Both sensors are commercially available.

2.1.1 EAS Tags

EAS tags (Figure 2.1) are normally used as shoplifting control devices and come in a variety of shapes and sizes. The tags used in this series of tests are 5-cm (2-in.) square and virtually paper thin. In air, they have a read range of 1-2 m (3-6 ft) and cost about $0.10 each (Novak, 2002). Their electrical circuit contains

an inductor coil and capacitor and the measured characteristic frequency is approximately 8 MHz. An adhesive layer allows the EAS tags to be affixed to the surface of almost any object. The EAS tags were studied because they had already been used in the development of the crack weld detection sensor discussed in Chapter 1, and therefore, they satisfy three of the four required sensor attributes: affordability, reliability and passivity.

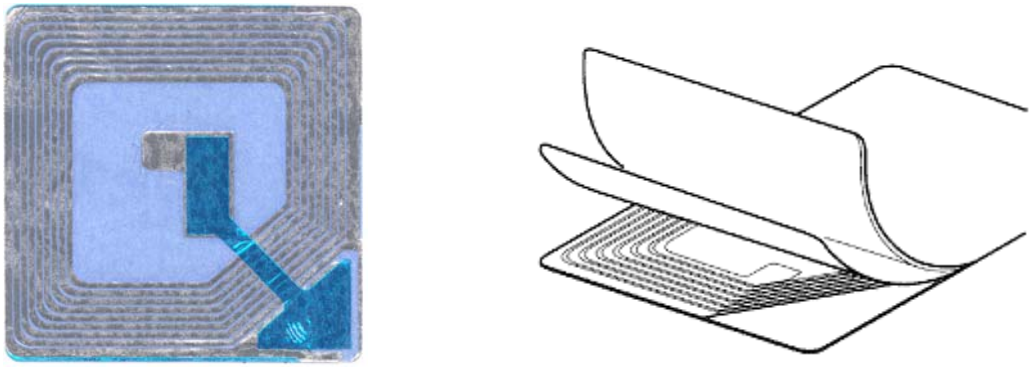

Figure 2.1 Typical EAS Tag

2.1.2 3M™ Disc Markers

3M™ disc markers (Figure 2.2) are used in the water, gas, and telecommunications industries (3M™, 2003). The markers are attached to the underside of access ports over buried pipes and conduits and allow for the utilities to be located under backfill, snow, or overgrown vegetation. Like the EAS tags, the markers consist of an inductor coil and capacitor, but unlike the EAS tags, the electrical components are enclosed in a sealed plastic container (Figure 2.3). Markers with different characteristic frequencies are used to locate different types of pipes, such as water, wastewater, and gas. The markers used in this series of tests were the water markers which have a frequency of 145 kHz. They have a read range of up to 1.5 m (5 ft). They are circular in shape and have a 10 cm (4-in.) diameter and 1.8 cm (0.7-in.) height and cost about $5.00 each. The 3M disc

markers were studied because they had already been proven to be durable through their use in rugged environments. They were also passive and affordable.

Figure 2.2 Typical 3M™ Disk Marker

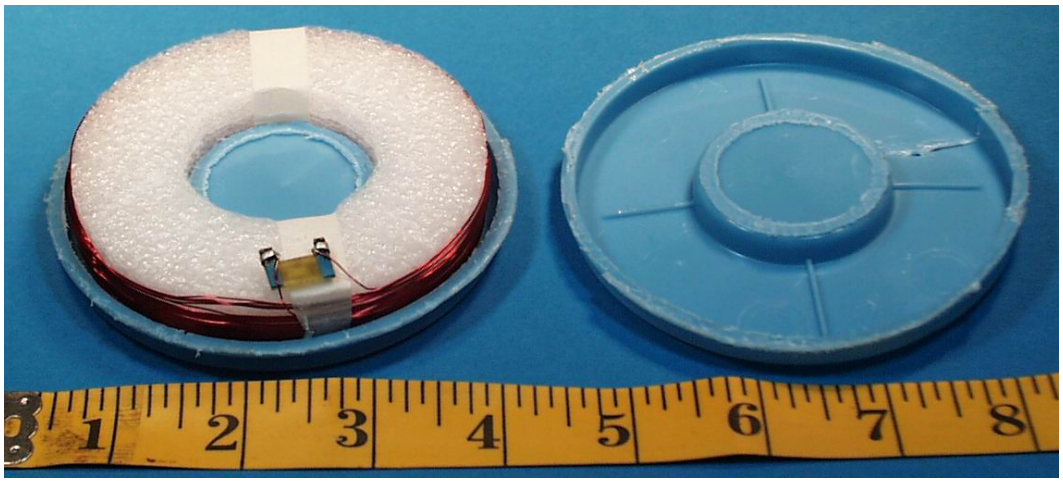

Figure 2.3 Inside of Typical 3M™ Disk Marker

2.2 EAS TAGS EMBEDDED IN CONCRETE

Two series of tests were conducted to evaluate the feasibility of embedding EAS tags in concrete. The bare tags were placed in the fresh concrete

in the first series and were wrapped or protected before being placed in the fresh concrete in the second series. The results from both series of tests are summarized below.

2.2.1 Bare EAS Tags

In the first series of tests, the EAS tags were tested without any form of external protection, in concrete prisms measuring 10.2 x 10.2 x 35.6 cm (4 x 4 x 14 in.). EAS tags were placed at different depths during casting: 1¼, 2½, 3¾, and 5 cm (½, 1, 1½, and 2 in.). Note that the sensors could also be interrogated at depths of 6½, 7½, and 9 cm (2½, 3, and 3½ in.) by simply turning the prisms over. The prisms were cured in a steam room for two weeks and subsequently air dried for two more weeks. A month after casting, all the sensors were interrogated, and none transmitted a signal to the reader. Based on the results of this first test, it was not clear if the signal from the tags could not be transmitted through the concrete or if the tags had been damaged during the casting process.

In order to separate the signal transmission from the durability issues, several concrete slices, each with a different thickness, were cut and placed over an EAS tag. The tag was then interrogated and readings were obtained through each concrete slice. The maximum concrete thickness tested was 7.6 cm (3 in.). This experiment confirmed that the tags could transmit through a medium such as concrete, and that they must have been damaged at some point during the construction process.

A few of the prisms were cut open in order to inspect the tags for possible damage. Small slices of concrete were cut until the tags were obtained. It was extremely difficult to determine where some of the tags were located, so some of them were cut in the slicing process. Even when a tag was successfully extracted from the concrete, it was impossible to determine why the tag was no longer

functioning. One reason could have been that alkaline environment in the concrete somehow damaged the integrity of the tag. Another possibility was that the tags were damaged by the placement of the fresh concrete. This hypothesis seemed more likely.

Regardless of which hypothesis was correct, it was determined that the sensors would have to be protected from the environment within the concrete in order to survive. Thus, three different ways to protect the sensors were considered and tested: wrapping with packing tape, wrapping with foam tape, and encapsulating in epoxy within a plastic petri dish. The results from the tests are described in the next section.

2.2.2 Protected Tags

Three options for protecting the EAS tags were investigated: wrapping with packing tape (Figure 2.4), wrapping with foam tape (Figure 2.5), and encapsulating in epoxy within a plastic petri dish (Figure 2.6). The first two options were simple to construct. Packing tape and foam tape (1.5 mm, 0.060 in.) was folded over the sensor to ensure that the sensor was completely covered. A 2-in. circular plastic petri dish with tight lid and five-minute epoxy were used for the third protection scheme. The EAS tag was placed inside the bottom half of the petri dish. The corners had to be gently folded up because the square sensor did not fit into the round dish. After placement inside the dish, the dish was filled with a five-minute epoxy. The lid was placed on top and the epoxy was left to cure for 24 hours.

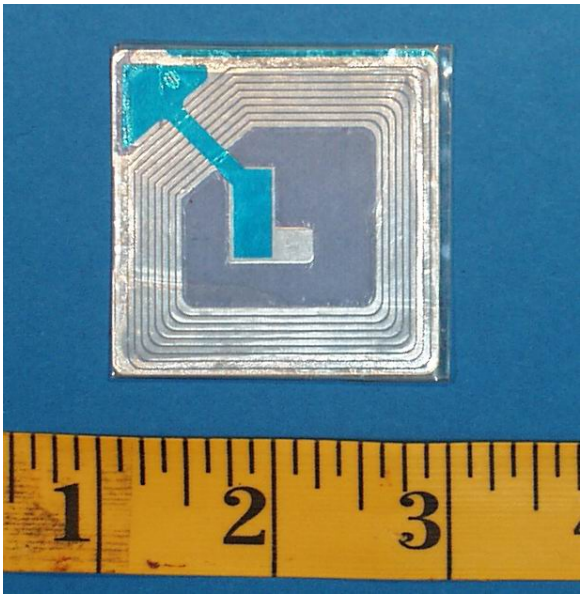

Figure 2.4 EAS Tag Protected with Clear Packing Tape

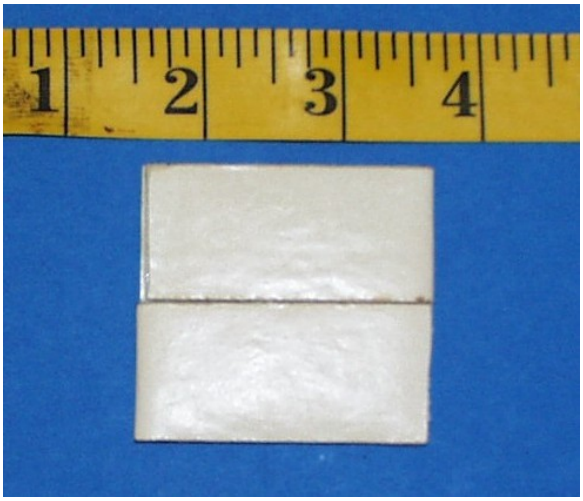

Figure 2.5 EAS Tag Protected with Foam Tape

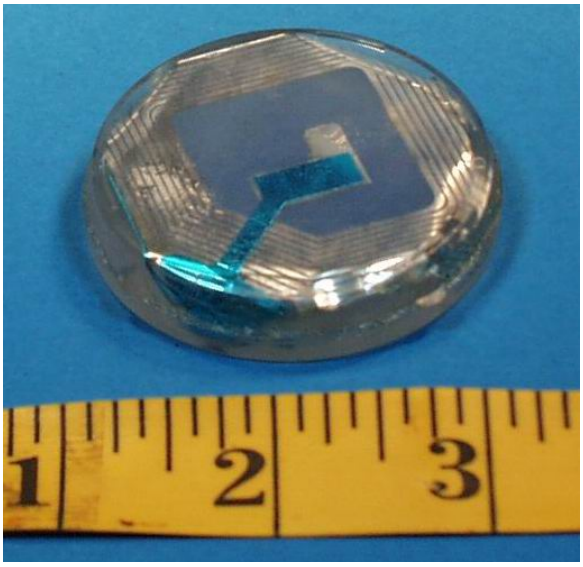

Figure 2.6 EAS Tag Protected Inside Epoxy-filled Petri Dish

The protected sensors were then cast in concrete prisms of the same size at depths of 2.5 and 5.1 cm (1 and 2 in.). Six prisms were cast with two sensors in each. These specimens were cured for one week in a steam room and subsequently air dried for three weeks. A month after casting, the sensors were interrogated and could be read at any depth within the 10-cm (4-in.) deep concrete. The sensors were believed to be undamaged, so all types of protection were successful.

Because the protected EAS tags survived the construction process and could be interrogated when embedded in concrete, the next objective was to determine the protection method which interfered with the transmission the least. Also, it was important to determine how the response was affected by embedment depth. To achieve these two objectives, a phase-gain analyzer was used to monitor the variation of phase angle and impedance data with the frequency of the transmitter. A representative plot of the variation of phase angle and impedance with frequency is shown in Figure 2.7. In this case, the EAS tag was not

protected and was not embedded in concrete. As discussed by Novak (2002), the characteristic frequency is defined as the frequency corresponding to the minimum phase angle. The absolute value of the phase angle variation, and magnitude of the impedance response, depends on a variety of factors including the drive coil and the length of the cable connecting the drive coil to the phase-gain analyzer. Therefore, only the relative values of phase angle and impedance are of interest. Data recorded for all the protected sensors are plotted in Appendix A.

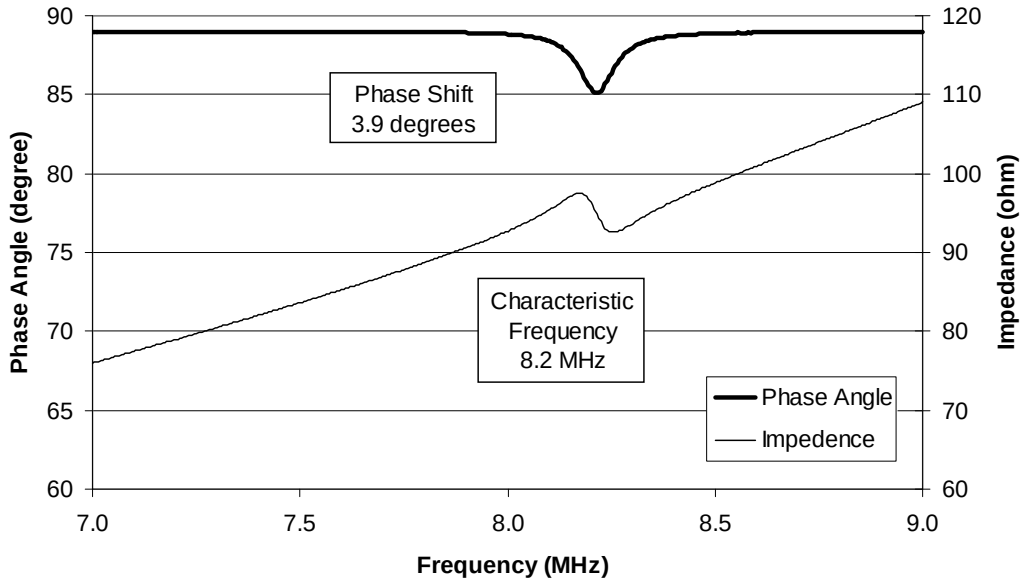

Figure 2.7 Variation in Phase Angle and impedance for Bare EAS Tag

The EAS tag interrogated in Figure 2.7 had a characteristic frequency of 8.2 MHz, and the phase angle shift at this frequency was 3.9 degrees. The amplitude of the phase shift is related to the strength of the signal relayed back to the transmitter. The distance from the sensor to the transmitter and the medium through which the sensor and transmitter are coupled both affect the signal

strength. Each of the embedded EAS tags was subjected to two frequency sweeps. The average amplitudes of the phase shifts are shown in Figure 2.8.

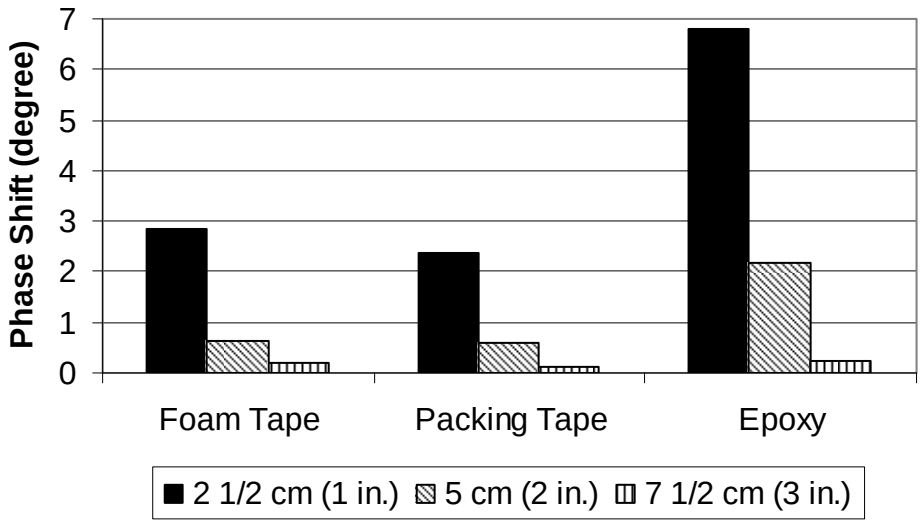

Figure 2.8 Variations of Phase Shift with Protection Type and Embedment Depth

Independent of the type of protections, the amplitude of the phase angle shift decreases with increasing embedment depth, indicating that the strength of the signal decreases with embedment depth. In addition, the EAS tags protected in the epoxy-filled petri dish exhibited larger phase shifts at all embedment depths compared with tags protected using foam and packing tape. Due to the larger phase shift, a transmitter would be able to read the tag protected by the epoxy-filled petri dish at a further distance and with more concrete cover than the other two protection alternatives. Overall, the epoxy-filled petri dish provided the best protection alternative for the EAS tag.

2.3 3M™ DISC MARKER TESTING IN CONCRETE

3M™ disc markers were embedded in concrete at the same depths and with the same prism sizes as used in the previous series of tests using the protected EAS tags. As with the EAS tag tests, a phase-gain analyzer was used to evaluate variations of phase angle and impedance data with frequency. Figure 2.9 shows the plot for a 3M™ marker in air. Data from all the embedded markers are plotted in Appendix A. The 3M™ marker interrogated in Figure 2.9 had a characteristic frequency of 147.4 kHz, and the phase shift at this frequency was 55.0 degrees.

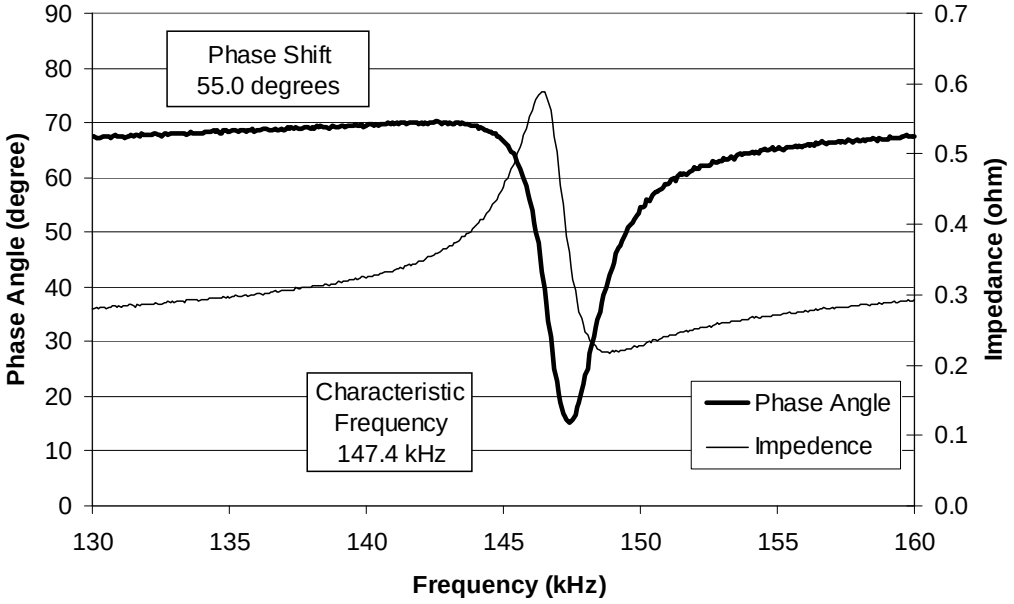

Figure 2.9 Variations of Phase Angle and Impedance for 3M™ Disc Marker

Each of the embedded markers was subjected to two frequency sweeps. The average amplitudes of the phase shifts are shown in Figure 2.10. The results of the 3M™ marker tests confirm those from the protected EAS tag tests. As the

depth of embedment into concrete increases, the magnitude of the phase shift decreases.

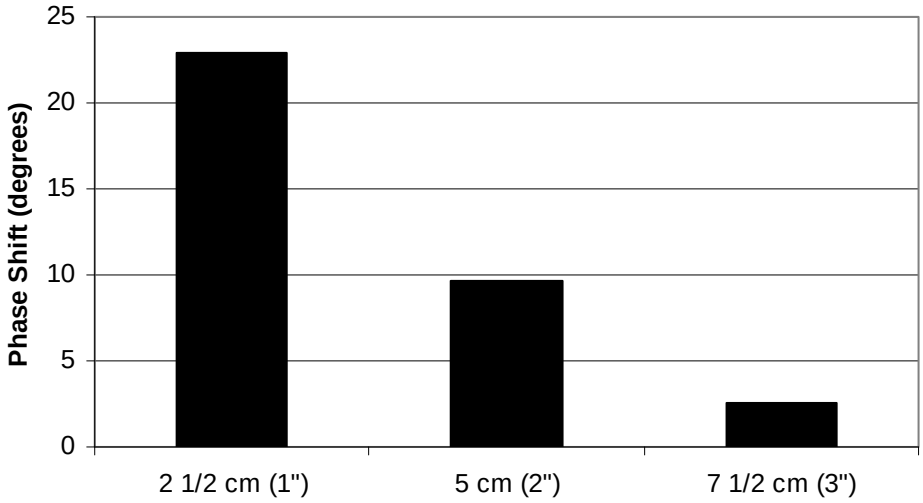

Figure 2.10 Variations of Phase Shift for Embedment Depths of 3M^{TM} Disc Markers

2.4 CONCLUSIONS

Based on the tests of the EAS tags and 3M^{TM} disc markers, it was concluded that RF technology can be used to transmit information through a dense and non-homogeneous medium such as concrete. When the EAS tags were embedded in concrete without any protection, they did not survive the construction process. When the tags were protected with either packing tape, foam tape, or an epoxy-filled petri dish, they did survive. Of the protection alternatives tested, the epoxy-filled petri dish yielded the best signal and sturdiest option. The tests run on the 3M^{TM} disc markers confirmed that as the depth of embedment increases, the magnitude of the reading or phase shift received by the transmitter decreases.

CHAPTER 3
Design of Switch for State Sensor

3.1 INTRODUCTION

The conceptual sensor design, as explained in Chapter 1, consists of at least one state switch added to an LC circuit. For the prototype corrosion sensor, the state switch was fabricated from annealed steel wire. This material was selected because the corrosion rates were expected to be comparable to those for deformed reinforcement and prestressing strand. When sufficient corrosion occurs, the wire will fracture, thereby opening the state switch and changing the characteristic frequency of the state sensor.

The purpose of this phase of testing is to quantify the corrosion rates in the deformed reinforcement and annealed steel wire. Accelerated corrosion tests were used for this purpose.

3.2 PHASE ONE: ACCELERATED CORROSION TESTS USING STEEL WIRE AND DEFORMED REINFORCEMENT

There were two objectives for this phase of testing. The main objective was to determine the rates of corrosion in deformed reinforcement corresponding to complete corrosion of steel wires. Both the reinforcement and wires were exposed to the same environment for the same amount of time. Several wire gauges were tested to determine if the amount of corrosion damage in the reinforcing steel could be related to the area of the wire. A second objective was to determine the quickest way to obtain these results. Three different

environments were tested to establish which induced the highest corrosion rates. That environment would be utilized in all future testing.

3.2.1 Testing Environments

Corrosion of reinforcing steel in reinforced concrete is a slow process. It takes time for the chloride ions to permeate through the concrete, to break down the passive layer naturally formed by the concrete, and to cause enough corrosion for visible or structural damage. The whole process can take several months in the laboratory and often takes years in the field. Thus, in the laboratory, it is often useful to expedite the corrosion process by using a simulated concrete solution as opposed to real concrete. This option has two advantages. Not only does it speed up the corrosion process by removing the time for permeation and break down of the passive layer, but it also allows the corrosion specimens to be inspected visually at any time. A major drawback to corrosion testing in reinforced concrete is that the corrosion specimen can never be visually inspected unless the concrete is cut open, thereby destroying the test specimen. Corrosion testing in a simulated concrete solution allows visual inspection at any time by simply removing the specimen from the solution.

Several simulated concrete solutions have been used by other researchers, and the one that has proven most useful is a saturated calcium hydroxide solution containing 1.85 g/L $Ca(OH)_2$. A saturated calcium hydroxide solution closely models the concrete environment surrounding the reinforcing steel because calcium hydroxide crystals occupy 20-25% of cement paste volume (Kitowski, 1993). Also, calcium hydroxide forms the initial passive layer around the reinforcing steel (Jones, 1996).

Three different environments were used for the accelerated corrosion tests of steel wire and deformed reinforcement. One of the environments used was

constant exposure to the saturated calcium hydroxide solution (SCS-C). A sodium chloride (NaCl) solution with a concentration of 3.5% by weight is normally used to simulate seawater in the laboratory to induce corrosion because corrosion rate reaches a peak around this concentration (Figure 3.1). This concentration was desired for the simulated concrete solution, unfortunately, a 3.5% by volume concentration was used in phase one. A 3.5% by volume concentration resulted in around a 7% concentration by weight and a slight decrease in the expected corrosion rate. The desired concentration of 3.5% by weight was used in phase two.

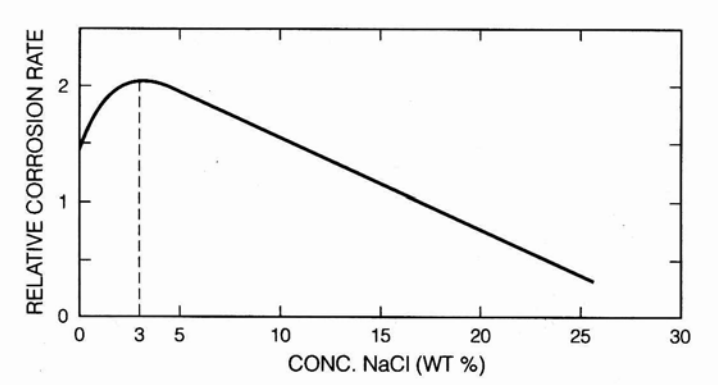

Figure 3.1 Effect of NaCl Concentration on Corrosion of Iron in Aerated Solutions (From Jones, 1996)

The saturated calcium hydroxide solution was also used as the second environment, but instead of exposing the specimens continuously, the specimens were submitted to wetting and drying cycles (SCS-W/D). It has been proven that specimens exposed to wetting and drying cycles experience a higher rate of corrosion than those specimens that are constantly wet (Jones, 1996). This rate increase is due to an increase of the presence of dissolved oxygen during the drying cycle. Dissolved oxygen is required for the cathodic reduction reaction of

corrosion in alkaline environments such as concrete (Jones, 1996). A 3.5% NaCl solution was also added to this environment to induce corrosion.

The last environment used was direct exposure to the chlorides that cause corrosion through a 3.5% sodium chloride solution (NaCl-C).

3.2.2 Specimens Submitted to Environments

For the state switch design, four gauges of wire were tested: No. 21, 22, 24, and 26 gauges (Figure 3.2). These gauges were the smallest available at the time of testing. The measured average diameters of the gauge 21, 22, 24, and 26 wires were 0.834 mm (0.034 in.), 0.787 mm (0.031 in.), 0.559 mm (0.022 in.), and 0.432 mm (0.017 in.), respectively. Each wire specimen was cut to lengths of approximately 75 cm (30 in.).

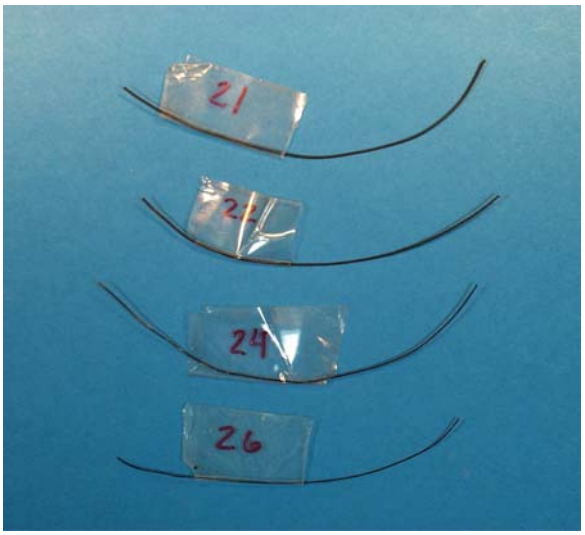

Figure 3.2 Gauges of Wire Used in Accelerated Corrosion Tests

For the purpose of correlating corrosion in the wire to corrosion in the reinforcing steel, #5 rebar was used. The nominal diameter of a #5 bar is 1.6 cm (0.625 in.). No. 5 rebar was chosen because it is a typical size used in bridge decks, one of the structural elements most vulnerable to corrosion attack. Rebar

specimens were cut to lengths of approximately 15 cm (6 in.). More corrosion was expected at the freshly cut ends of the rebar because mill scale is not present on these surfaces. To get a more uniform corrosion attack, a small layer of five-minute epoxy was applied to the ends of the rebar to prevent corrosion from occurring there. One small hole was drilled close to one end of the rebar so that it could be suspended and completely submerged in a solution.

3.2.3 Test Set-up and Procedure

In this phase, the four gauges of wire were tested in each of the three different environments, and duplicates were made of each combination, giving a total of 24 specimens (Table 3.1). Twenty-four 3-liter beakers were set up with one steel wire and one rebar in each. The steel wire was hung in a loop from a bar above the beaker and allowed to suspend in the solution. Either string or fishing line was used to suspend the rebar from the bar above. The rebar was suspended in the solution and completely submerged. An example of the beaker set-up is shown in Figure 3.3. Figure 3.4 shows a close-up of one of the beakers.

Table 3.1 Data for Accelerated Corrosion Test Specimens

	SCS-C				SCS-W/D				NaCl-C			
Bar #	1	2	3	4	5	6	7	8	9	10	11	12
Wire Gauge	21	26	24	22	21	26	24	22	21	26	24	22
Bar #	13	14	15	16	17	18	19	20	21	22	23	24
Wire Gauge	21	26	24	22	21	26	24	22	21	26	24	22

Figure 3.3 Test Set-up for Accelerated Corrosion Test

Figure 3.4 Rebar and Wire in Accelerated Corrosion Test Beaker

Before being subjected to their corrosive environments, each rebar specimen was weighed and the diameter measured at three locations along the length. All the specimens were placed in their simulated environments on the same day. Routine maintenance of the tests included replacement of evaporated water daily to ensure that the original concentrations of chemicals did not vary (ASTM G44, 1994). The specimens in the wet/dry environment were subjected to cycles of six days wet, and one day dry. For the dry cycle, the specimens were left to hang freely outside of the solution. Half-cell potential readings were taken with a saturated calomel electrode and voltmeter every couple of days to monitor corrosion probabilities. To take the readings, the saturated calomel electrode was connected to the negative port of the voltmeter and its tip was placed in the solution. The positive port of the voltmeter was connected to the steel wire and a corrosion potential reading was observed. Corrosion of the steel wire specimens was also monitored daily by visual inspection.

When a wire was observed to break due to corrosion, the wire and the corresponding rebar were removed from the solution. (It should be noted that due to the daily fluctuations in solution levels, a small section of wire at the solution/air interface underwent frequent wet/dry cycles, which caused premature wire breaks. When this occurred, the wire was simply twisted back together in that area and left to fail at another location that was fully submerged in the solution.) The rebar was then cleaned, and a final weight was taken to determine weight loss due to corrosion.

Several possible solutions can be used to remove the corrosion products from the steel (ASTM G1, 1999). A solution containing 500 mL of hydrochloric acid, 3.5 g of hexamethylene tetramine and 500 mL reagent water was used (ASTM G1, designation C.3.5). Also after cleaning, diameter measurements were taken to find a percent reduction in cross-sectional area.

3.3 PHASE TWO: ACCELERATED CORROSION TESTS USING STEEL WIRE IN PROTOTYPE SENSOR CONFIGURATION, DEFORMED REINFORCEMENT, AND PRESTRESSING STRAND

During the first phase of accelerated corrosion tests, it was observed that wire breaks often occurred in the vicinity of a kink in the wire. There were concerns that the wires may be kinked during fabrication of the sensors; therefore, a second phase of accelerated corrosion tests was initiated using wires embedded in petri dishes, which were filled with a potting compound (Chapter 4). Concerns were also raised that the highest rates of corrosion would be observed immediately outside the petri dish.

The wires were tested in two configurations during the second phase of corrosion tests: exposed loops of wire that extended beyond the petri dishes and loops of wire that encircled the petri dishes. The configuration of the state switches is discussed in Chapter 4. Small holes were drilled through the center of each petri dish, and the wire specimens were suspended in the solution.

In addition to testing deformed reinforcement, prestressing strands were also examined during the second phase of testing. Again, a No. 5 rebar was used, and specimens with lengths of approximately 15 cm (6 in.) were used. Standard ½-in. (1.3-cm) diameter strand was tested.

Twelve beakers were used in this phase. Six beakers contained rebar, and six contained prestressing strand. The rebar specimens were numbered 25-30, while the prestressing strand specimens were numbered 31-36. Each beaker contained two petri dishes, one with each wire configuration. Only 26 and 24-gauge wires were used in this phase. Of the six beakers that contained rebar, three contained gauge 26 wire and three contained gauge 24 wire, and similarly with the six beakers that contained prestressing strand.

All specimens were subjected to wet/dry exposure in the simulated concrete solution environment, because the fastest corrosion rates were observed in this environment during phase one. A similar daily maintenance routine was continued in this phase of testing. The duration of the wet/dry cycles were the same, and water was replaced daily. Half-cell readings were monitored during the first few weeks of testing. Because corrosion was visible soon after the first week and the half-cell readings indicated that corrosion potential was high, the readings were deemed unnecessary and were discontinued.

3.4 DATA FROM ACCELERATED CORROSION TESTS

3.4.1 Half-Cell Potentials

The progress of the half-cell potential readings for bars #1-12 in the three environments is plotted in Figures 3.5, 3.6, and 3.7. Each plot contains lines indicating regions where corrosion is probable, not probable, and uncertain. A corrosion potential reading between 0 and -0.13 V indicates a less than 10% chance of corrosion occurring. The corrosion probability is uncertain in the region between -0.13 and -0.28 V. If a reading exceeds -0.28 V the probability of corrosion is more than 90% (ASTM C876, 1999). All three environments yielded the same corrosion probability patterns. Within a few days, the corrosion potentials had risen above the greater than 90% probability of corrosion level and remained above this threshold throughout the duration of testing. Thus, the specimens were constantly corroding. The half-cell potential readings for the duplicates, bars #13-24, show very similar trends and are plotted in Appendix B.

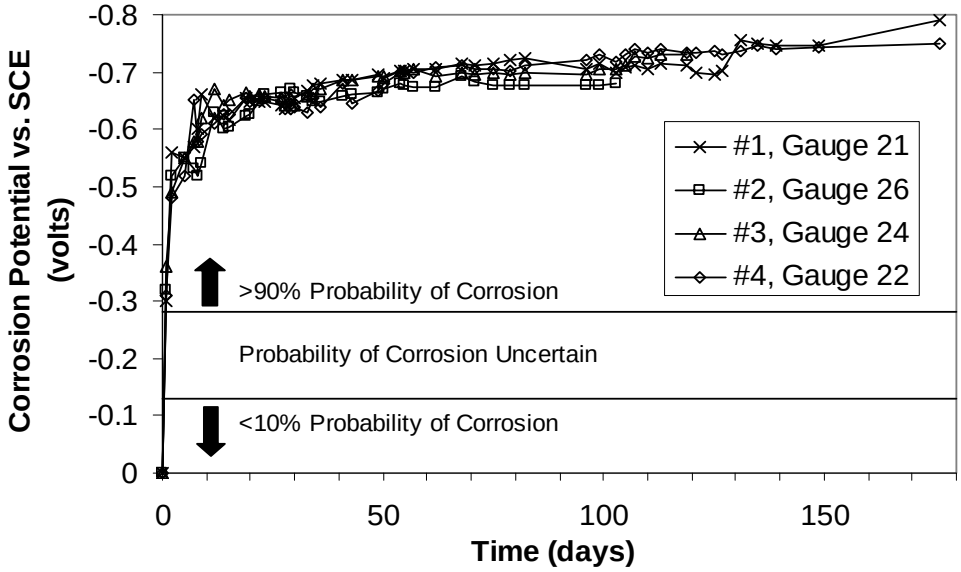

Figure 3.5 Corrosion Potential Progress for Bars #1-4 in SCS-C Environment

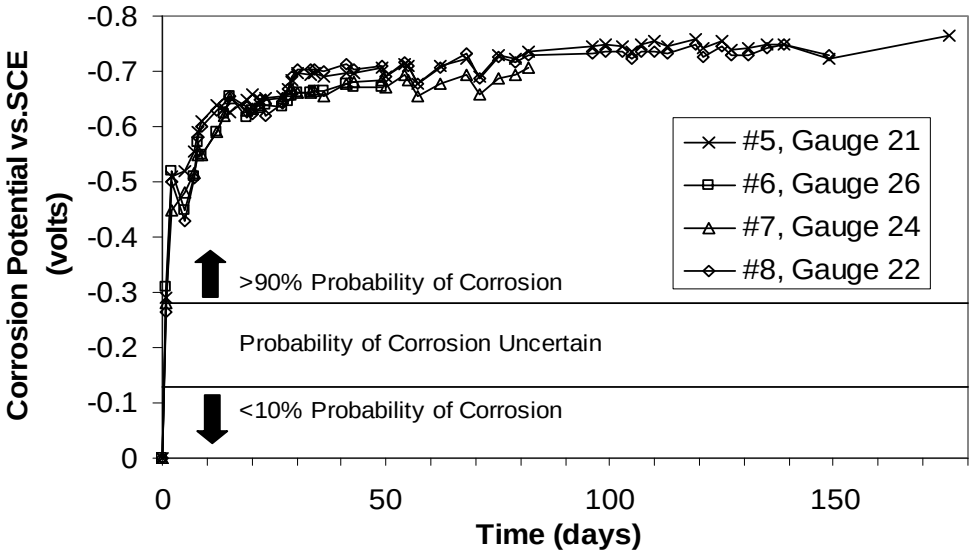

Figure 3.6 Corrosion Potential Progress for Bars #5-8 in SCS-W/D Environment

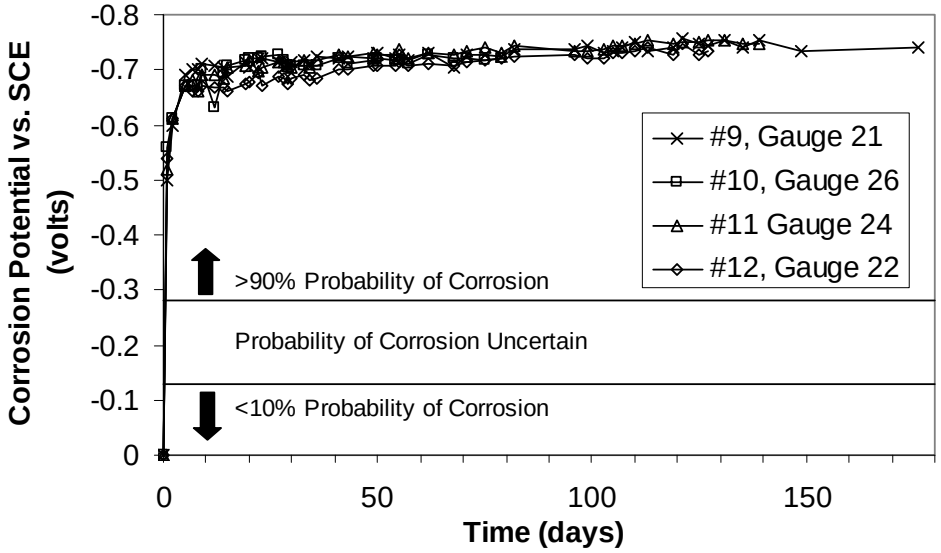

Figure 3.7 Corrosion Potential Progress for Bars #9-12 in NaCl-C Environment

3.4.2 Corrosion Rate

At the time of writing, 16 of the 24 steel wires from the first phase of testing had broken due to corrosion. Also, three wire specimens from the second phase of testing had broken, providing data about corrosion rates for two rebar specimens. (Two wire specimens were paired with one rebar or prestressing strand in each beaker.) Unless otherwise noted, all data presented in this section includes 16 of the 24 specimen from the first phase of testing and the two specimens from the second phase of testing. Pictures of the corroded steel wire and their corresponding corroded rebar are shown in Appendix D.

A corrosion rate was determined for each rebar using Eq. 3.1 where weight loss, *W*, is in milligrams; density, *D*, is in g/cm^3; surface area, *A*, is in in^2; and time, *T*, is in hours.

$$Rate = \frac{534W}{DAT} \tag{3.1}$$

When using these units, the corrosion rate calculated will be in units of mils per year (mpy), where one mil equals 0.001 in. When calculating the surface area, the end surfaces where the rebar was cut were excluded. The ends were covered with epoxy so that no corrosion would occur in that area. Unfortunately, some corrosion did occur even underneath the epoxy. The area was still calculated the same. In future testing a marine epoxy should be used to ensure that no corrosion occurs.

Table 3.2 shows the corrosion rates as well as the percentage of cross-sectional area reduction and time required to break each of the wire specimens. A more detailed list of all the variables needed for the computation of corrosion rate and cross-sectional area reduction for each specimen is listed in Appendix B.

Table 3.2 Corrosion Rates and Cross-Sectional Area Reductions

Bar #	Wire Gauge	Time to Wire Break *(days)*	Cross-Sectional Area Reduction in Rebar *(%)*	Corrosion Rate *(mpy)*	Bar #	Wire Gauge	Time to Wire Break *(days)*	Cross-Sectional Area Reduction in Rebar *(%)*	Corrosion Rate *(mpy)*
2	26	105	0.25	0.62	15	24	110	0.37	0.95
3	24	121	0.01	1.07	17	21	192	2.61	4.69
6	26	50	2.59	3.14	18	26	71	0.24	4.57
7	24	96	1.65	3.68	19	24	96	2.16	4.52
8	22	176	2.29	9.36	22	26	135	0.24	2.08
10	26	96	0.99	3.97	23	24	103	2.23	2.76
11	24	149	0.39	3.93	24	22	149	2.01	4.51
12	22	135	0.82	2.09	25	26	47	1.11	2.30
14	26	79	1.77	0.93	26	26	65	0.11	2.13

A frequency distribution of the measured corrosion rates for all rebar was plotted to determine a mean corrosion rate (Figure 3.8). The resulting plot does not resemble a normal distribution because of a lack of ample data. It is expected that as more wires break, the distribution will become more defined. Another reason for the undefined distribution might be the use of the slightly different

testing environments. However, the mean corrosion rates for the reinforcing bars appear to be between 2 and 3 mpy.

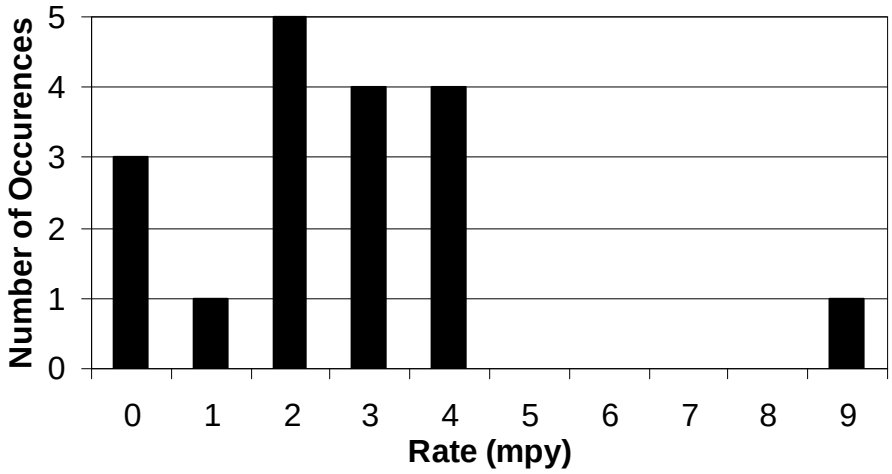

Figure 3.8 Distribution of Corrosion Rates

3.4.3 Corrosion Time to Wire Break

Ideally, each steel wire should corrode at the same rate. Therefore, the only parameter that distinguishes the different wires is the time it takes for the corrosion to penetrate the entire cross-sectional area. These times are listed in Table 3.2 for each specimen. The time to wire break for each gauge of wire was averaged and the results plotted (Figure 3.9). The average time to wire break of the smallest gauge wire, No. 26, was the least amount of time out of all the gauges tested. Likewise, the No. 21 gauge wire, the largest wire, displayed the highest average time to wire break. These results are expected to continue throughout the duration of phase one and two testing.

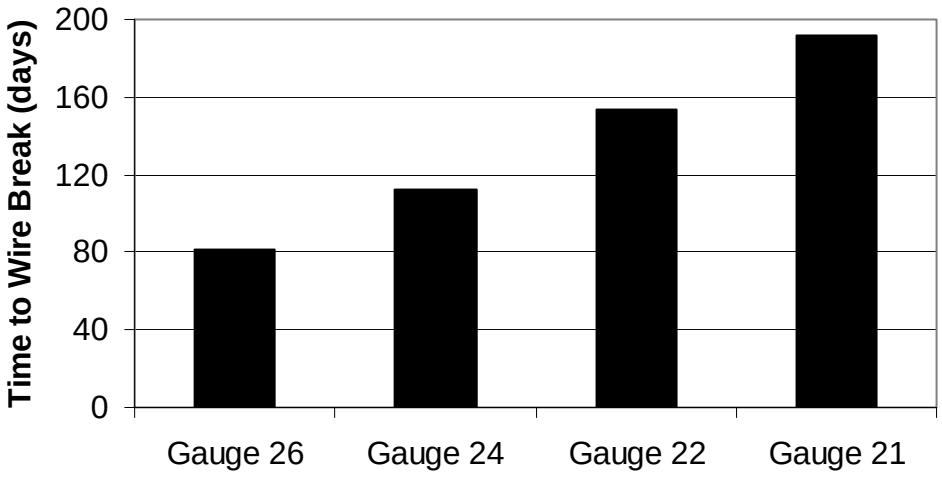

Figure 3.9 Time to Wire Break for Different Gauges of Wire

One of the objectives of phase one was to determine which environment, SCS-C, SCS-W/D, or NaCl-C, would produce the fastest corrosion. Only the results from wire gauges 26 and 24 were considered because many of the 22 and 21 gauge wires were not broken. Therefore, there were not ample data to compare between the three environments for those two wire gauges. Average time to wire break for each solution are plotted (Figure 3.10). The plot shows that for both the gauge 26 and gauge 24 wires, the SCS-W/D environment produced the fastest corrosion rates. Also, for both wire gauges, the SCS-C environment was on average the second fastest corroding environment and the NaCl-C environment was the slowest. With these results it was decided that future tests would solely use the SCS-W/D environment. Using the SCS-W/D environment would yield the fastest results and closely resemble the environment that reinforcing steel experiences inside concrete.

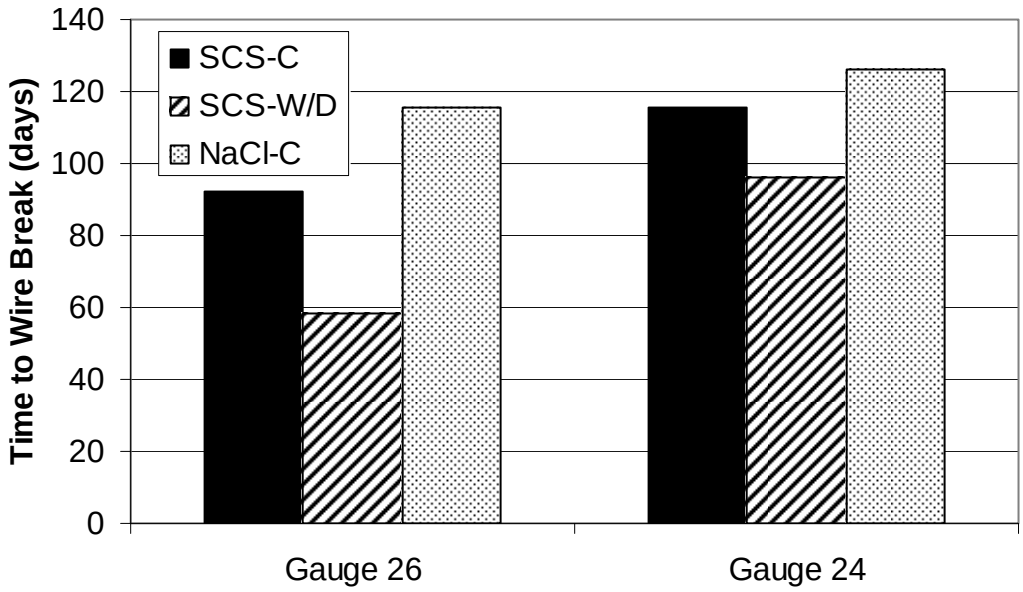

Figure 3.10 Comparison of Time to Wire Break for Different Environments

3.4.4 Cross-Sectional Area Reduction

An important parameter for a structural engineer is the cross sectional area reduction that the reinforcing steel experiences as corrosion damage occurs. As the cross sectional area of the reinforcing steel decreases, the force that the steel can resist also decreases. The cross-sectional area reduction for each specimen is listed in Table 3.2. The average reduction for each wire gauge was calculated and plotted (Figure 3.11). As expected, the area reduction increased as the diameter of the wire increased. The smallest wire, gauge 26, had the lowest cross-sectional area reduction, and likewise, the largest wire, gauge 21, had the highest reduction. As mentioned before, the average values obtained here are very important to a structural engineer. When a sensor is interrogated, it will relay to the user which state switches have and have not been broken. Knowing whether or not a state

switch has broken can provide information on how much cross-sectional area has been lost.

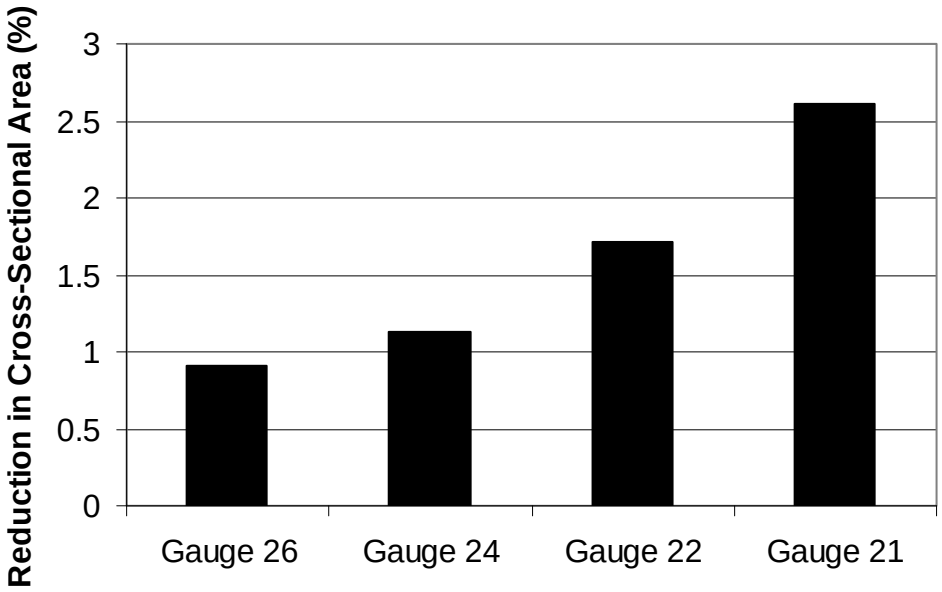

Figure 3.11 Percentage of Cross-Sectional Area Reduction in Reinforcing Bars for Different Wire Gauges

The calculated values for cross-sectional area reduction listed in Table 3.2 are highly variable. Corrosion is a highly variable and unpredictable phenomenon. Although all attempts were made to provide a uniform surface for corrosion to attack, corrosion was still accelerated at nicks and other areas of inconsistencies not seen by the naked eye.

3.5 CONCLUSIONS

The results obtained from the accelerated corrosion tests closely resemble what was expected, but more data are still needed. More data are needed to define fully the distribution of corrosion rates and to verify the time to wire break and cross-sectional area reduction patterns already observed.

The half-cell potential results indicated that corrosion probability quickly rose to over 90% within the first week. After that, half-cell potential readings were not necessary. If the same accelerated corrosion test setup is used in the future, half-cell potential readings would not be required. Also in future test, a marine epoxy should be used to cover the cut ends of the rebar to prevent corrosion from occurring there. The frequency distribution of the corrosion rates suggests that the average rate of corrosion of reinforcing steel is around 2-3 mpy. As expected, a smaller wire corrodes and breaks faster than a large wire. Likewise, the breakage of a smaller wire indicates a smaller reduction in area of reinforcing steel than a larger wire.

CHAPTER 4
Design and Testing of Prototype Wireless Corrosion Sensor

4.1 INTRODUCTION

The design of the prototype wireless corrosion sensor will be discussed in this chapter. Tests have been designed to demonstrate that the sensors provide reliable data about corrosion of embedded steel reinforcement. Prototype sensors have been embedded in reinforced concrete prisms, which are being subjected to wet/dry cycles in salt water. These tests are ongoing; therefore, final results are not available. However, the data obtained to date are discussed. Conceptual design of the corrosion sensor is discussed in Chapter 1. Detailed information about the construction and performance of the prototype sensors are discussed in this chapter.

4.2 DESIGN CONCEPT

Although the corrosion sensor can be designed with any number of state switches, the prototype sensor developed during this project utilized a single switch. As discussed in Chapter 3, information about the extent of corrosion can be obtained b using different wire sizes to fabricate the switch. Therefore, the corrosion sensor will provide information about when corrosion of reinforcement within the concrete have exceeded given thresholds.

4.2.1 Electrical Components of Prototype Sensor

Four basic electrical components are used to fabricate the prototype sensor developed in this project: an inductor, two capacitors, and a switch. Design and selection of each component is discussed below.

4.2.1.1 Inductor

The inductor for the prototype sensor was wound using No. 24 gauge, enamel-coated copper wire. The coils in the prototype sensor were fabricated using of wire, but coils with one, two, five, and ten turns were investigated. The choice of coil size was a trade-off between the desires to build the smallest sensor with the largest read distance from the transmitter. The physical size of the sensor is governed by the diameter of and number of turns in the coil, and the transmission distance increases with an increasing number of turns.

Equation 4.1 shows the relationship between inductance, L; coil radius, a; number of turns, N; and coil length, l (Lee, 1998):

$$L = \frac{(aN)^2}{22.9l + 25.4a} \tag{4.1}$$

Figure 4.1 illustrates the coil length, l, and coil radius, a, used in Eq. 4.1.

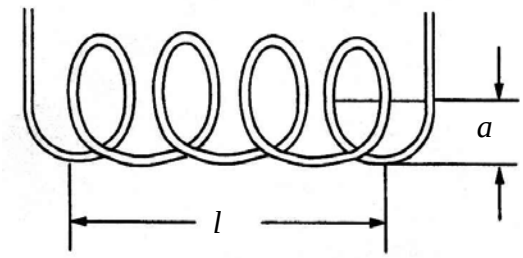

Figure 4.1 Diagram of Coil Length and Radius (From Lee, 1998)

Increasing the inductance will increase the coupling efficiency between the sensor and transmitter, thereby increasing the signal strength at a given distance between the sensor and transmitter. Consequently, the minimum

distance required to achieve a given signal strength will increase with increasing inductance.

In the applications envisioned for the prototype sensors, the sensors will be attached to the outer layers of reinforcement. Therefore, the transmitter-receiver system must be capable of penetrating the concrete cover.

For the tests described in Section 4.3, a concrete cover of 1¼ cm (½ in.) was used. Preliminary tests indicated that the one- and two-turn coils did not have sufficient inductance to read a signal through 1¼ cm (½ in.) of concrete. However, the five- and ten-turn coils were sufficient to transmit through this thickness. The five-turn coil was selected for the prototype sensor because it was easier to fabricate, and the resulting sensor size was smaller.

Although the five-turn coil was selected in the case for the prototype sensor, it should be noted that the American Concrete Institute requires that the reinforcing steel be placed with a minimum concrete cover of 4 – 5 cm (1½ – 2 in.) for structures exposed to weather (ACI 318, 2002). Thus, the current prototype sensor and transmitter combination are not likely to be sufficient in a real world situation. Either the inductor in the sensor or the transmitter will have to be altered to produce a transmitter-receiver system suitable for standard structures.

4.2.1.2 Capacitors

Capacitors were chosen that had tinned, copper leads, and a capacitance of 151 pF (picofarads). The tinned leads allowed for easy soldering. A capacitance of 151 pf was chosen because when the capacitor was combined with the chosen 5-turn coil inductor, the combination yielded a resonant frequency of approximately 8 MHz. When the steel wire state switch and second capacitor were added, the final resonant frequency was approximately 6 MHz. Figures 4.2a

and 4.2b show the change in phase angle and impedance, respectively, of a test sensor when the state switch is opened and closed. For this particular exposed loop sensor, the characteristic frequency was 6.03 MHz when the state switch was closed and 8.62 when the state switch was open. As defined (Novak, 2002), the characteristic frequency corresponds to a minimum in the phase angle response and an inflection point in the impedance response.

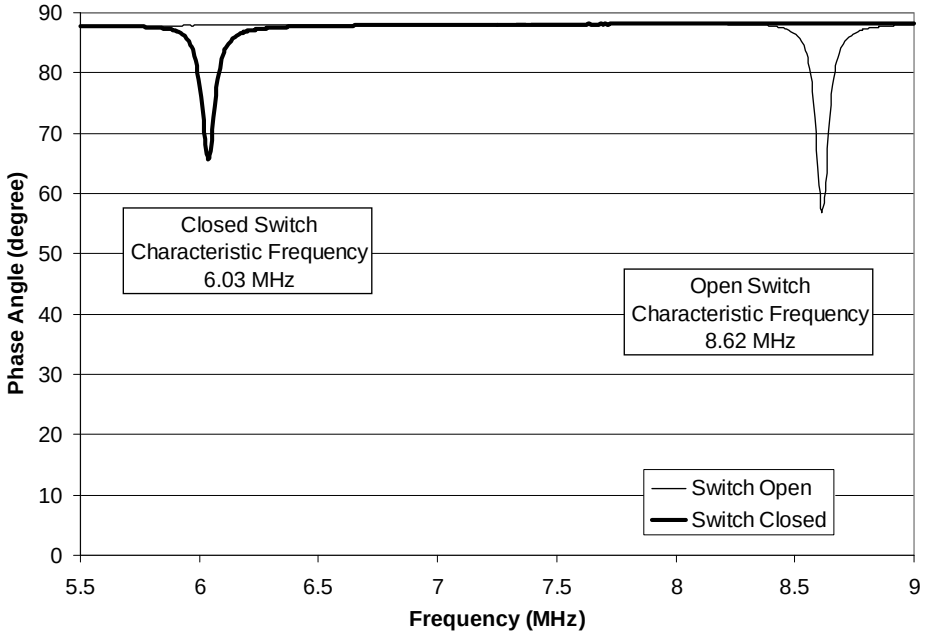

Figure 4.2a Variation in Phase Angle for Exposed Loop Sensor

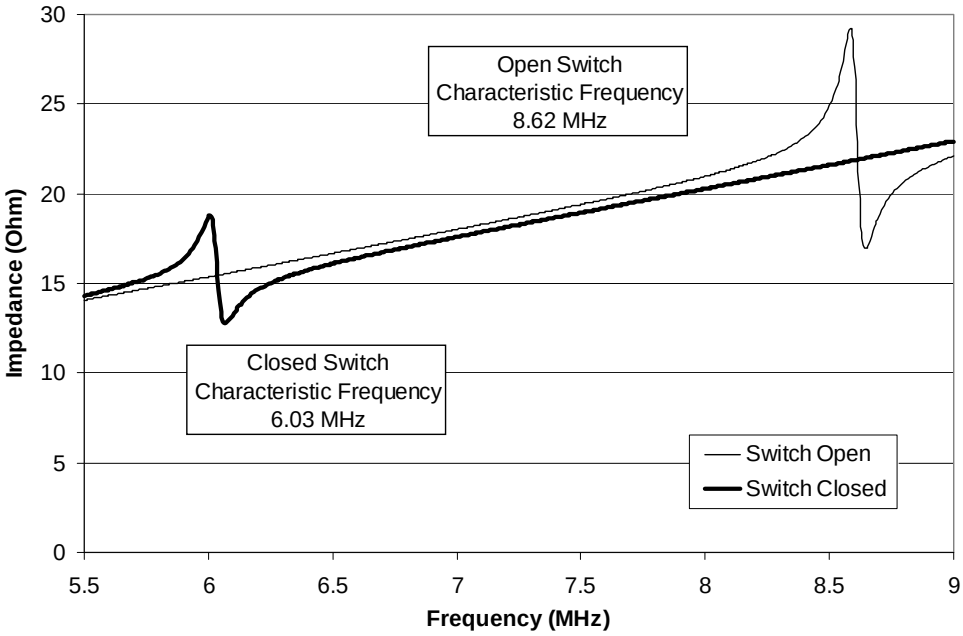

Figure 4.2b Variation in Impedance for Exposed Loop Sensor

4.2.1.3 State Switch

The state switch was fabricated from the annealed steel wire discussed in Chapter 3. Half of the prototype sensors were fabricated with state switches from No. 24 gauge wire and half were fabricating using a No. 26 gauge. These wire sizes were selected because they corroded quickly in the accelerated corrosion tests discussed in Chapter 3, and it was believed that they were sufficiently large to survive the construction process.

The prototype sensors were constructed with two configurations for the state switches: circumferential loops and exposed loops. The circumferential loop configuration consists of the steel wire being wound around the outside of the sensor. The exposed loop configuration consists of the steel wire extending outside of the sensor in a loop formation. Figures 4.3 and 4.4 illustrate the

circumferential and exposed loop state switches, respectively. Both configurations were tested to determine which was more likely to survive the construction process and which yielded more accurate corrosion results.

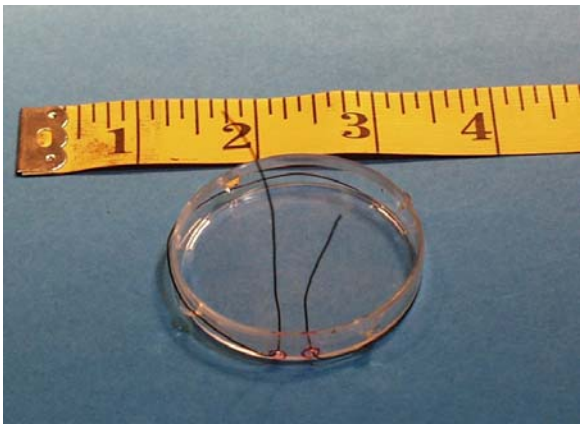

Figure 4.3 Circumferential Loop State Switch

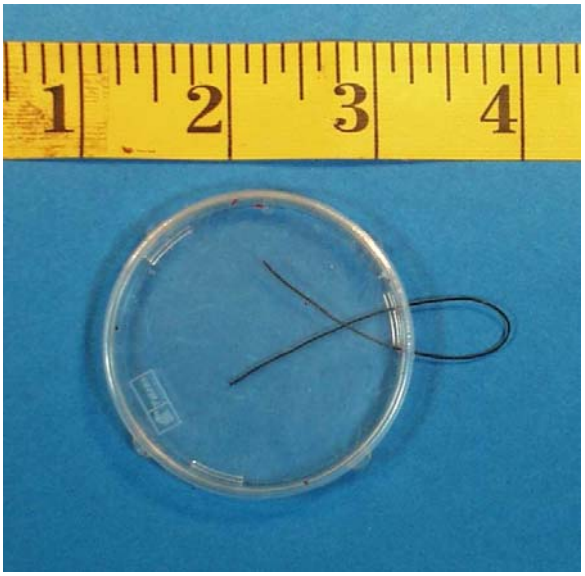

Figure 4.4 Exposed Loop State Switch

4.2.2 Non-electrical Components of Prototype Sensor

Several non-electrical components were also required to assemble the prototype sensor. The components included: a PVC pipe, a petri dish, and an electrical potting compound.

4.2.2.1 PVC Pipe

A cylindrical object was used to wind the copper wire that formed the inductor. The cylindrical object kept the coil intact after winding. A material that was both sturdy and easily cut into small slices was preferred. PVC pipe, a plastic pipe which is commonly used in plumbing projects and commercially available at hardware stores, fit all these requirements. PVC pipe is available in a variety of diameters. A 4-cm (1½-in.) PVC pipe was selected for the prototype sensor.

4.2.2.2 Petri Dish

A major concern with the sensor is its ability to survive the concrete construction process. An object was needed to encapsulate the electrical components of the sensor and protect them from the construction environment. A plastic petri dish was chosen for this purpose. This is the same petri dish used to protect the EAS tag in the initial feasibility study (Chapter 2). A petri dish with a 5-cm (2-in.) diameter, 8.5-mm (0.33-in.) height, and tight lid was selected.

4.2.2.3 Electrical Potting Compound

An electrical potting compound was used to fill the petri dish in order to protect the sensor. GE Silicones® makes several high-strength silicone rubber compounds ranging in color and viscosity that protect electronic components against vibration, moisture, chemicals and other environmental hazards. RTV615A was chosen because its color and viscosity were suitable for the prototype sensor. RTV615A is colorless, so even after it has been applied and

cured, the electrical circuit is still visible. Its viscosity is 4300 cP (centipoise), which is about the same viscosity as honey. This low viscosity allows the silicone to flow easily around complex parts. At room temperature, the silicone takes about six days to cure completely.

4.2.3 Desired Attributes of the Sensor

The desired attributes of the sensor (durable, affordable, passive, and reliable) were discussed in Chapter 1. The prototype sensor discussed in this chapter possesses three of the four desired attributes. The protective layers of the silicone and the petri dish and the self-sustaining power source due to inductive coupling combine to satisfy the durability requirement. All materials used to fabricate the sensor are affordable. At the time of writing, the total cost for raw materials of one prototype sensor is $1.58, making this sensor a much less expensive option than any existing forms of corrosion detection described in Chapter 1. Table 4.1 summarizes the costs of each raw material needed for the prototype sensor. Although it is expected, current testing of the prototype sensor will soon determine if it satisfies the last attribute: reliability.

Table 4.1 Cost of Raw Materials for One Prototype Sensor

Item	Amount	Unit Cost	Cost
Capacitor	2	$0.100 / each	$0.20
Copper coil	62	$0.001 / cm	$0.06
Steel wire	20	$0.001 / cm	$0.02
PVC Pipe	8	$0.001 / mm	$0.01
Petri Dish	1	$0.200 / each	$0.20
Silicone	16.7	$0.066 / cm^3	$1.09
		Total Cost:	**$1.58**

A detailed procedure for fabricating the prototype sensors is presented in Appendix C.

4.3 CORROSION TESTS OF PROTOTYPE SENSORS EMBEDDED IN CONCRETE PRISMS

4.3.1 Overview of Tests

The sensors were embedded in reinforced concrete prisms, which were then immersed in a 3.5% NaCl solution and subjected to wetting and drying cycles designed to corrode the reinforcement. Each cycle consisted of five days wet and two days dry. Sensors were interrogated weekly at the end of each dry cycle to determine the state of the switch.

4.3.1.1 Concrete Specimens

Twelve concrete prisms measuring 15.2 x 15.2 x 53.3 cm (6 x 6 x 21 in.) were cast with two #5 bars and three sensors in each. The rebar were positioned with 1¼ cm (½ in.) of concrete cover. The thickness of the concrete cover was selected such that the chloride ions in the NaCl solution could permeate rapidly.

Three sensors were positioned in each prism. The sensors were placed at the same level as the reinforcing steel, so that they would experience the same concentrations of chloride ions as the rebar. Two # 2 transverse bars were tied to the bottom of the longitudinal bars with a spacing of approximately 1¼-cm (½-in.). The transverse bars provided a platform to support the sensors during construction (Figure 4.5). The sensors were attached to the transverse bars with epoxy and wires to ensure that they stayed in place during construction (Figure 4.6).

In order to initiate corrosion as quickly as possible inside the concrete prisms, crack initiators were formed into the top of the prism over each sensor. The crack initiators were formed by using a piece of sheet metal to form a thin indention in the concrete just after casting the prisms.

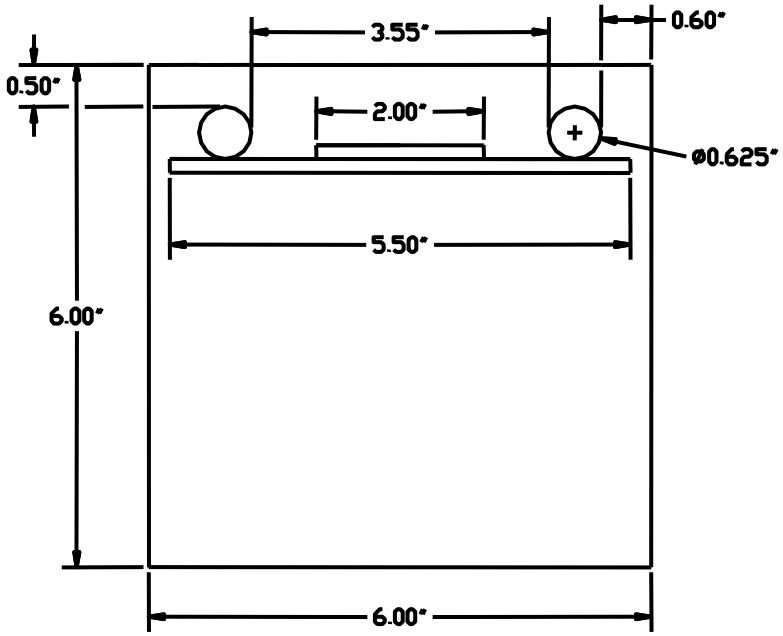

Figure 4.5 Cross Section of Prism Used in Prototype Sensor Testing

The specimens were designed such that half-cell potential readings could be used to track corrosion probabilities in the prisms. Half-cell potential readings require a direct connection to the steel (ASTM C876, 1999). To allow for this, reinforcing steel had to extend beyond the concrete. Holes were drilled in the concrete prism forms at the desired locations.

The reinforcing steel was 61 cm (24 in.) long, which allowed about 4 cm (1½ in.) to extend beyond the forms at each end. Each piece of reinforcing steel was drilled and tapped near one end in the region that would beyond outside the forms. A ¼ x 1-in. galvanized screw was inserted into the threaded hole. This screw served as a connection point for the half-cell potential readings. Figure 4.5 shows the plan view of a completed form, including screws, longitudinal bars, transverse bars, and sensors, just before casting.

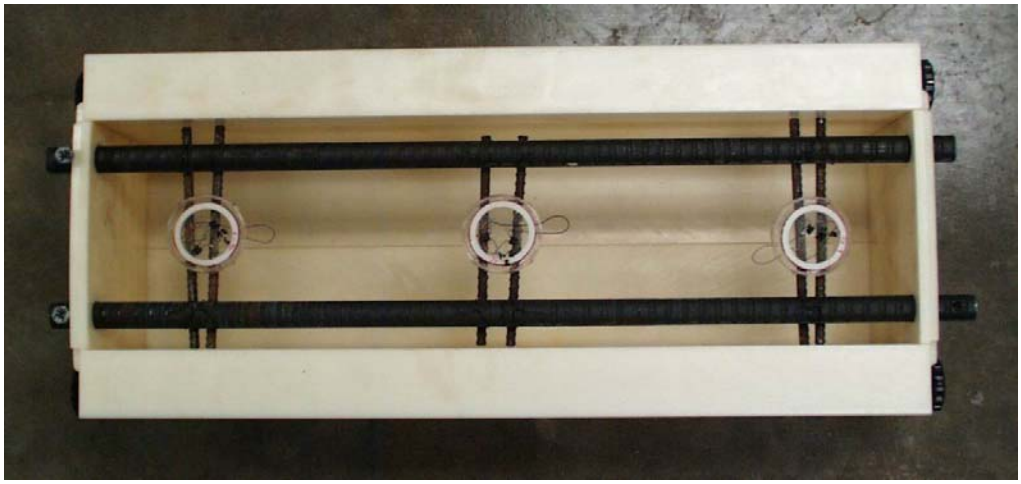

Figure 4.6 Photograph of Form, Reinforcement, and Sensors

4.3.1.2 Embedded Sensors

As mentioned previously, three sensors were placed in each prism. Sensors were placed at three points along the length of the prism: at the midpoint and 6 cm (2½ in.) from each end (Figure 4.6). A total of thirty-six sensors were cast in the prisms. The prisms and sensors are identified in Figure 4.6. The prisms are numbered 1 through 12 and the sensors are identified using two letters to identify the configuration of the state switch, CL for the circumferential loop and EL for the exposed loop, and two numbers to identify the wire gauge, 24 and 26. Each prism contained three sensors with the same loop configuration. Both wire sizes were used in each prism. To date none of the state switches have broken. However, the concrete prisms will be demolished to inspect the reinforcement and sensors after the sensor readings indicate that the state switches have corroded and fractured. The longitudinal bars will then be weighed to calculate weight loss and corrosion rate.

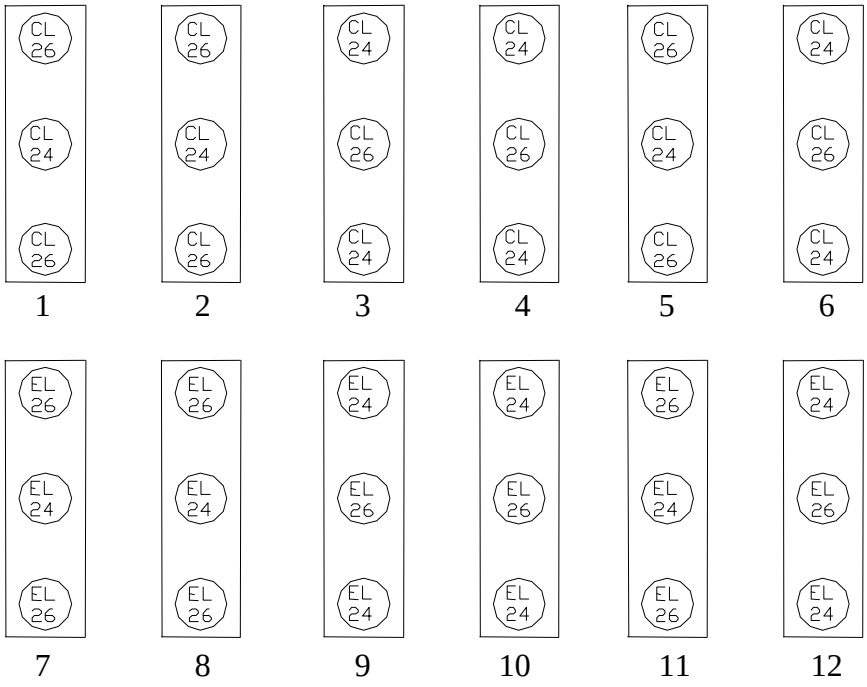

Figure 4.7 Sensor Locations in Concrete Prisms

4.3.1.3 Concrete Mix Design and Casting Procedure

The concrete used to cast the prisms was not a normal mixture design; the mixture was designed to promote corrosion of the embedded reinforcement. A similar mixture had been used successfully to promote corrosion (Fuentes, 1999). The mixture was designed to have a very high water-cement ratio, as well as a high slump. Consequently, the concrete would be highly permeable and vulnerable to corrosion attack. Also, instead of waiting for the chloride ions to permeate through the concrete, chlorides were added to the concrete during mixing by adding salt to the mixing water. The time required for chloride penetration can be substantial. By including chloride ions in the concrete, this time to initiation of corrosion is reduced. The mixing water contained 3.5% salt by weight. Table 4.2 summarizes proportions of the concrete mixture.

Table 4.2 Concrete Mixture Design

	Weight, lb	
	Design	Actual
Coarse Aggregate	243	243
Fine Aggregate	224	224
Water	47	37
Cement	68	68
Salt	1.65	1.35

A total of twelve prisms were cast: six on January 23, 2003 and six on January 24, 2003. A total of ten 10x20-cm (4x8-in.) cylinders, five each day, were also cast. The cylinders were used to determine the compressive strength and chloride content of the concrete.

Before casting, each sensor was interrogated to determine its characteristic frequency. During casting, special care was taken to not damage the sensors. Immediately after casting, the crack initiators were formed. The specimens were removed from the molds a day after casting and cured in an environmental chamber (72° F, 100% humidity) for one week and in air for an additional week. The prisms were then immersed in a tank containing a 3.5% NaCl solution. A photograph of the prisms in the tank is shown in Figure 4.8.

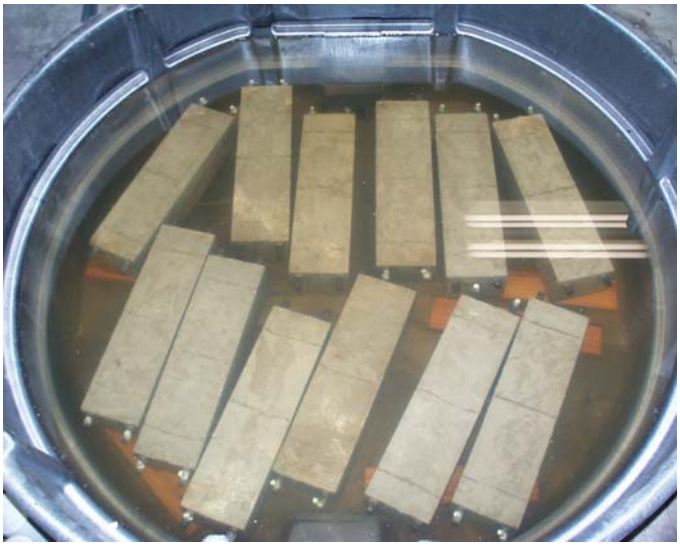

Figure 4.8 Concrete Prisms Immersed in 3.5% NaCl Solution

4.3.2 Measured Data

4.3.2.1 Rebar Specimen

Initial length, weight, and diameter measurements of the rebar were taken before the placement of concrete (Appendix F). These measurements will be used in conjunction with the final measurements to determine corrosion rates and reductions in cross-sectional area.

4.3.2.2 Half-cell Potential Readings

Half-cell potential readings were taken during the first few weeks of testing. After the first week, all half-cell readings were above the greater than 90% probability level, so the half-cell potential readings were deemed unnecessary and discontinued.

4.3.2.3 Compressive Strength Testing

Eight of the ten cylinders, were tested 30 days after casting. An average compressive strength of the concrete cast on January 23, 2003, and January 24, 2003 were 6050 and 6000 psi, respectively. The compressive strength of each cylinder is listed in Table 4.3.

Table 4.3 Compressive Strengths of Cylinders Cast on January 23 and 24, 2003

	f'_c, psi	
	1/23/2003	1/24/2003
	6314	5929
	6190	6006
	5997	6004
	5684	6063
Average:	**6050**	**6000**

The measured strengths were much higher than what was expected. The desired slump for the concrete mixture was 6 in. As a result of reaching the desired slump when only a portion of the mixing water had been added, the remaining water was not included in the mixture. Consequently, the water/cement ratio was decreased, and the compressive strength increased. The actual concrete mixture, including the reduced water and salt amounts, is listed in Table 4.2. It is not yet known whether or not the unexpected increase in concrete strength will affect the time to corrosion of the reinforcing steel.

4.3.2.4 Chloride Content of Concrete

The initial chloride content, before the prisms were immersed in the NaCl solution, was measured. Tests were conducted on the two remaining cylinders, which were not exposed to the NaCl solution. AASHTO T 260-97 (2001) guidelines for testing chloride ion content were followed. Six samples were taken from the side of each cylinder. Samples were taken at three points along the length of each cylinder: at the centerline and 5 cm (2 in.) from each end.

Samples were also taken at two different depths: 1¼ cm (½ in.) and 3¼ cm (1¼ in.) The first depth corresponds to the distance from the top of the prism to the top of the rebar, and the second depth corresponds to the distance from the top of the prism to the bottom of the rebar.

The chloride content from each of the 12 samples is plotted in Figures 4.9 and 4.10. The chloride threshold for corrosion is indicated on each plot at 0.03% by weight of concrete. This value is intended as a guideline only, and is based on a chloride threshold value of 0.2% of weight of cement. (ACI 222, 1996) Two lines representing the depths at the top and bottom of the rebar are also shown. Both plots indicate that the chloride content in each concrete mix was well above the chloride content threshold for corrosion. Therefore, each prism cast had enough chlorides present to initiate corrosion of the reinforcing steel. This was expected to accelerate the corrosion process.

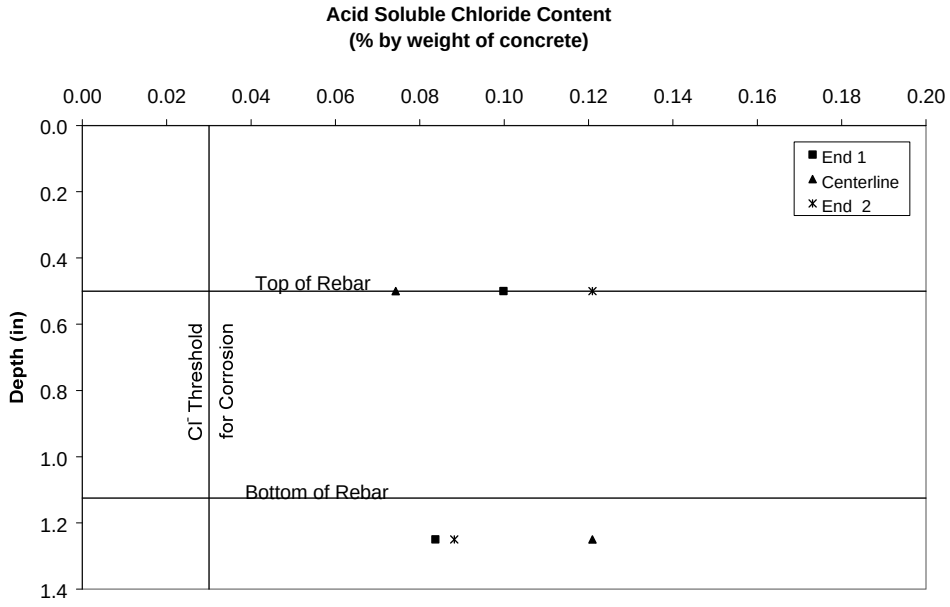

Figure 4.9 Soluble Chloride Content Measured from Cylinder Cast on January 23, 2003

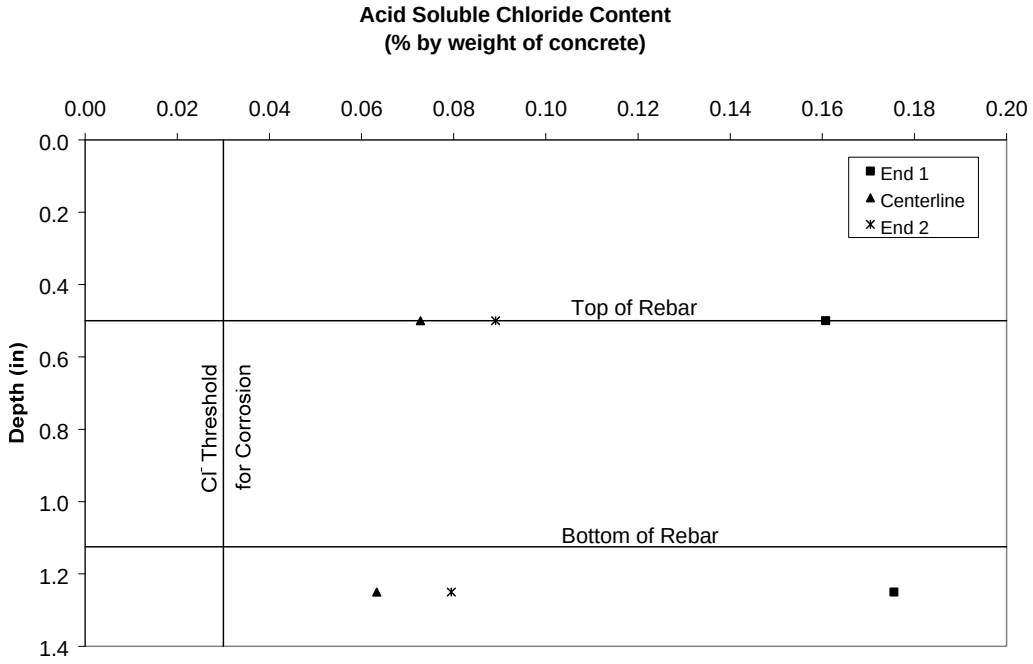

Figure 4.10 Soluble Chloride Content Measured from Cylinder Cast on January 24, 2003

4.3.2.5 Characteristic Frequencies of Sensors

Each sensor was interrogated two weeks after casting the prisms and before the prisms were immersed into the NaCl solution. Each sensor was successfully interrogated through the concrete. To date, each sensor still resonates at a characteristic frequency corresponding to a closed switch (Table 4.4).

Table 4.4 Measured Characteristic Frequencies of Sensors Embedded in Prisms

Circumferential Loop, No. 26 Wire

Sensor	Prism	Frequency *(MHz)*
CL-26-1	1	6.36
CL-26-2	1	6.40
CL-26-3	2	6.38
CL-26-4	2	6.31
CL-26-5	3	6.36
CL-26-6	4	6.32
CL-26-7	5	6.00
CL-26-8	5	6.31
CL-26-9	6	6.37

Circumferential Loop, No. 24 Wire

Sensor	Prism	Frequency *(MHz)*
CL-24-1	1	6.30
CL-24-2	2	6.22
CL-24-3	3	6.32
CL-24-4	3	6.31
CL-24-5	4	6.29
CL-24-6	4	5.69
CL-24-7	5	6.32
CL-24-8	6	6.31
CL-24-9	6	6.29

Exposed Loop, No. 26 Wire

Sensor	Prism	Frequency *(MHz)*
EL-26-1	7	6.10
EL-26-2	7	6.12
EL-26-3	8	6.10
EL-26-4	8	6.15
EL-26-5	9	6.12
EL-26-6	10	6.14
EL-26-7	11	6.10
EL-26-8	11	6.19
EL-26-9	12	6.08

Exposed Loop, No. 24 Wire

Sensor	Prism	Frequency *(MHz)*
EL-24-1	7	6.01
EL-24-2	8	6.13
EL-24-3	9	6.04
EL-24-4	9	6.09
EL-24-5	10	6.04
EL-24-6	10	6.00
EL-24-7	11	6.06
EL-24-8	12	6.05
EL-24-9	12	6.11

4.4 SENSOR TESTING IN CONSTRUCTION PROCESS

During casting of the concrete prisms, special care was taken so that the sensors would not be damaged. This delicate handling would not normally occur, so it was decided to test if the sensors could survive a typical concrete placement. Twelve sensors were attached to a rebar cage constructed for another research project at the Ferguson Structural Laboratory. Concrete was placed using a crane supported bucket, and internal vibrators were used to consolidate the concrete.

Two specimens were cast, and six sensors were placed in each specimen. The specimens measured 0.8 x 0.8 x 3.7 m (2.5 x 2.5 x 12 ft). The sensors were attached to stirrups with epoxy and plastic zip ties. Figure 4.11 shows a sensor attached to the top of the stirrup in the rebar cage. Figure 4.12 shows a photograph of the team placing the concrete and a photograph of one sensor after a portion of the concrete had been placed.

Figure 4.11 Sensor Attached to the Rebar Cage

Figure 4.12 Placement of Concrete

Locations of the sensors were measured before the concrete was placed, so that they could be easily located and interrogated afterwards (Appendix E). The concrete cover for each sensor was approximately 4 cm (1½ in). Characteristic frequencies for the sensors were measured before the concrete was placed and are summarized in Appendix E.

The sensors were interrogated two weeks after casting with the portable transmitter. Readings were not obtained with the portable transmitter because the concrete cover was too thick. Thus, the phase-gain analyzer was used to interrogate the sensors, and it was successful in reading all twelve sensors. All twelve sensors survived the concrete placement process. Two of the twelve sensors had very faint readings, which was probably because they were moved or tilted during the placement of concrete. Variations of phase angle and impedance for two of the embedded prototype sensors are plotted in Appendix E.

CHAPTER 5
Conclusion

5.1 SUMMARY OF TEST RESULTS

The objective of this thesis was to develop a prototype wireless sensor to detect corrosion in reinforced concrete infrastructure. The inexpensive, durable, and reliable state sensor discussed in this thesis is intended to provide the owner with information about the level of corrosion occurring inside the concrete. The sensors can detect levels of corrosion that can not be observed visually, thereby reducing the cost of the necessary structural repairs.

A sketch of the electrical circuit for the proposed wireless corrosion sensor is in Chapter 1 (Figure 1.4). It consists of an inductor, two capacitors, and a state switch. The sensor resonates at a certain characteristic frequency when the state switch is closed. The state switch (steel wire) was designed so that it corrodes at the same rate as reinforcing steel. When the state switch is broken, the sensor resonates at a different characteristic frequency, indicating that a certain amount of corrosion has occurred.

RF technology was implemented in the prototype sensor design. In Chapter 2, verification of data transmission through concrete is presented. Protected and non-protected EAS tags and 3M^{TM} disc markers were embedded in concrete at different depths and interrogated. The results indicate that the depth of embedment of the sensor affects the magnitude of the variation in phase angle, which is used to identify the characteristic frequency of the sensor. As the thickness of concrete cover increases, the magnitude of the phase shift decreases.

The development of the state switch was presented in Chapter 3. An annealed steel wire was used as the state switch, or "corrosion detector," for the prototype sensor. Annealed steel wire, deformed reinforcement, and prestressing strand were exposed to accelerated corrosion tests in simulated concrete solutions in an attempt to quantify the corrosion rates in the reinforcements and steel wire. The average observed corrosion rates currently fall between 2 and 3 mpy. This series of tests concluded that a smaller wire gauge would take less time to corrode than a thicker wire gauge. Thus, a small gauge wire break would indicate a smaller reduction in cross-sectional area in the reinforcement than a thicker gauge wire break. The wire gauges tested indicate cross-sectional area reductions around 1-3% for the deformed reinforcement. The amount of corrosion that has occurred at this stage is far less than the amount of corrosion required to cause spalling of the concrete, thus the sensor would be able to detect the onset of corrosion in embedded reinforcement.

The design of the prototype sensor was discussed in Chapter 4. Thirty-six sensors were fabricated and embedded in concrete. The prototype sensor consists of two 151-pF capacitors and a copper wire inductor coil, all encapsulated in a petri dish filled with a potting compound, and a steel wire state switch extending outside of that area. The prototype sensors resonate at approximately 6 MHz when the switch is closed and 8 MHz when the switch is open. Testing of the prototype sensor embedded in concrete prisms immersed in salt water and exposed to wet/dry cycles was begun. The concrete mix used for the prisms contained sodium chloride, to accelerate the corrosion process. To date, all 36 sensors are functioning as expected, but none of the state switches has broken.

The durability of the proposed sensor was also discussed in Chapter 4 by exposing the sensors to the normal construction process. Twelve prototype sensors were attached to the reinforcement cages in a large-scale test specimen at

the Ferguson Structural Engineering Laboratory. The sensors were interrogated two weeks after casting, and all sensors survived the construction process. Two of the twelve sensors had very faint readings, and that is probably due to the fact that they were moved or tilted during the placement of the concrete. If sensors are securely attached to rebar, and placement is known, the sensors should have no problem surviving the construction process.

5.2 RECOMMENDATIONS FOR FUTURE WORK

The results of this thesis demonstrate that development and implementation of a wireless corrosion sensor is feasible; however, more research is needed before the sensor can be installed in a structure exposed to deicing salts or a marine environment. To continue the development of the sensor, the following recommendations are proposed:

- Continue the existing accelerated corrosion tests on deformed reinforcement and prestressing strand. Data acquired from these tests should define the distribution of corrosion rates for given sizes of steel wire. Additional tests may be required to define these distributions.
- Continue the exposure tests of the prototype sensors embedded in reinforced concrete prisms. After the sensors indicate that corrosion has occurred, the concrete prisms should be broken apart to determine corrosion rates and reductions in cross-sectional area of the reinforcement. These results should be compared with those from the accelerated corrosion tests.
- Embed prototype sensors in a large-scale specimen that are subjected to continuous loading and wet/dry cycles using ponded salt water.

- Investigate the feasibility of developing of a sensor that provides analog readings of corrosion, as opposed to the threshold detection provided by the prototype sensor.

APPENDIX A
Results from Feasibility Study of RF Technology in Concrete

A.1 EAS TAGS

Measured variations of phase angle and impedance for the protected EAS tags are plotted in this section of Appendix A. Three types of protected sensors (clear packing tape, foam tape, and epoxy-filled petri dish) embedded at three different depths of 2½, 5, and 7½ cm (1, 2, and 3 in.) are presented. Plots for protected tags in air are also presented.

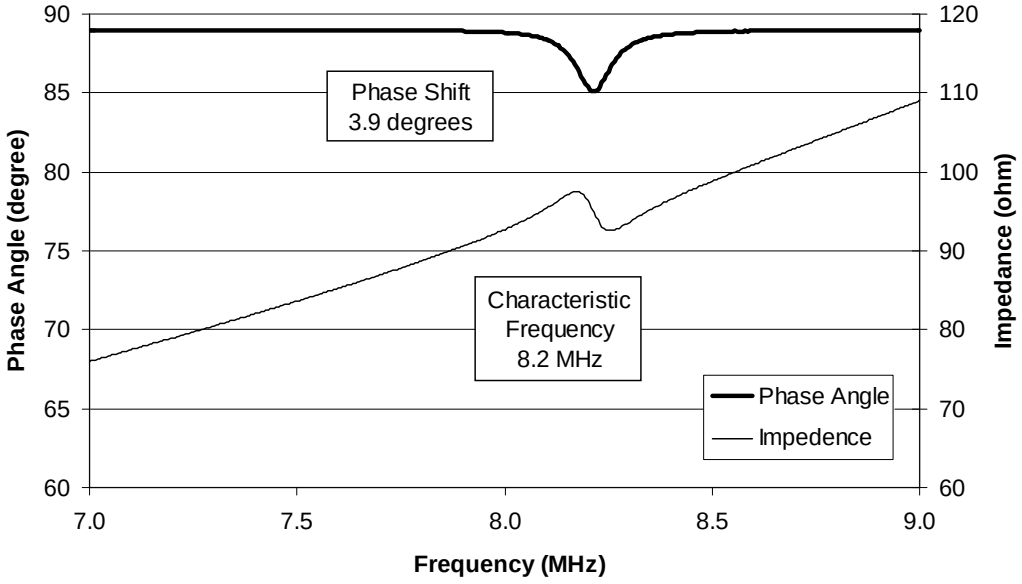

Figure A.1 Bare EAS Tag – Sweep 1

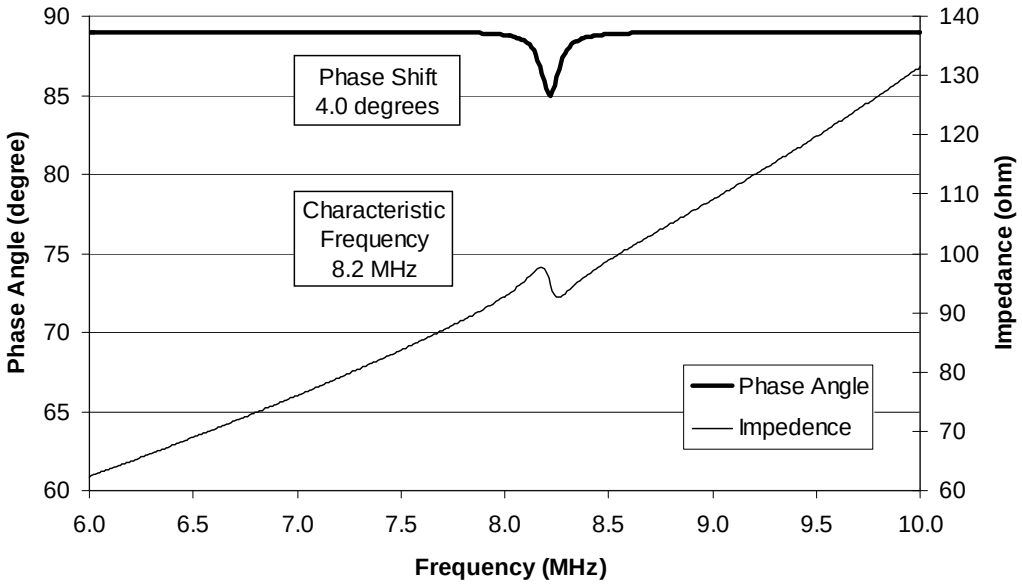

Figure A.2 Bare EAS Tag – Sweep 2

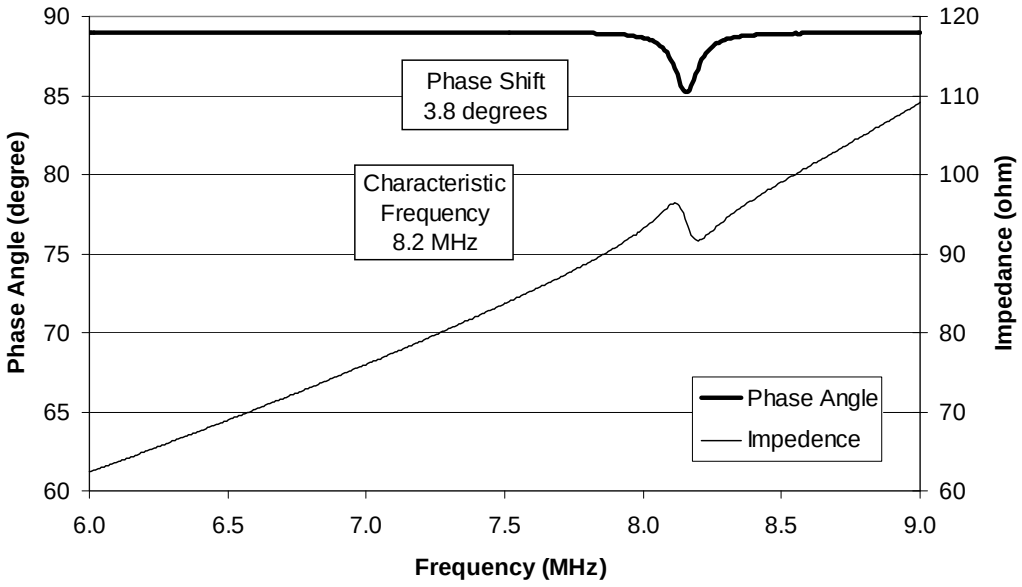

Figure A.3 EAS Tag Protected Using Foam Tape in Air – Sweep 1

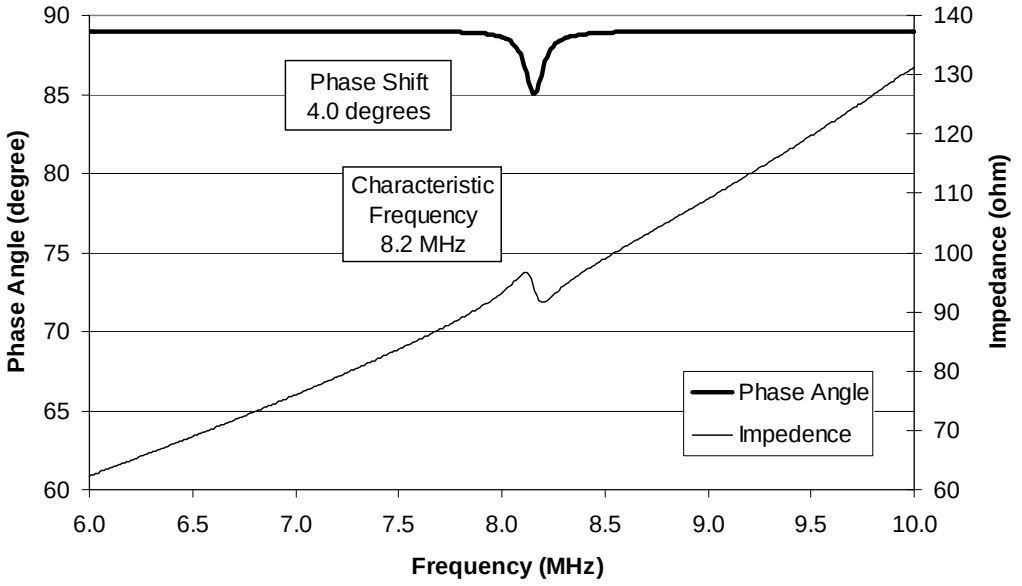

Figure A.4 EAS Tag Protected Using Foam Tape in Air – Sweep 2

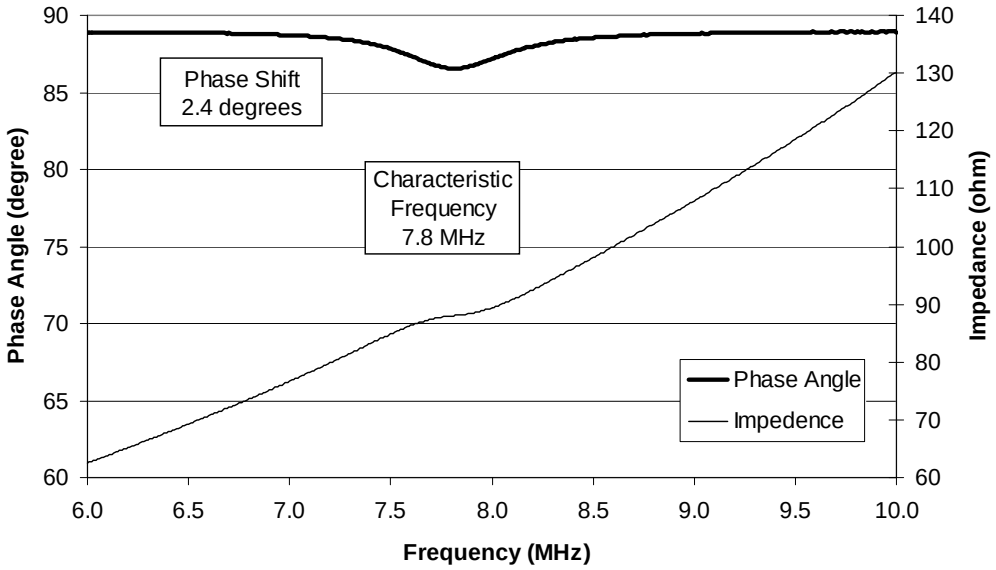

Figure A.5 EAS Tag Protected Using Foam Tape Embedded 2½ cm (1 in.) in Concrete – Sweep 1

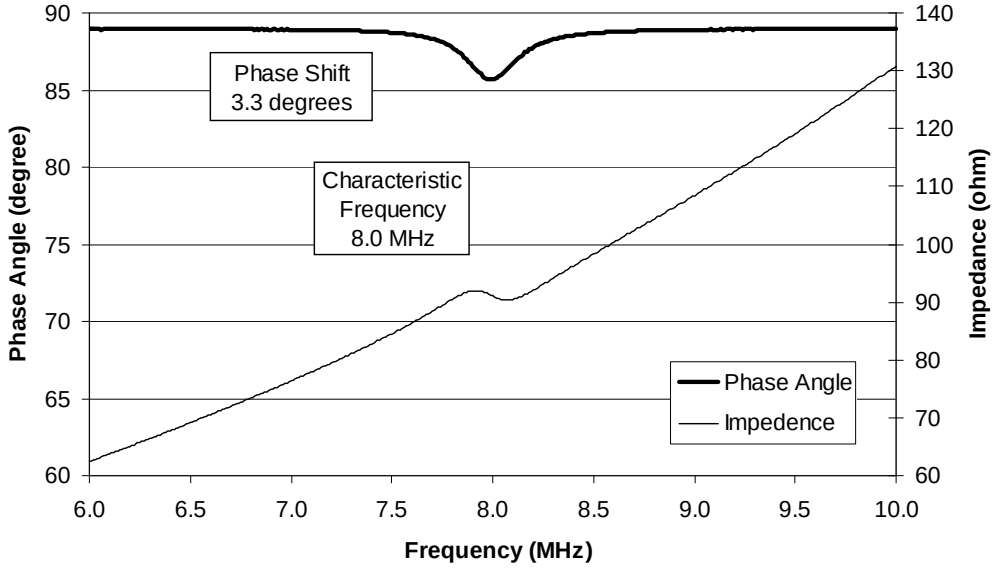

Figure A.6 EAS Tag Protected Using Foam Tape Embedded 2½ cm (1 in.) in Concrete – Sweep 2

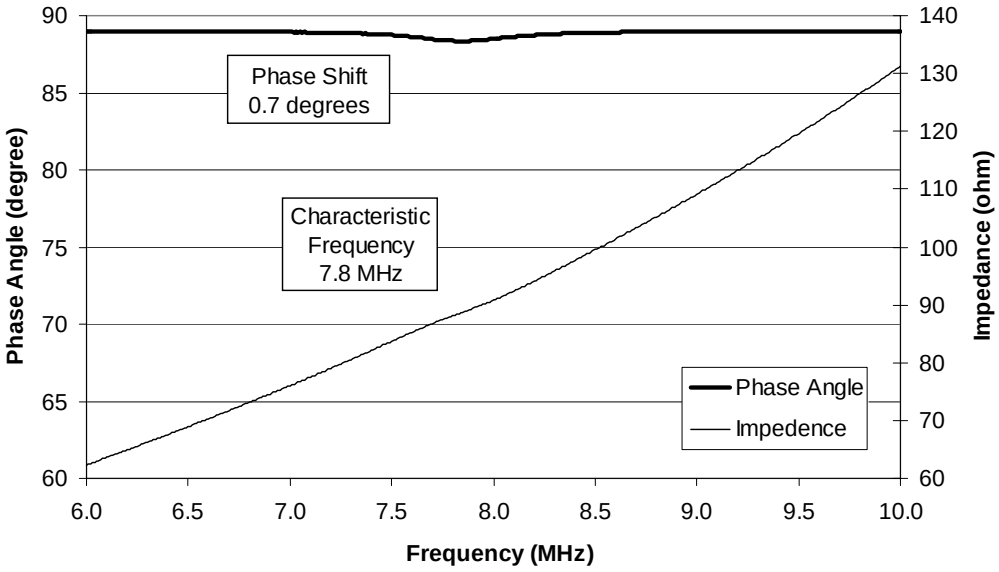

Figure A.7 EAS Tag Protected Using Foam Tape Embedded 5 cm (2 in.) in Concrete – Sweep 1

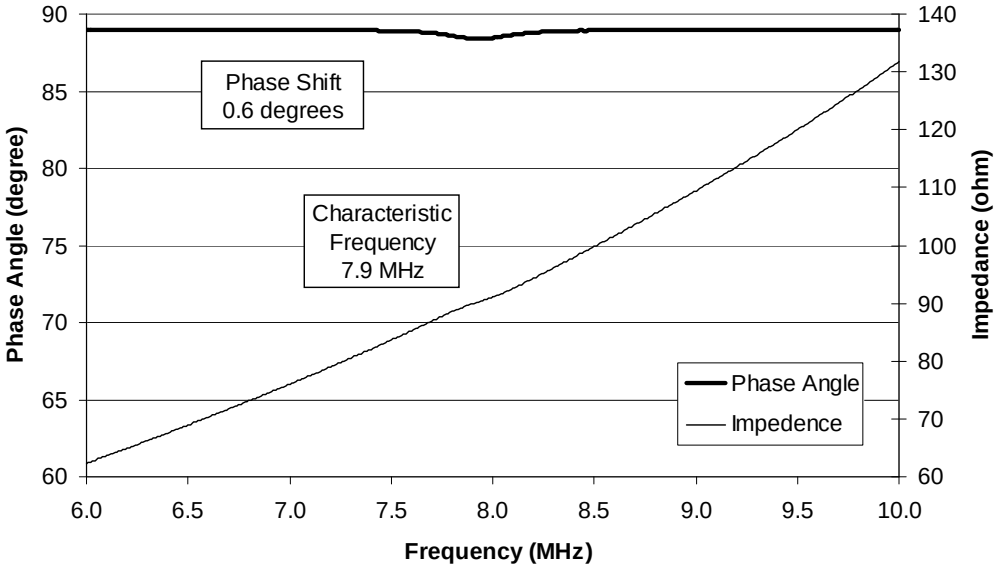

Figure A.8 EAS Tag Protected Using Foam Tape Embedded 5 cm (2 in.) in Concrete – Sweep 2

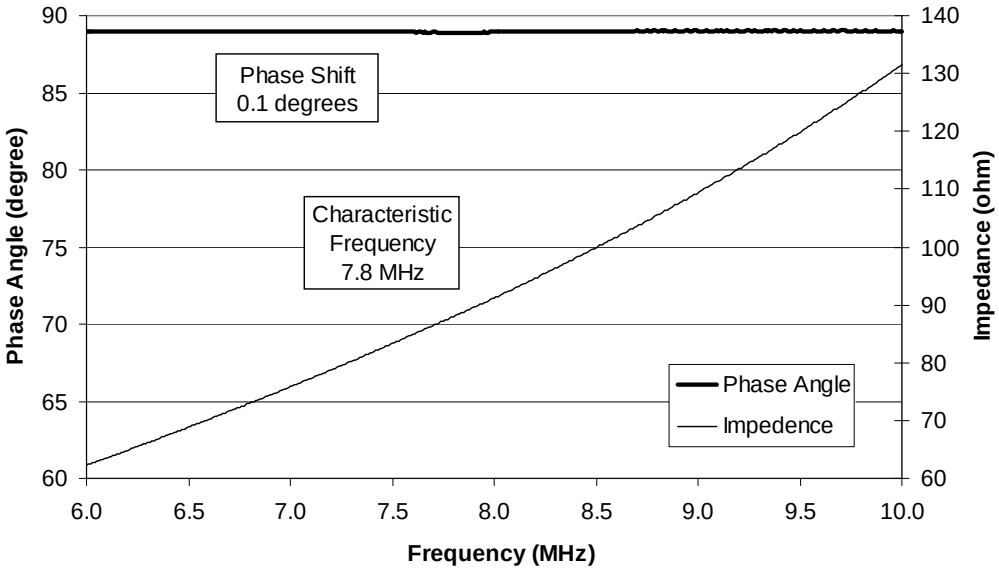

Figure A.9 EAS Tag Protected Using Foam Tape Embedded 7½ cm (3 in.) in Concrete – Sweep 1

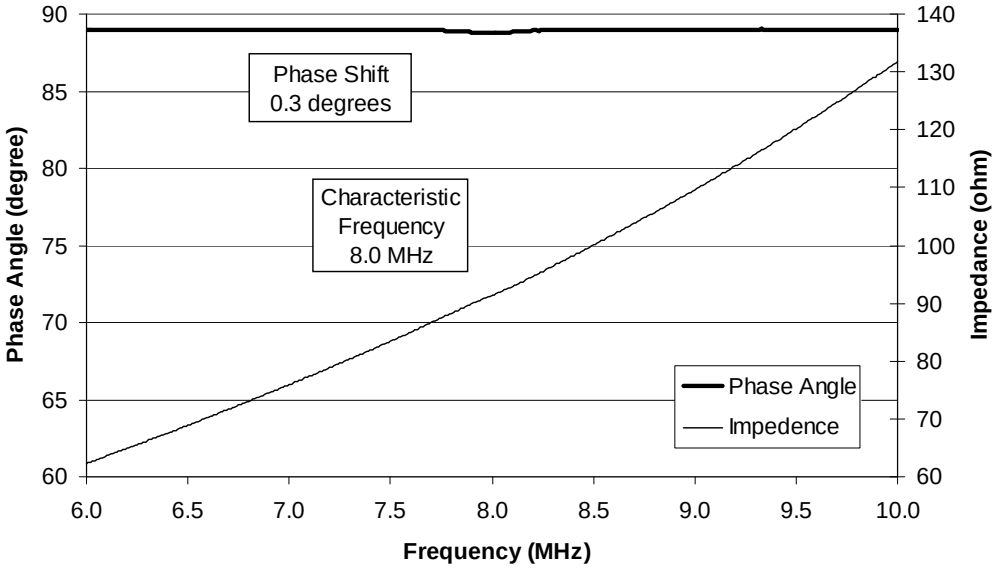

Figure A.10 EAS Tag Protected Using Foam Tape Embedded 7½ cm (3 in.) in Concrete – Sweep 2

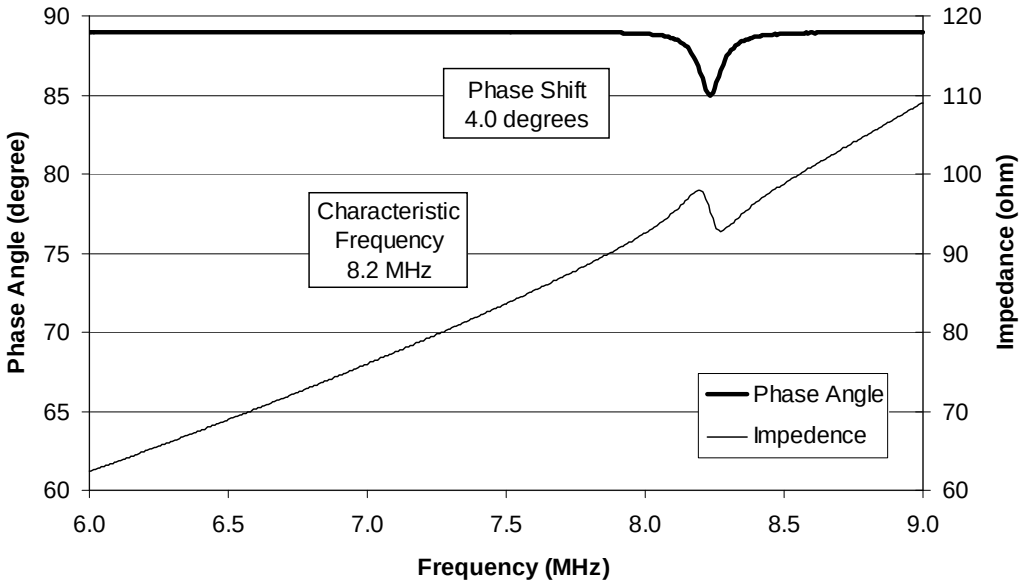

Figure A.11 EAS Tag Protected Using Packing Tape in Air – Sweep 1

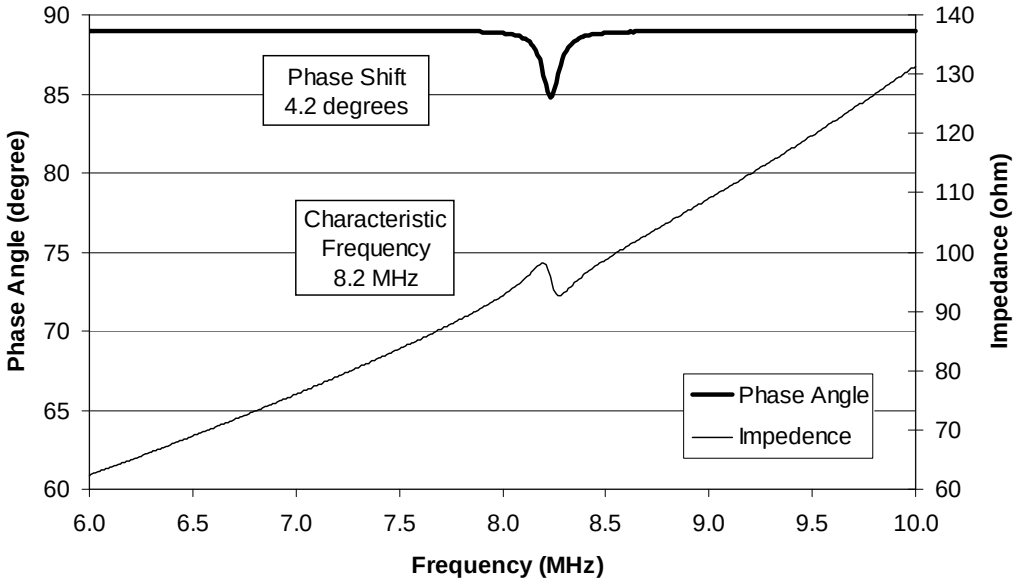

Figure A.12 EAS Tag Protected Using Packing Tape in Air – Sweep 2

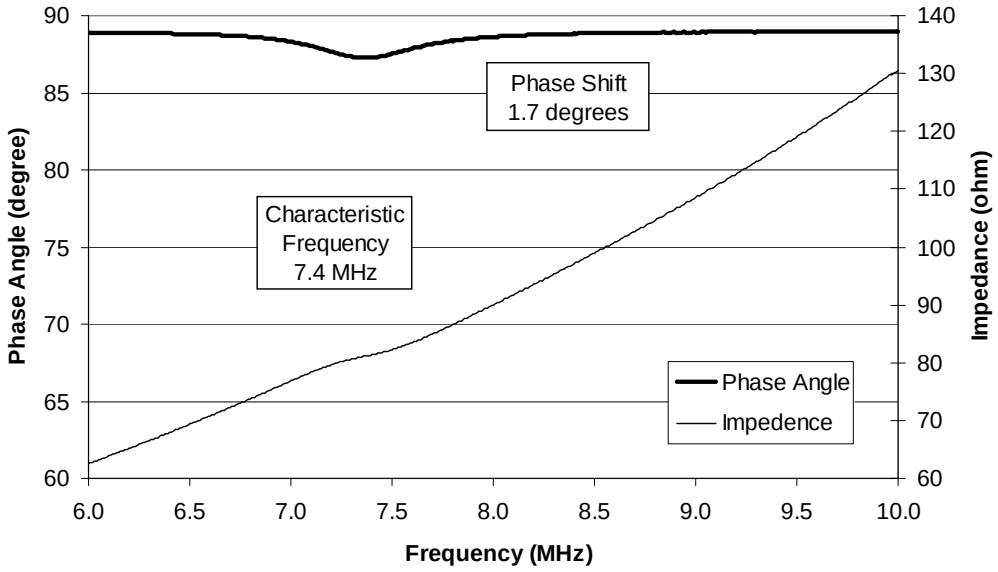

Figure A.13 EAS Tag Protected Using Packing Tape Embedded 2½ cm (1 in.) in Concrete – Sweep 1

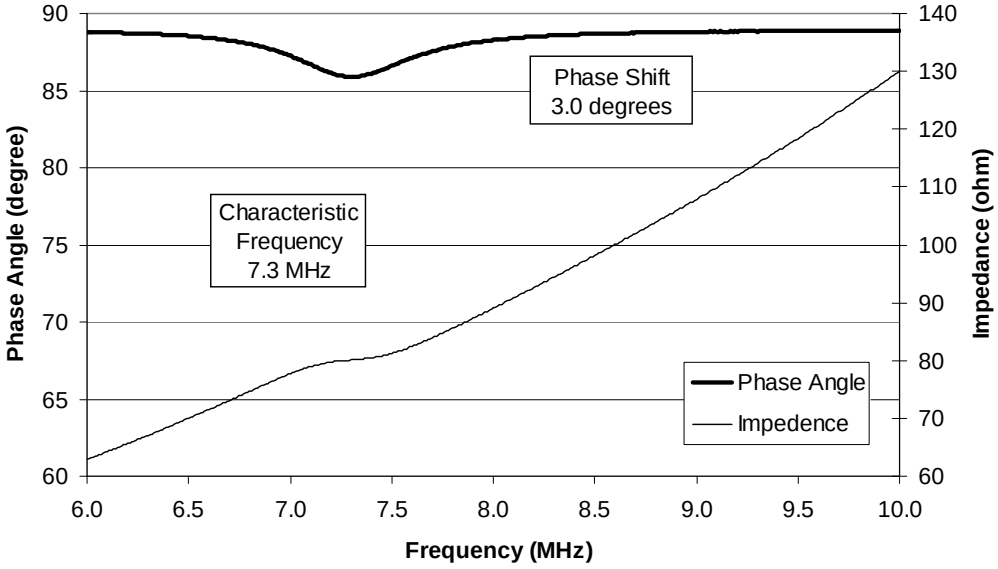

Figure A.14 EAS Tag Protected Using Packing Tape Embedded 2½ cm (1 in.) in Concrete – Sweep 2

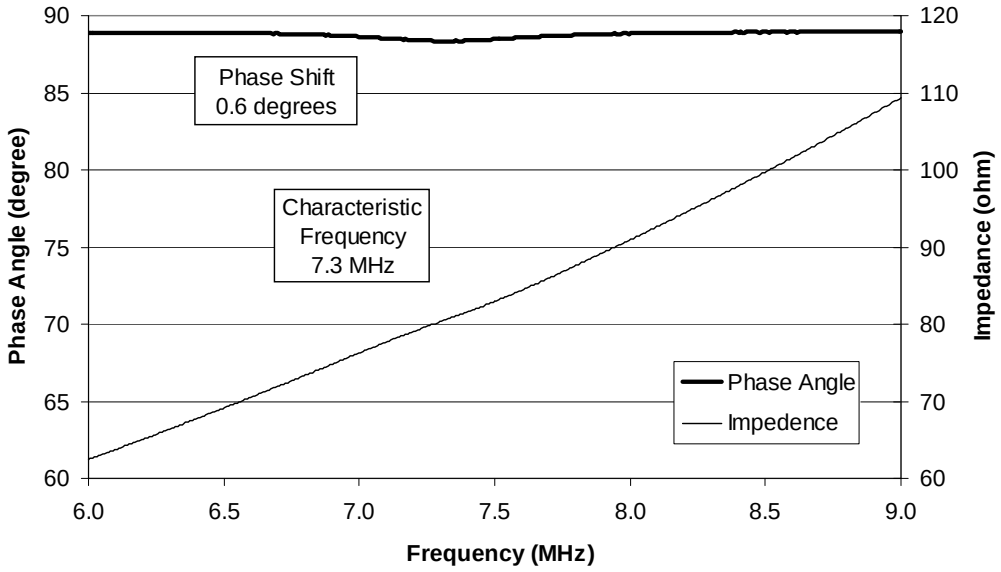

Figure A.15 EAS Tag Protected Using Packing Tape Embedded 5 cm (2 in.) in Concrete – Sweep 1

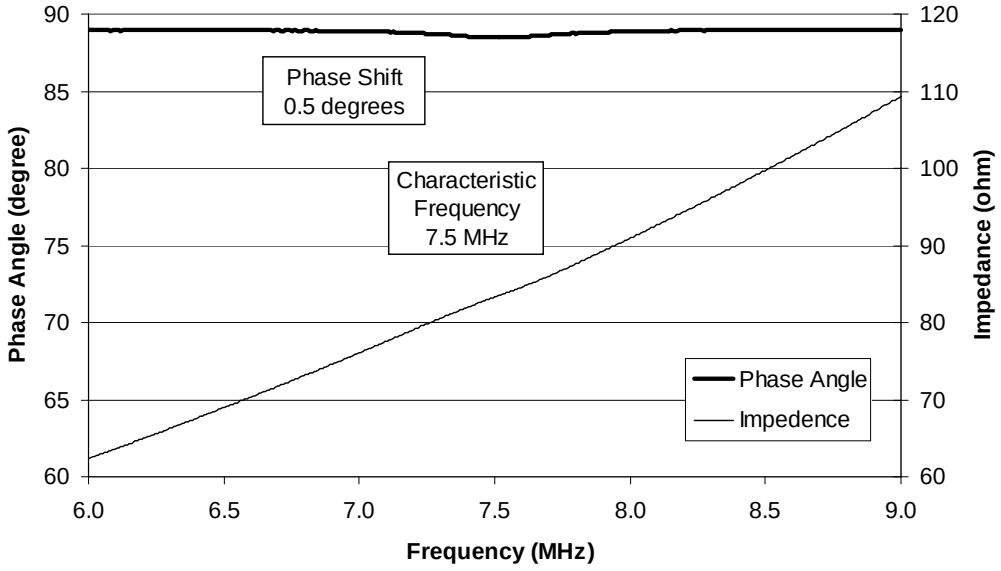

Figure A.16 EAS Tag Protected Using Packing Tape Embedded 5 cm (2 in.) in Concrete – Sweep 2

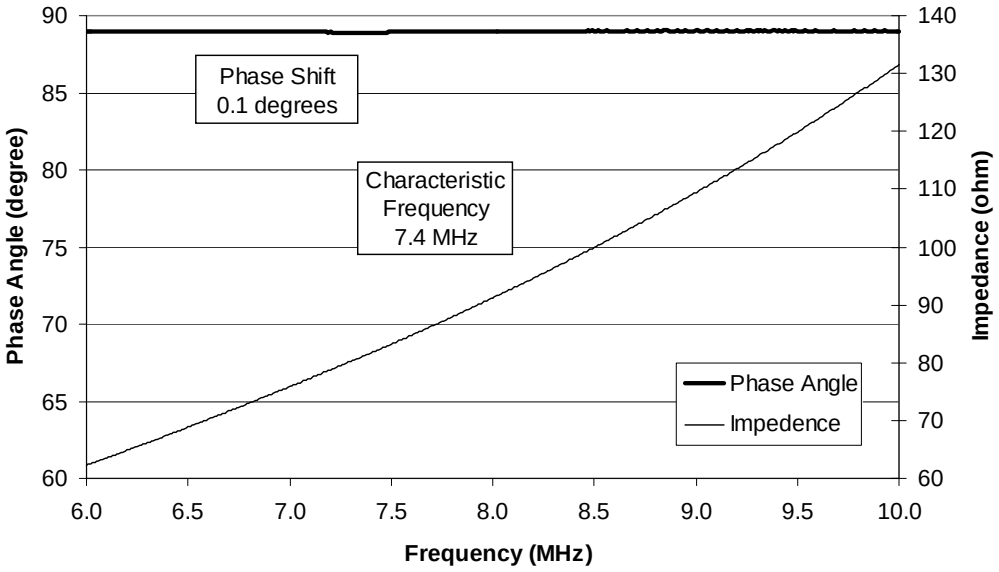

Figure A.17 EAS Tag Protected Using Packing Tape Embedded 7½ cm (3 in.) in Concrete - Sweep 1

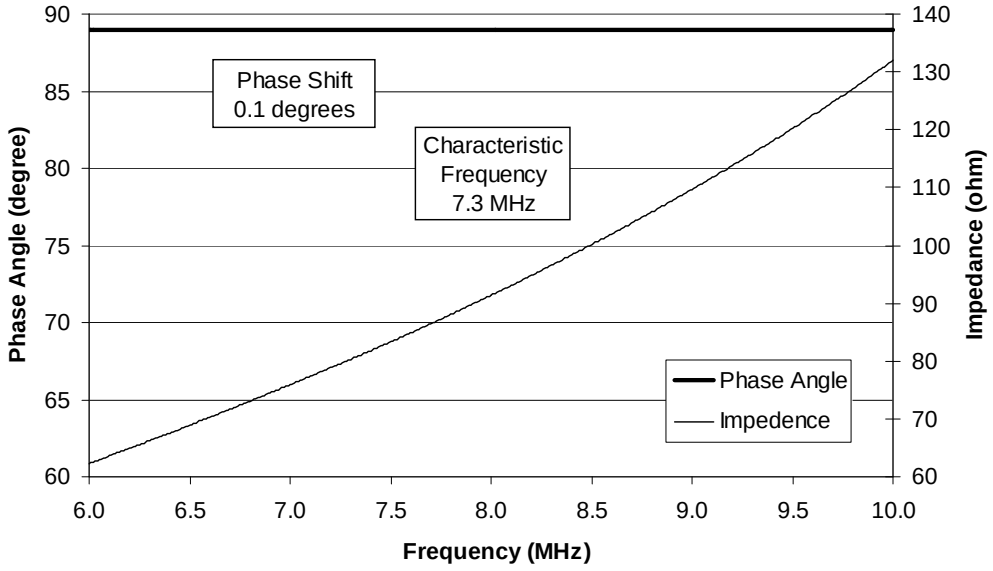

Figure A.18 EAS Tag Protected Using Packing Tape Embedded 7½ cm (3 in.) in Concrete - Sweep 2

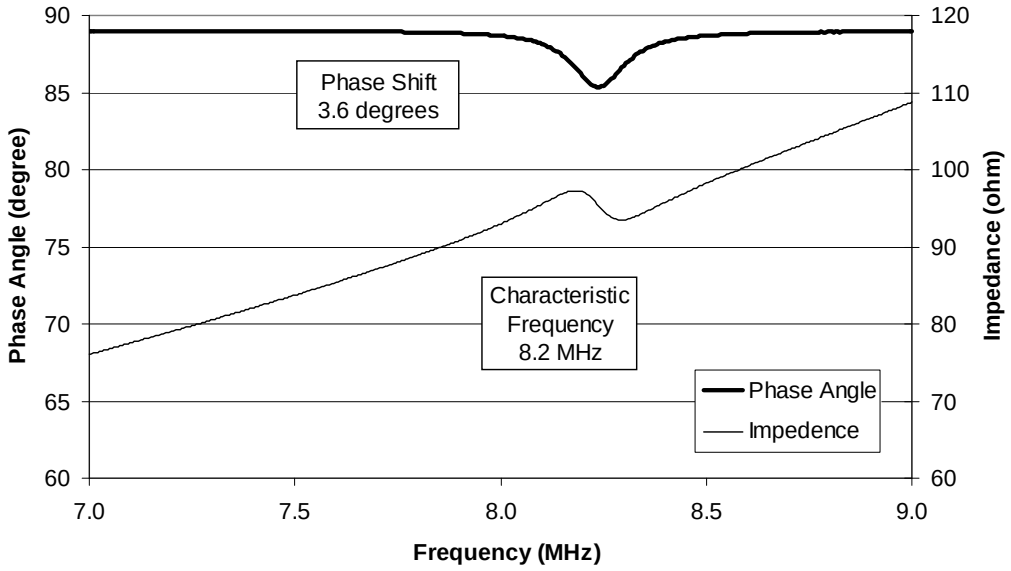

Figure A.19 EAS Tag Protected Using Epoxy-filled Petri Dish in Air - Sweep 1

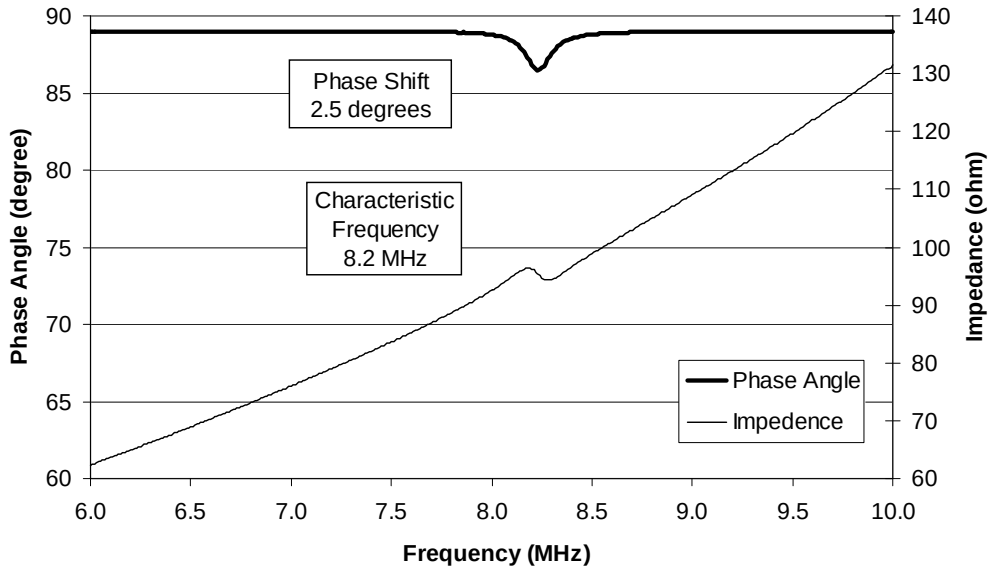

Figure A.20 EAS Tag Protected Using Epoxy-filled Petri Dish in Air - Sweep 2

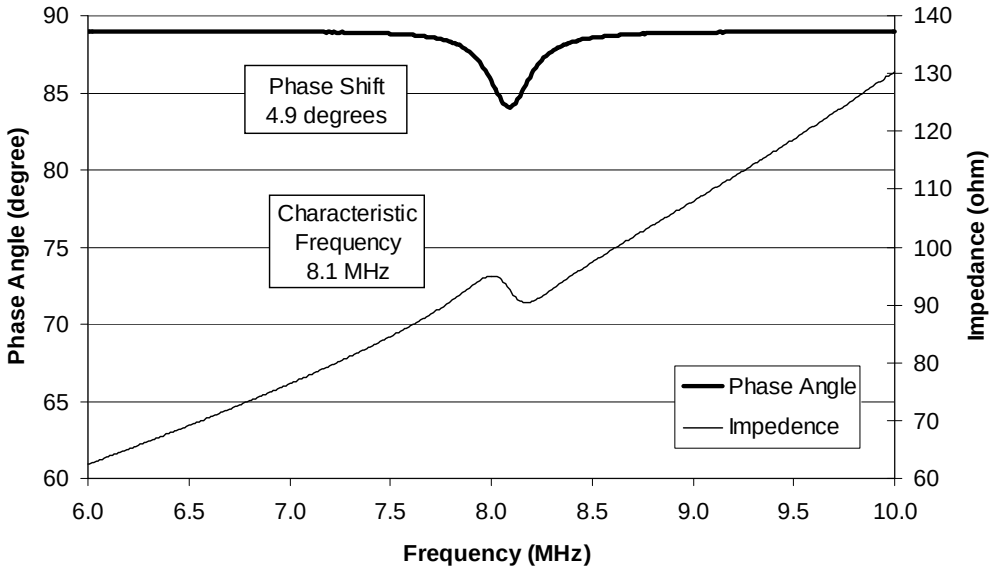

Figure A.21 EAS Tag Protected Using Epoxy-filled Petri Dish Embedded 2½ cm (1 in.) in Concrete - Sweep 1

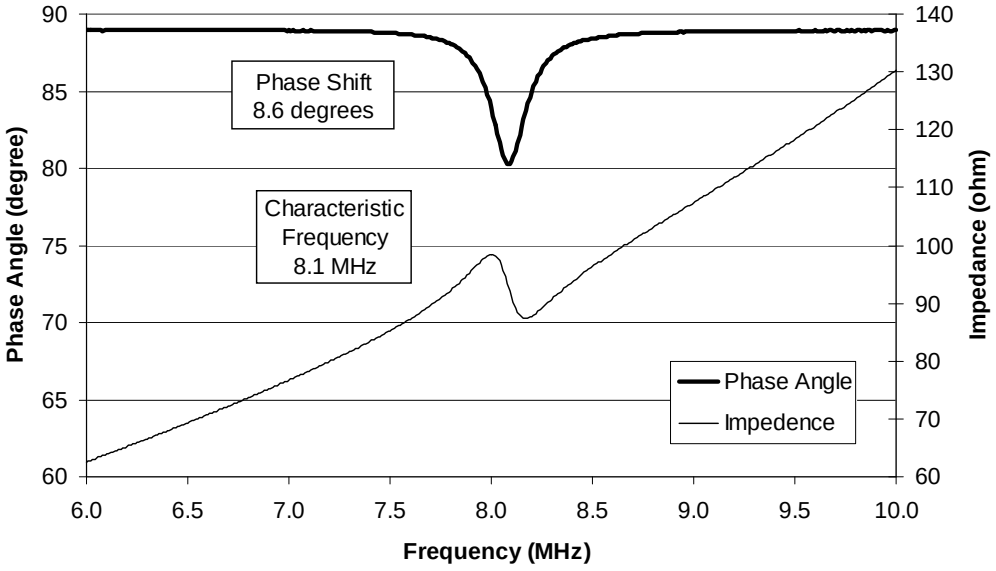

Figure A.22 EAS Tag Protected Using Epoxy-filled Petri Dish Embedded 2½ cm (1 in.) in Concrete - Sweep 2

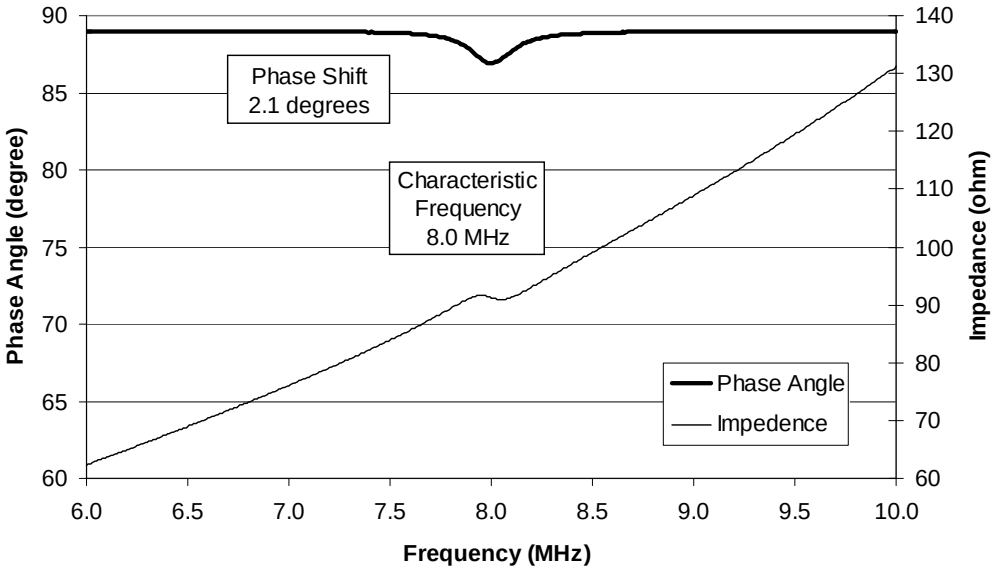

Figure A.23 EAS Tag Protected Using Epoxy-filled Petri Dish Embedded 5 cm (2 in.) in Concrete - Sweep 1

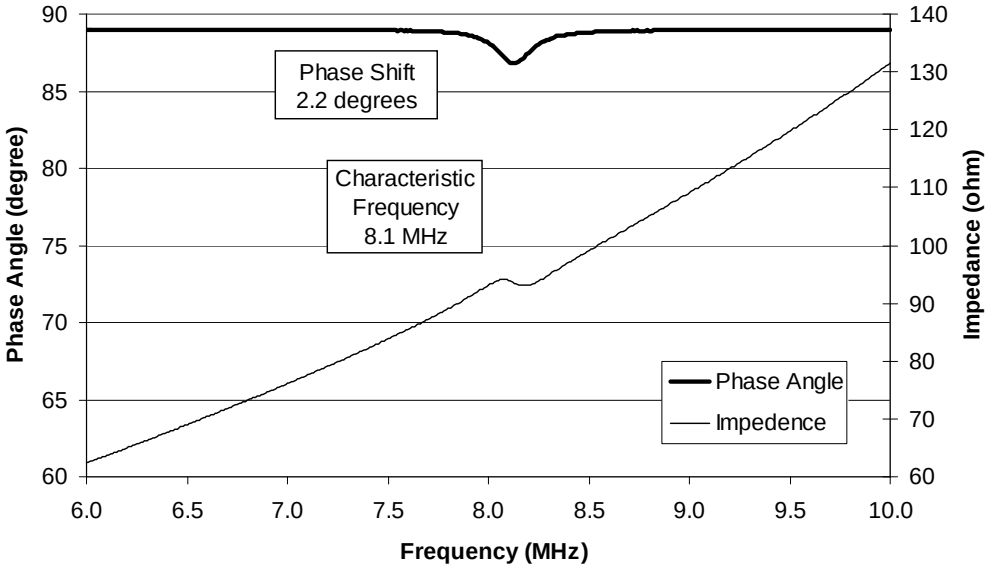

Figure A.24 EAS Tag Protected Using Epoxy-filled Petri Dish Embedded 5 cm (2 in.) in Concrete - Sweep 2

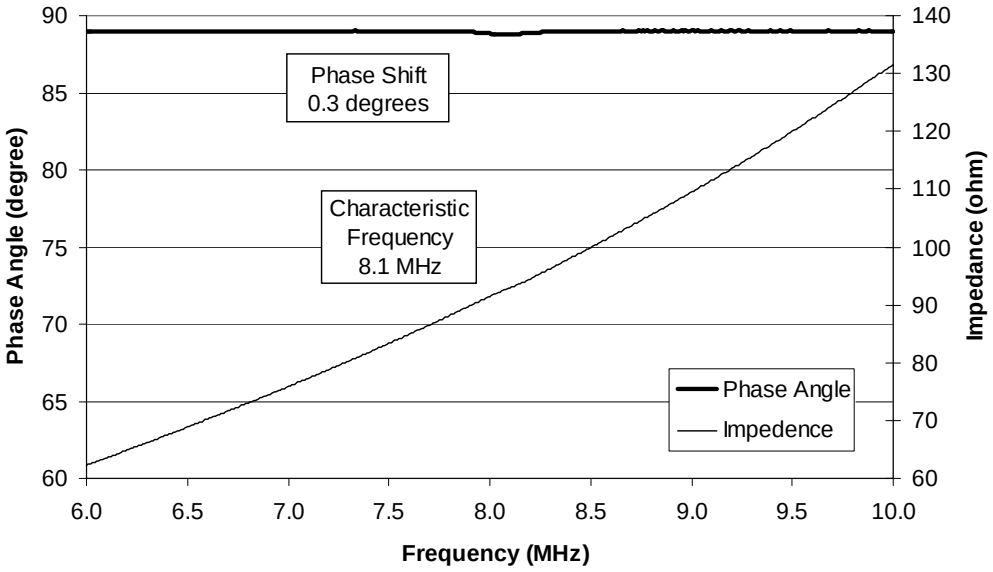

Figure A.25 EAS Tag Protected Using Epoxy-filled Petri Dish Embedded 7½ cm (3 in.) in Concrete - Sweep 1

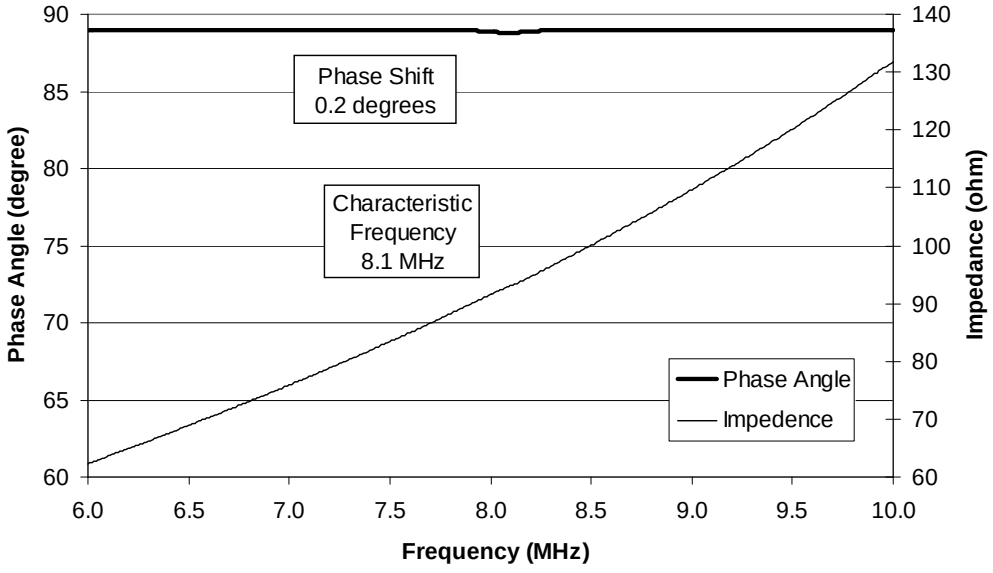

Figure A.26 EAS Tag Protected Using Epoxy-filled Petri Dish Embedded 7½ cm (3 in.) in Concrete - Sweep 2

A.2 3M™ DISC MARKERS

Measured variations of phase angle and impedance for 3M™ Disc Markers embedded in concrete at depths of 2½, 5, and 7½ cm (1, 2, and 3 in.) are plotted in this section of Appendix A.

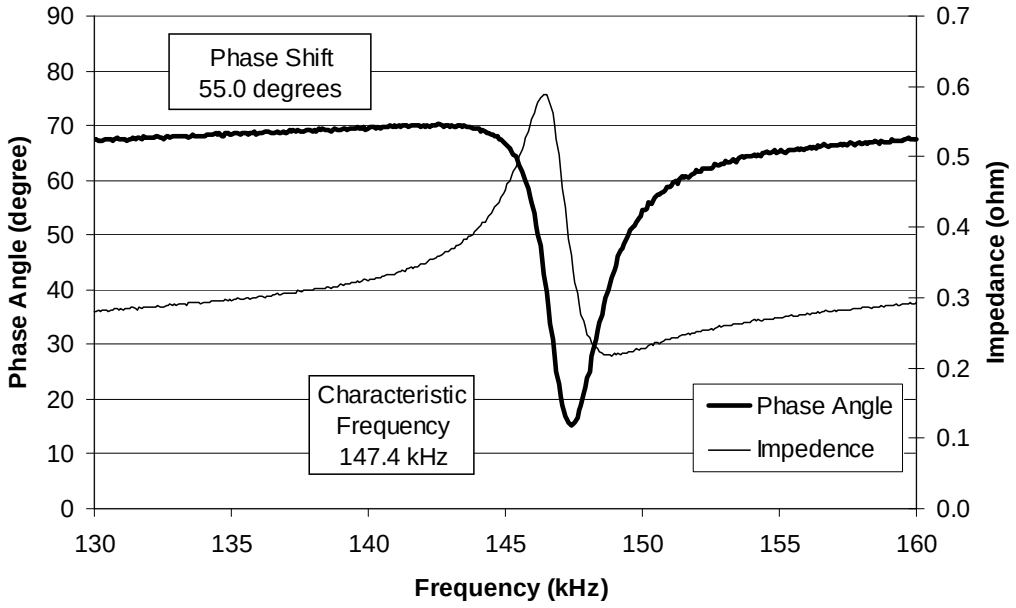

Figure A.27 3M^{TM} Disc Marker in Air – Sweep 1

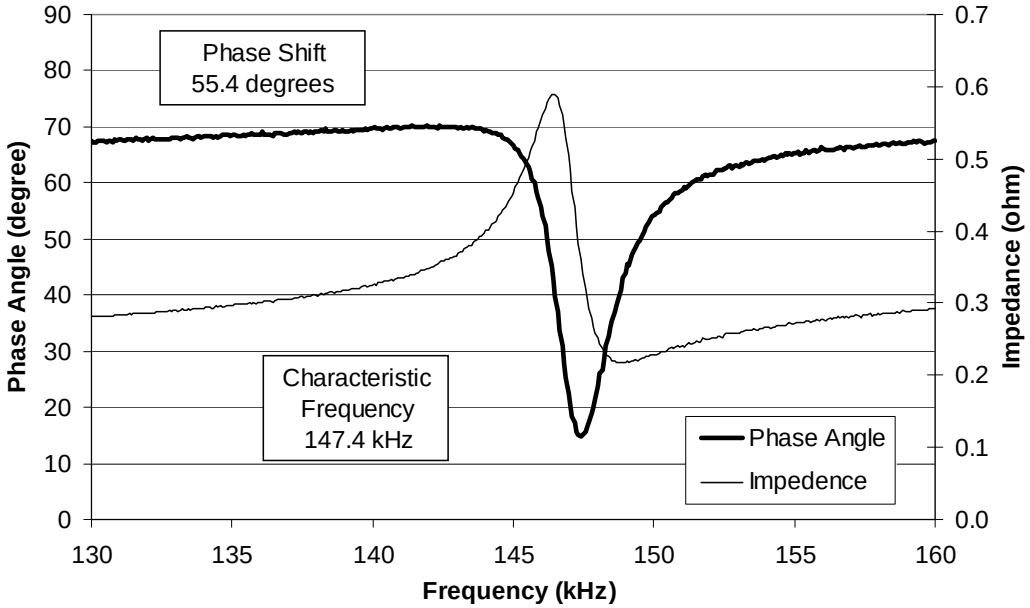

Figure A.28 3M^{TM} Disc Marker in Air – Sweep 2

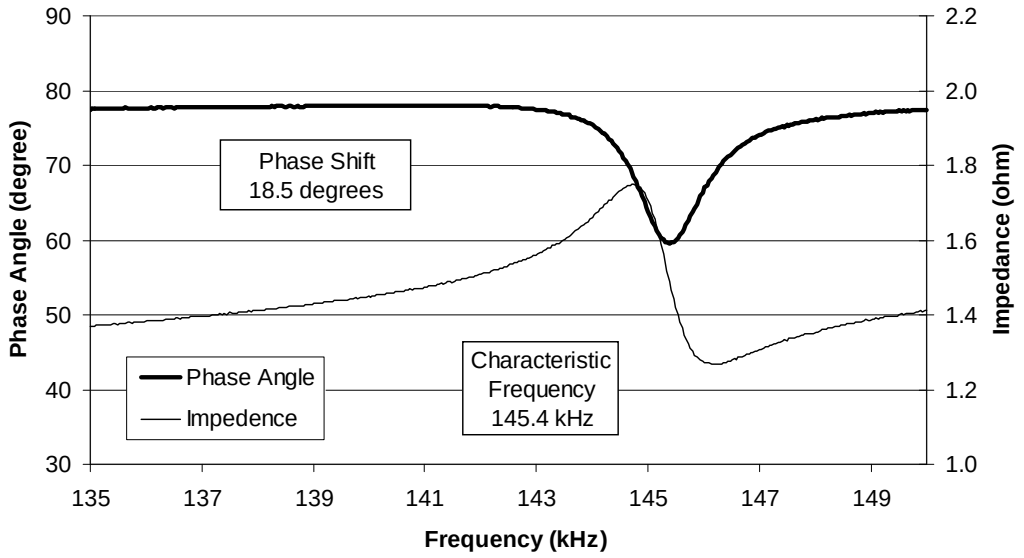

Figure A.29 3M™ Disc Marker Embedded 2½ cm (1 in.) in Concrete – Sweep 1

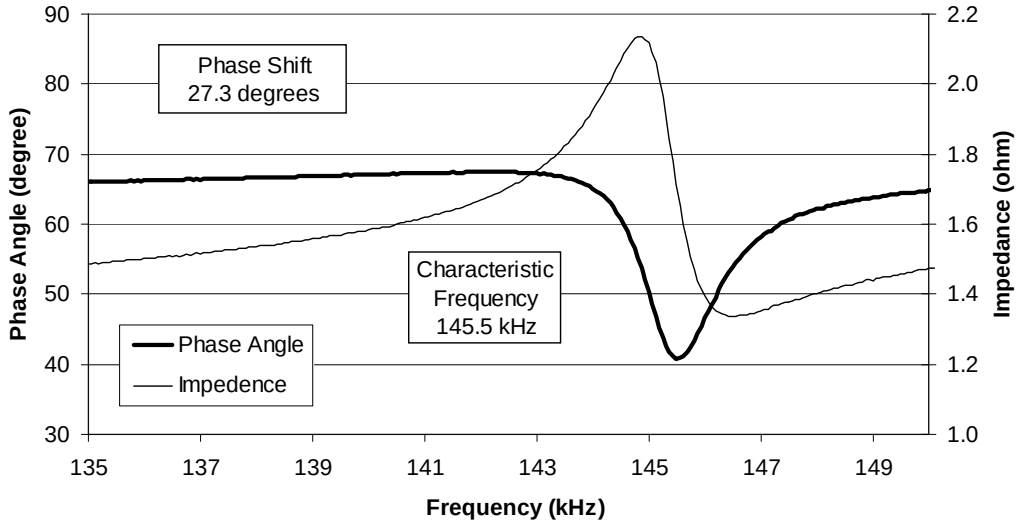

Figure A.30 3M™ Disc Marker Embedded 2½ cm (1 in.) in Concrete – Sweep 2

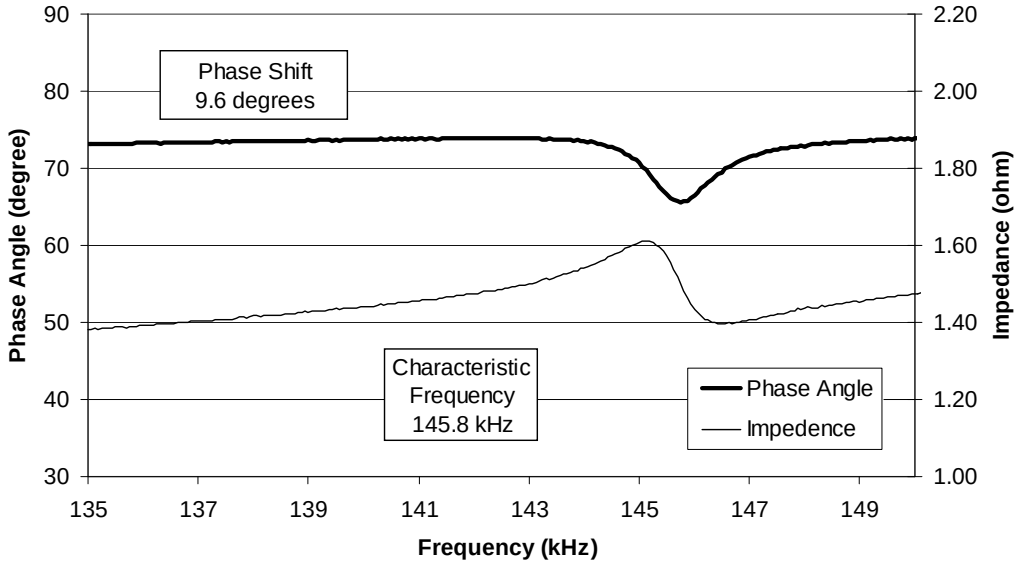

Figure A.31 3M™ Disc Marker Embedded 5 cm (2 in.) in Concrete – Sweep 1

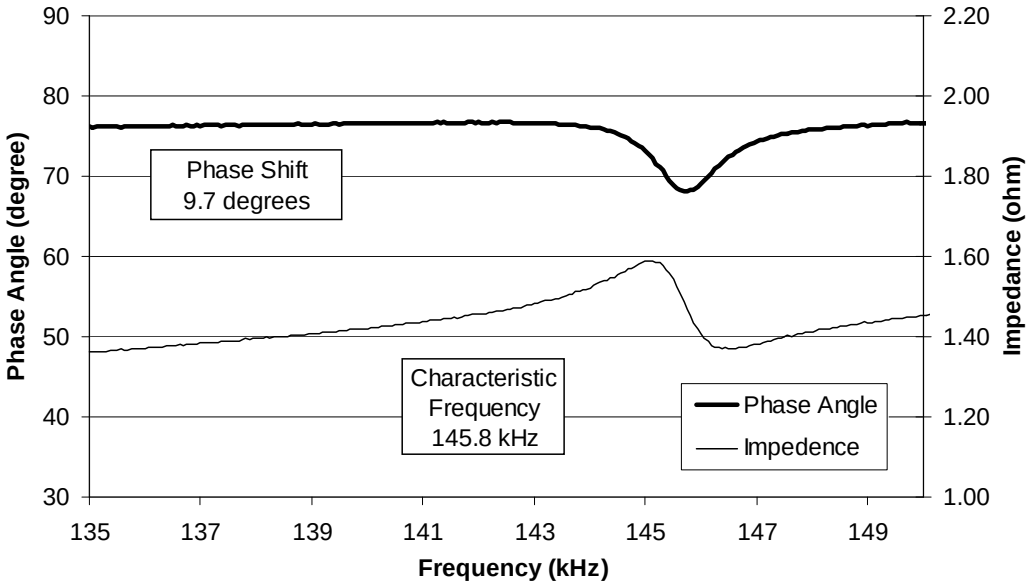

Figure A.32 3M™ Disc Marker Embedded 5 cm (2 in.) in Concrete – Sweep 2

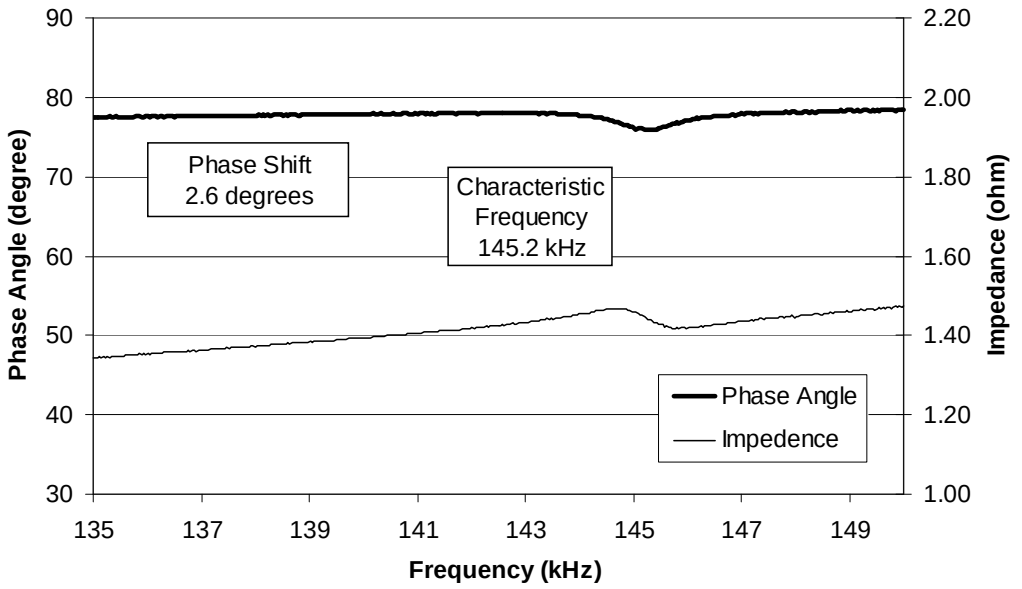

Figure A.33 3M™ Disc Marker Embedded 7½ cm (3 in.) in Concrete – Sweep 1

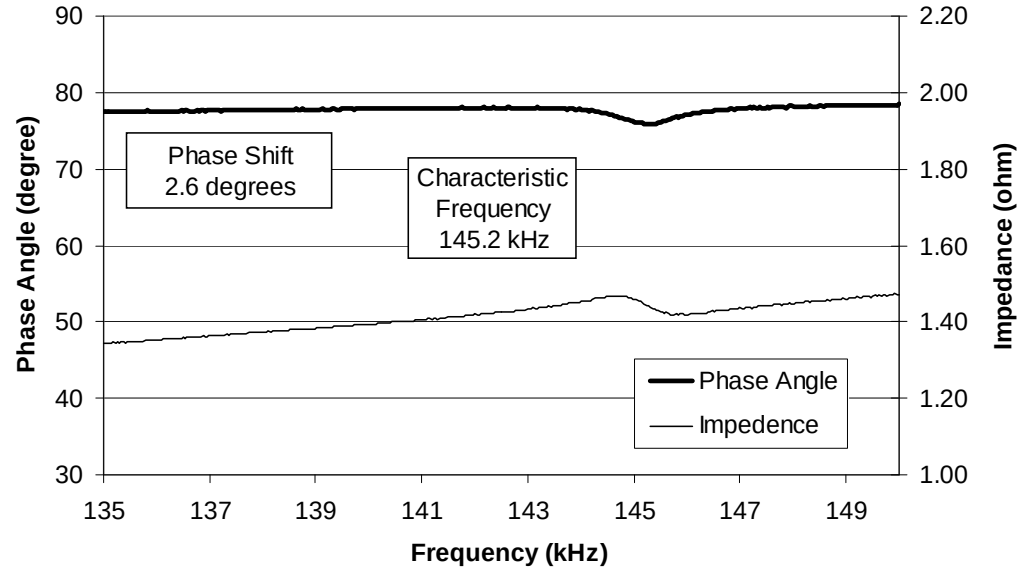

Figure A.34 3M™ Disc Marker Embedded 7½ cm (3 in.) in Concrete – Sweep 2

APPENDIX B

Results from Phase One and Two of Accelerated Corrosion Tests on Steel Wire

B.1 HALF-CELL POTENTIAL READINGS

The half-cell potential readings for bars #13-24 are plotted in Figure B.1 through B.3.

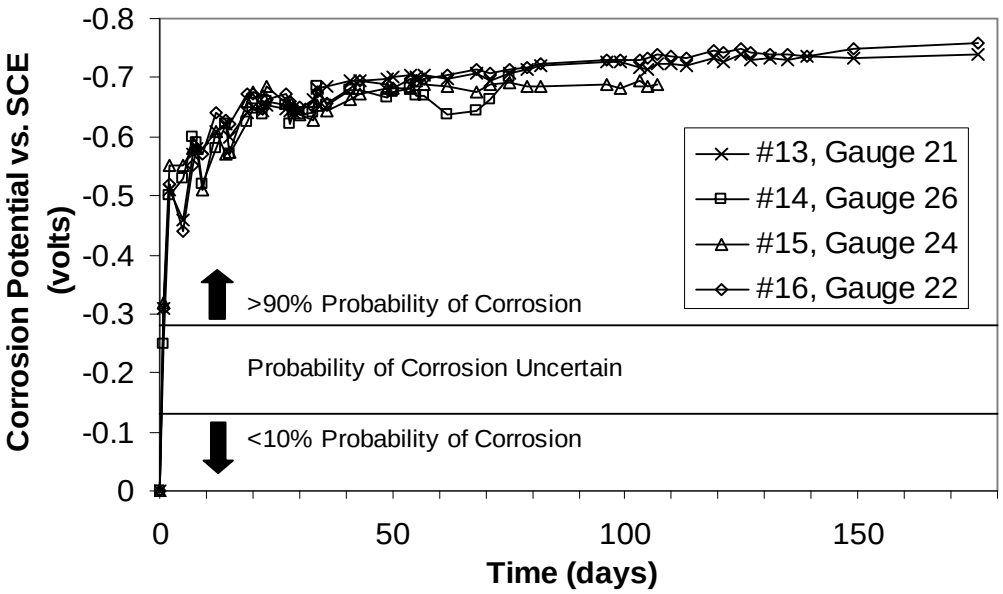

Figure B.1 Corrosion Potential Progress for Bars #13-16 in SCS-C Environment

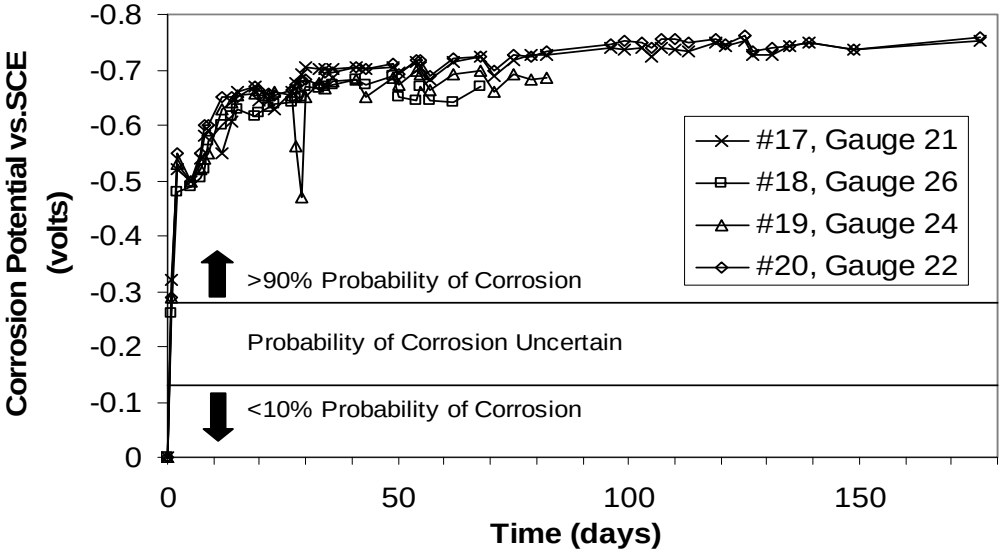

Figure B.2 Corrosion Potential Progress for Bars #17-20 in SCS-W/D Environment

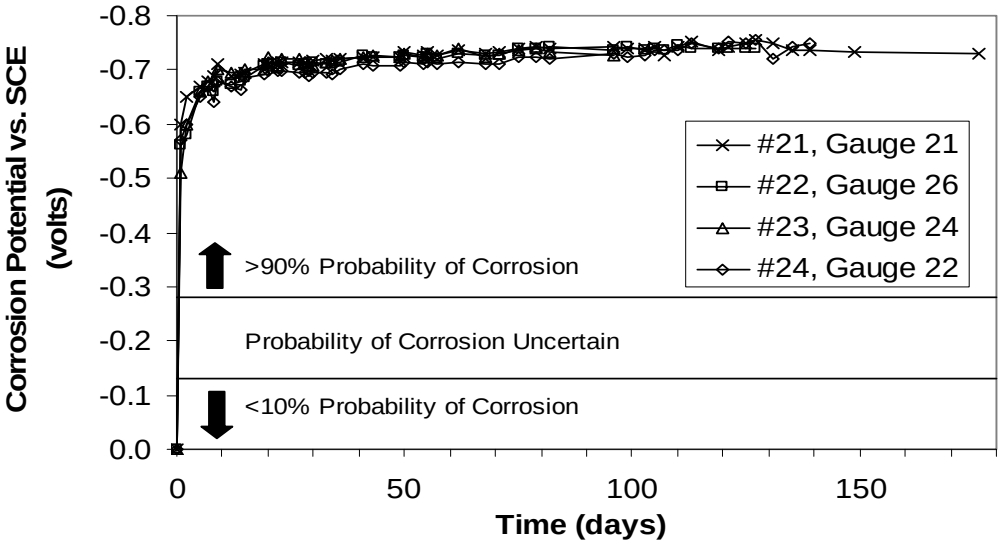

Figure B.3 Corrosion Potential Progress for Bars #21-24 in NaCl-C Environment

B.2 SPECIMEN DATA FROM ACCELERATED CORROSION TESTS

The detailed measurements used to calculate corrosion rate and cross-sectional area reduction are summarized in Table B.1. Both the initial and final diameter measurements listed are averages of three measurements taken along the length of the rebar. The measurements were taken with a micrometer and measured to within 0.001 in. The initial and final weights were measured to within 0.01 g. Surface area calculations for corrosion rate do not include the area of the ends of the rebar, because these areas were covered with epoxy and did not corrode.

Table B.1 Measured Values Used in Determining Corrosion Rate and Cross-Sectional Area Reduction for Each Specimen

Bar #	Length (in)	Diameter		Area		Area Reduction (%)	Density (g/cm^3)	Weight		Weight Loss (mg)	Surface Area (in^2)	Time (hours)	Corrosion Rate (mpy)
		Initial (in)	Final (in)	Initial (in^2)	Final (in^2)			Initial (g)	Final (g)				
2	5.906	0.538	0.537	0.227	0.227	**0.25**	7.87	225.74	225.51	230	9.981	2520	**0.62**
3	5.906	0.563	0.563	0.249	0.249	**0.00**	7.87	227.19	226.71	480	10.439	2904	**1.07**
6	5.906	0.563	0.555	0.249	0.242	**2.59**	7.87	225.45	224.87	580	10.439	1200	**3.14**
7	6.063	0.562	0.558	0.248	0.244	**1.65**	7.87	234.96	233.62	1340	10.711	2304	**3.68**
8	5.827	0.562	0.555	0.248	0.242	**2.29**	7.87	221.70	215.71	5990	10.284	4224	**9.36**
10	6.142	0.539	0.536	0.228	0.226	**0.99**	7.87	233.65	232.25	1400	10.393	2304	**3.97**
11	5.906	0.557	0.556	0.244	0.243	**0.39**	7.87	227.23	225.09	2140	10.335	3576	**3.93**
12	5.945	0.565	0.562	0.250	0.248	**0.82**	7.87	227.13	226.08	1050	10.546	3240	**2.09**
14	6.299	0.563	0.558	0.249	0.245	**1.77**	7.87	243.49	243.20	290	11.148	1896	**0.93**
15	5.787	0.536	0.535	0.226	0.225	**0.37**	7.87	220.87	220.51	360	9.751	2640	**0.95**
17	5.591	0.542	0.535	0.231	0.225	**2.61**	7.87	212.40	209.37	3030	9.521	4608	**4.69**
18	5.866	0.558	0.557	0.244	0.244	**0.24**	7.87	225.41	224.23	1180	10.277	1704	**4.57**
19	5.866	0.552	0.546	0.239	0.234	**2.16**	7.87	225.93	224.37	1560	10.173	2304	**4.52**
22	5.945	0.560	0.559	0.246	0.246	**0.24**	7.87	228.35	227.31	1040	10.459	3240	**2.08**
23	5.866	0.566	0.559	0.251	0.246	**2.23**	7.87	221.51	220.46	1050	10.425	2472	**2.76**
24	5.709	0.544	0.539	0.233	0.228	**2.01**	7.87	217.55	215.23	2320	9.765	3576	**4.51**
25	5.984	0.598	0.595	0.281	0.278	**1.11**	7.87	225.00	224.57	430	11.242	1128	**2.30**
26	5.866	0.597	0.597	0.280	0.280	**0.11**	7.87	224.10	223.56	540	11.002	1560	**2.13**

APPENDIX C
Fabrication of Prototype Wireless Corrosion Sensor

C.1 Materials Needed for Fabrication Process

All materials and tools needed for the fabrication of the prototype wireless corrosion sensor were inexpensive and also easily attainable. Both sensor configurations, exposed and circumferential loop, required the same materials and tools.

The electrical components needed for a complete circuit in the wireless sensor were two capacitors, an inductor, and a switch. The capacitors used in the prototype sensor had a capacitance of 151 pF (picofarads) with copper, tinned leads. The tinned leads allowed for easy soldering. The capacitors can be purchased at most electronics supply stores. Two types of 151-pF capacitors are shown in Figure C.1. The inductor was a coil made up of No. 24 gauge plain enamel-coated copper wire which can also be purchased at most electronics supply stores. The material used for the switch was annealed steel wire. In the prototype sensors, gauges 24 and 26 of the dark-annealed steel wire were used. The measured average diameters of the gauge 24 and 26 wires were 0.559 mm (0.022 in.) and 0.432 mm (0.017 in.), respectively.

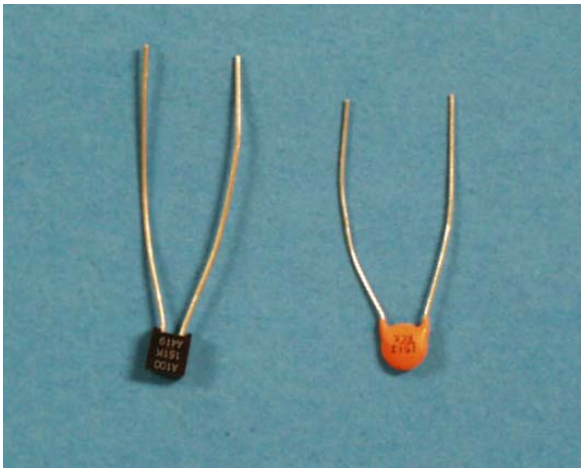

Figure C.1. Typical 151-pF Capacitors Used in Prototype Sensor

In addition to the electrical components, several non-electrical components were needed to aid in the fabrication of and also to protect the complete wireless sensor. Those components were a PVC pipe, a petri dish, an electrical potting compound, and solder. A thin slice of a 4-cm (1½-in.) PVC pipe was used as a sturdy, cylindrical object around which the coil was wound; it also aided in holding the coil in tact. A petri dish with a 5-cm (2-in.) diameter and 8.5-mm (0.33-in.) height and tight lid was used to enclose and protect the electrical circuit. The petri dish created a protected sensor area, where the contents were protected from the surrounding environment or concrete. Only one part of the circuit, the steel wire, extended outside of the protected sensor area so that it could corrode in the surrounding environment. Petri dishes can be purchased from most biology supply stores. General Electric® Silicone RTV615A was used as a potting compound in the petri dish to protect the electrical circuit from the environment under which it will be exposed. Two types of solder were needed: tin solder and silver solder and flux.

Access to some tools was needed for fabrication of the sensor. Those included a circular saw, a hand-held drill, a hot glue gun, a soldering iron, and a voltmeter.

C.2 WINDING THE COIL

The first step in the fabrication process was preparing the PVC pipe around which the coil of copper wire would be wrapped. The PVC pipe was cut using a circular saw into slices approximately 8 mm (5/16 in.) thick. Then four holes were drilled into the pipe with a No. 56-bit (1.17-mm, 0.046-in. diameter). These holes provided access for both the copper wire from the coil and the steel wire from the switch to pass through the pipe. One pair of holes was drilled towards the top of the PVC slice for the steel wire access. One of the holes for the copper wire access was drilled near the top of the slice, and one was drilled near the bottom. The pairs of holes were diametrically opposed (Figure C.2).

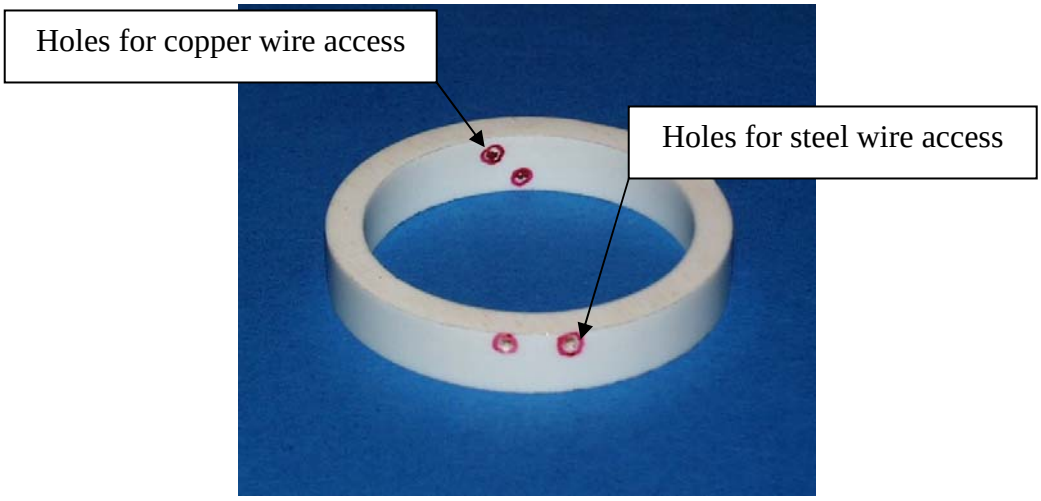

Figure C.2. Half-inch Wide PVC Pipe with Drilled Hole Layout

Next, the No. 24 gauge plain enamel-coated copper wire was wound around the prepared PVC pipe. For fabrication of the five-turn coil,

approximately 71 cm (28 in.) of the copper wire was needed. Approximately 2½ – 4 cm (1-1½ in.) of wire was inserted through one of the copper wire access holes to the inside of the pipe, and then the wire was wound tightly and closely spaced around the circumference of the pipe section five times. Special care was taken to ensure that rounds of the wire did not cross. If the coating was damaged during installation, and the wires were crossed, the circuit would not work properly. Upon completion of winding five times, another 2½ – 4 cm (1-1½ in.) of wire was inserted through the remaining copper wire access hole. Last, to ensure that the wire stayed in place, a small layer of hot glue was applied across the coil in three places around the circumference of the pipe: one covering the two copper wire access holes and the other two at third points around the circumference. Figure C.3 shows where the hot glue was applied. The lengths of wire extending on the inside of the pipe were used for soldering. Figure C.4 shows a top view of the completed coil and wires extending on the inside of the pipe section. While winding the wire, special care was taken to ensure that the steel wire access holes were not obstructed (Figure 4.5).

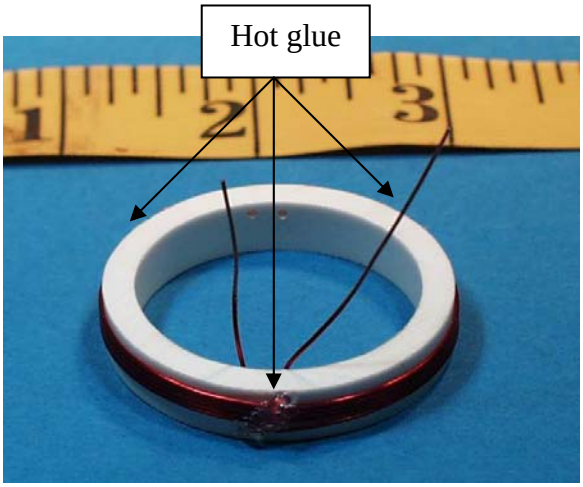

Figure C.3. Wound Coil Hot Glued at Three Points

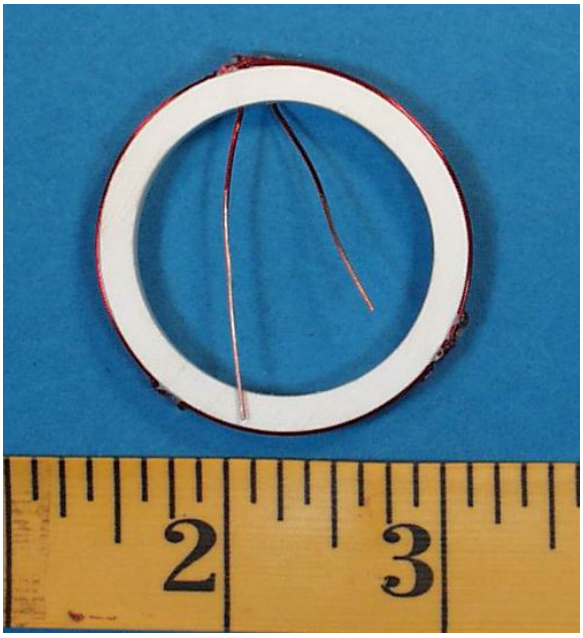

Figure C.4. Top View of Coil and Wires Extending to Inside of Pipe Section

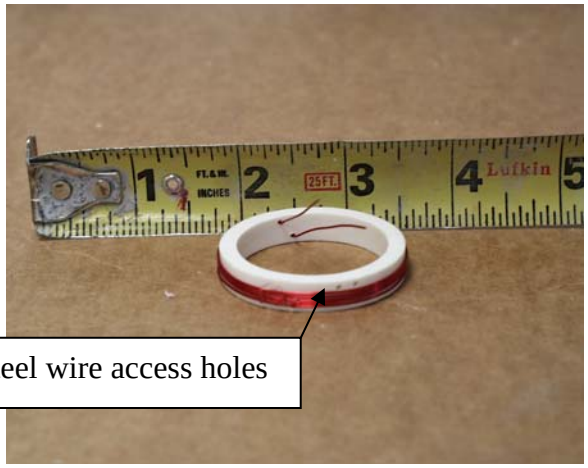

Figure C.5. Steel wire Access Holes Not Obstructed by Wound Coil

C.3 PREPARING CONNECTIONS FOR SOLDERING

After the coil was complete, the next step was to prepare the copper wire, steel wire, and capacitors for soldering. A steel wire, or state switch, was cut to size depending on which sensor configuration was going to be used: exposed loop or circumferential loop. The exposed loop configuration consists of a steel wire extending outside of the protected sensor area in a loop formation. The circumferential loop configuration consists of a steel wire extending outside of the protected sensor area and wrapping around the circumference of the petri dish. The advantages and disadvantages of each configuration are discussed in Chapter 3. Examples of the exposed- and circumferential loop configurations are shown in Figures C.6 and C.7, respectively. The sections of steel wire cut for the exposed loop configuration were 8 cm (3 in.) long, and the sections cut for the circumferential loop configuration were 20-cm (8-in.) long.

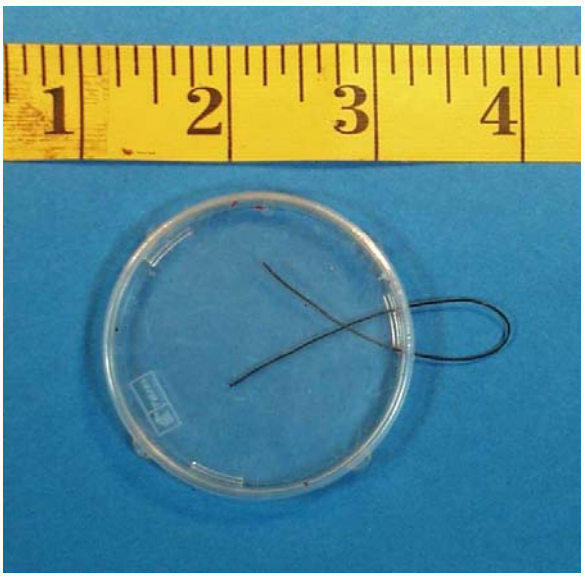

Figure C.6. Exposed Loop Configuration Option

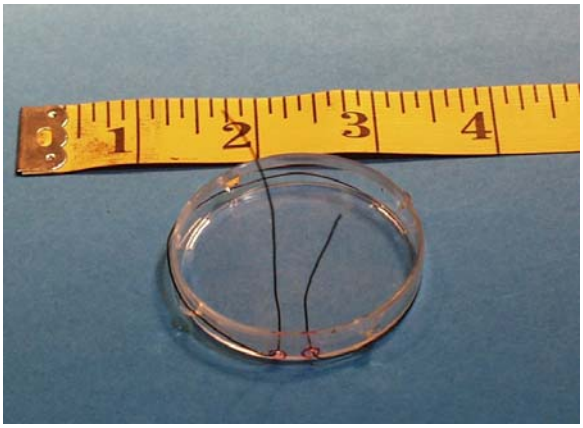

Figure C.7. Circumferential Loop Configuration Option

Next, all the electrical components (two capacitors, copper wire extending inside the PVC pipe, and steel wire state switch extending inside the enclosure) were trimmed so that they all fit inside the PVC pipe. Figure C.8 provides a diagram of the layout of the sensor components. This was used as a guide to determine the proper length of lead wires for each component so that they were long enough for a good soldering connection, yet still short enough to fit inside the PVC pipe.

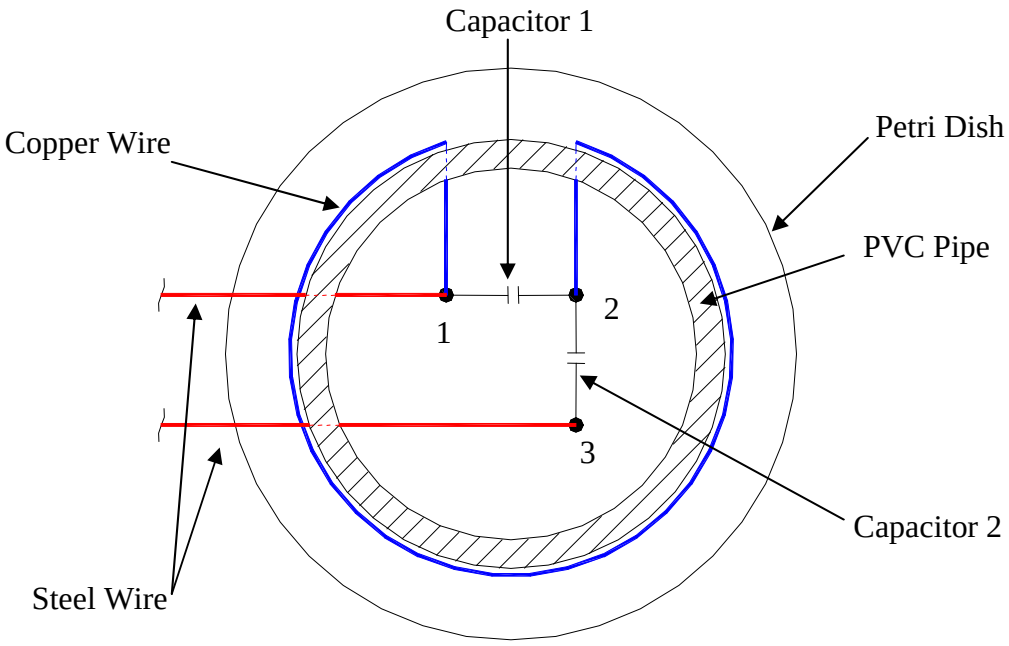

Figure C.8. Diagram of Approximate Sensor Component Location

Last, the surfaces of some of the wires had to be scraped in order to have a clean surface for a good solder connection. The wire leads extending from the capacitors came already cleaned and tinned, so no preparation besides the trimming was needed. The enamel on the copper wire leads was removed using a razor blade. Only the length needed for soldering, approximately 1 cm (½ in.), was cleaned. Special care was taken to ensure that the cleaned section did not extend outside the PVC pipe. A similar action was taken with the steel wire to remove the mill scale.

C.4 SOLDERING THE ELECTRICAL CIRCUIT

C.4.1 Soldering Connection Types

The prototype sensor included two types of soldering connections, which required different types of solder. The coil to capacitor and capacitor to capacitor connections were copper to copper wire connections and required the use of a tin

solder. The state switch to capacitor connection was a steel copper wire connection and required the use of a silver solder and flux. Figure C.8 illustrates the three soldered joints in the electrical circuit. Joints 1 and 2 link three wires, while only two wires are connected at Joint 3.

C.4.2 Soldering Connection Sequence

The first step in soldering was connecting the copper-lead wires from the coil to one of the capacitors (Joints 1 and 2). Each copper lead wire was soldered to a different capacitor lead wire as illustrated in Figure C.9. This completed one circuit. A voltmeter was used to ensure that the connections were sound and that the circuit was complete.

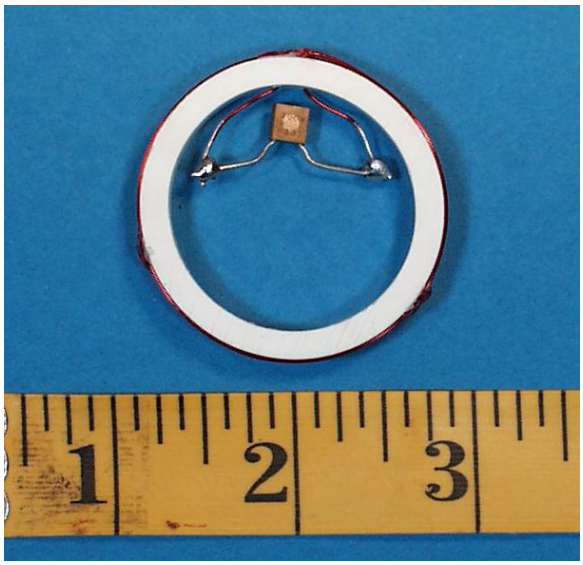

Figure C.9. Coil to Capacitor Connections

The next step was to solder the second capacitor to Joint 2, which is also a copper to copper connection. Figure C.10 shows the second capacitor soldered onto the circuit.

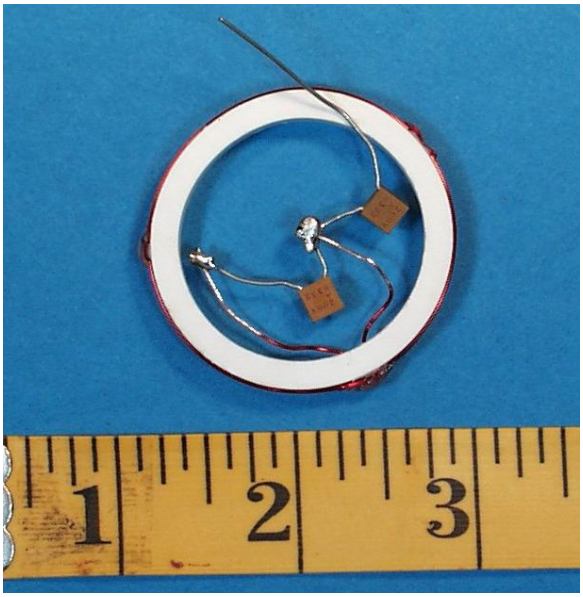

Figure C.10. Second Capacitor Connection

The next step was completing the second circuit by attaching the steel wire. Before the steel wire could be soldered to any other component, the petri dish had to be prepared so that the steel wire could extend outside of the petri dish. Two holes were drilled in the bottom half of the petri dish in the same manner that the steel wire access holes were drilled into the PVC pipe, with a No. 56-bit (1.17-mm, 0.046-in. diameter), and at approximately the same height and distance apart. Figure C.11 illustrates where the holes were drilled in the petri dish.

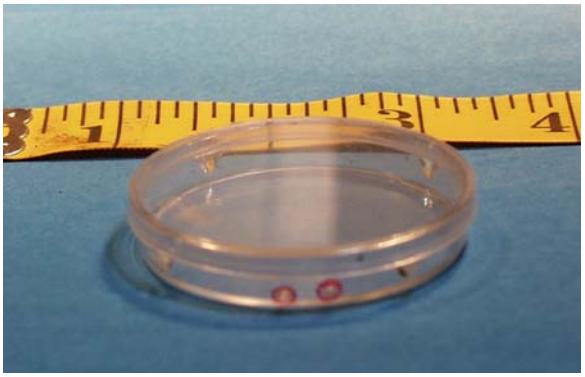

Figure C.11. Steel wire Access Holes Drilled in Petri Dish

Next, the steel wire state switch was formed outside the petri dish, based on the desired wire configuration. The lead wires were then stuck through the drilled holes in the petri dish and through the PVC pipe to extend to the inside of the PVC pipe. Figures C.6 and C.7 illustrate this step for the exposed and circumferential loop configurations, respectively. For the exposed loop configuration, a loop about 2 cm (¾ in.) long was formed outside of the petri dish. For the circumferential loop configuration, the wire was wrapped tightly around the circumference of the bottom half of the petri dish, and hot glue was applied at three places around the circumference to secure the wire in place. Then, one steel lead was soldered to Joint 1 to create a three wire connection, and the other steel lead was soldered to Joint 3 to create a two wire connection. Figures C.12 and C.13 show the completed circuits of the exposed and circumferential loop configurations, respectively. This soldering completed the second circuit. A voltmeter was used to ensure that the connections were sound and that the second circuit was complete.

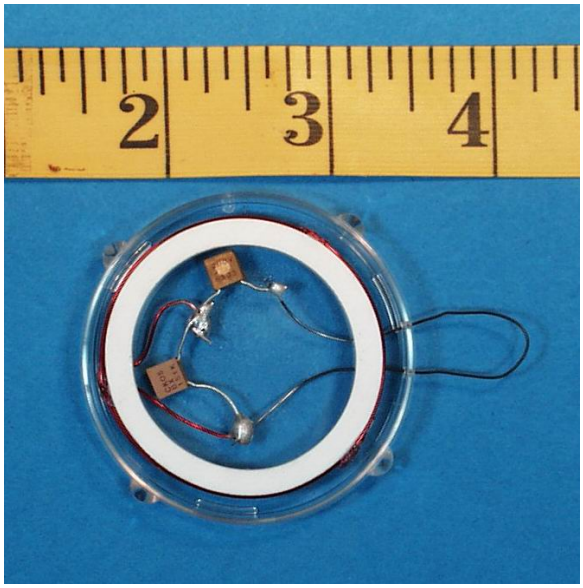

Figure C.12. Completed Circuits with Exposed loop Configuration

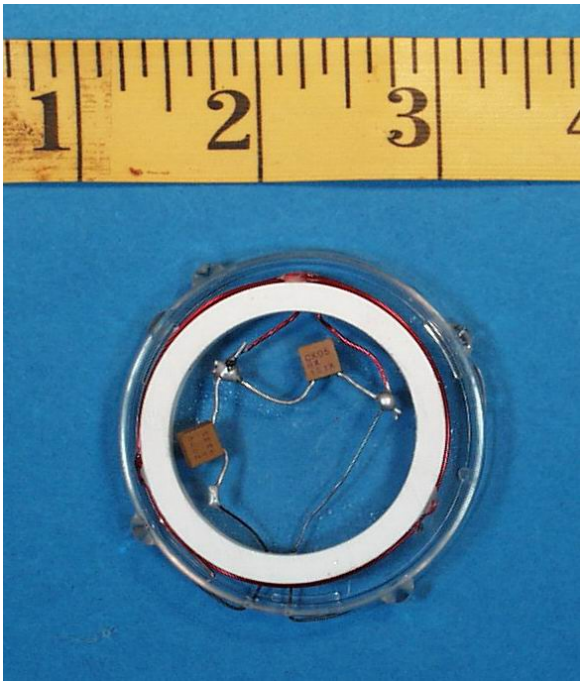

Figure C.13. Completed Circuits with Circumferential loop Configuration

C.5 PROTECTING THE SENSOR

The last step in the sensor fabrication was protecting the electrical circuit. An electrical potting compound, General Electric® Silicone RTV615A, was poured into the bottom of the petri dish and filled to the top. (Instructions on the proper use of the silicone came with the packaging.) The lid was placed on the petri dish and was left to set for 24 hours. After 24 hours, if air pockets existed inside the petri dish, the top was removed and more silicone was inserted into these air pockets. The lid was then replaced and left for six additional days to completely cure. After completely curing, if any silicone had squeezed out through the steel access holes and gathered around the steel, it was removed to ensure that the steel wire would be fully exposed to the surrounding environment when in place. An example of an air pocket is illustrated in Figure C.14. A picture of a completed prototype sensor with protection is illustrated in Figure C.15.

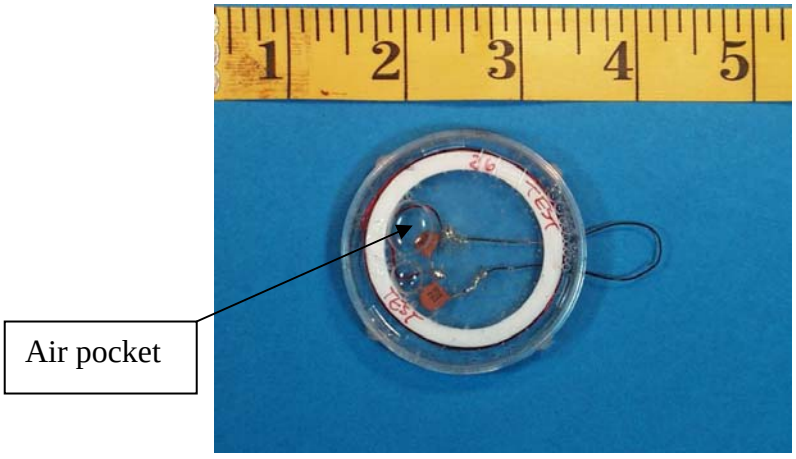

Figure C.14. Silicone-Filled Petri Dish with Air Pockets

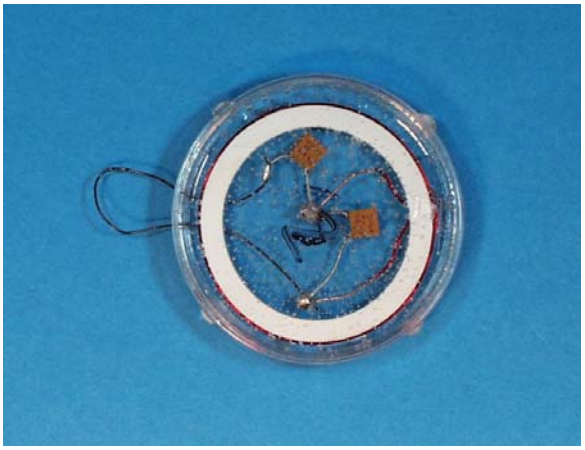

Figure C.15. Example of Completed Prototype Sensor

APPENDIX D

Steel Wire Accelerated Corrosion Test Pictures

Each corroded rebar specimen is shown with its corresponding corroded wire. The pictures were taken before the removal of corrosion products.

D.1 PHOTOGRAPHS OF REBAR AND WIRE AT CONCLUSION OF ACCELERATED CORROSION TESTS

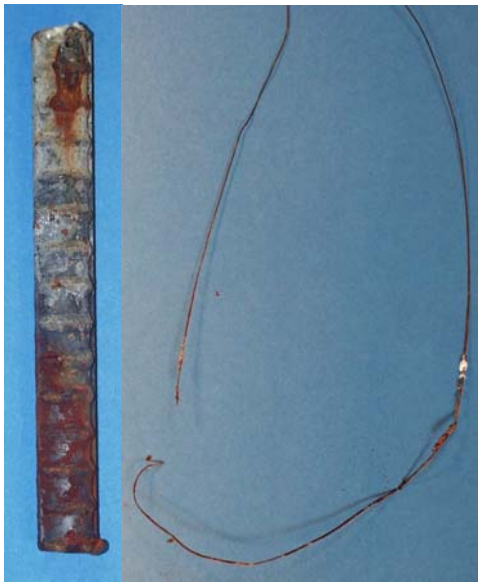

Figure D.1 Bar #2, No. 26 Gauge Wire

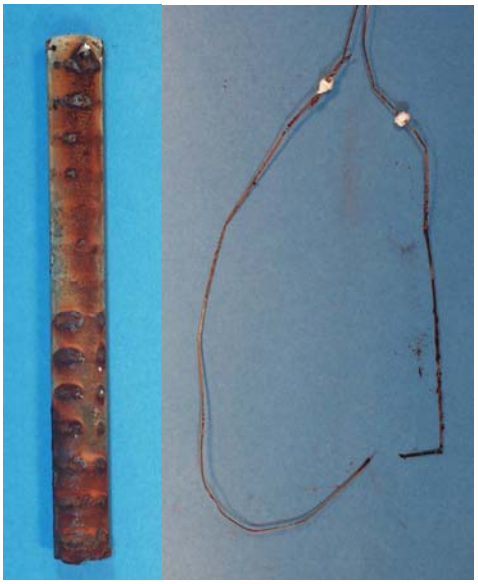

Figure D.2 Bar #3, No. 24 Gauge Wire

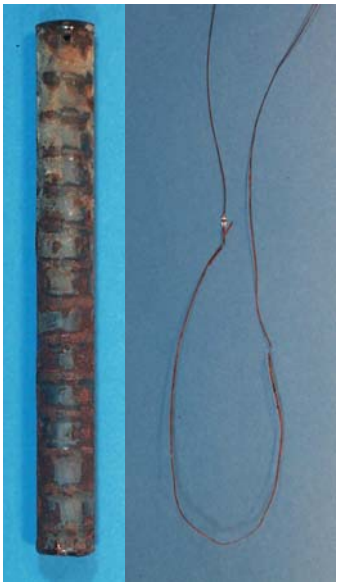

Figure D.3 Bar #6,
No. 26 Gauge Wire

Figure D.4 Bar #7,
No. 24 Gauge Wire

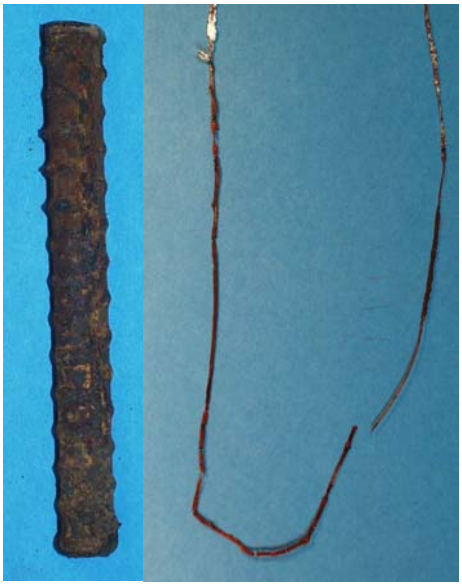

Figure D.5 Bar #8,
No. 22 Gauge Wire

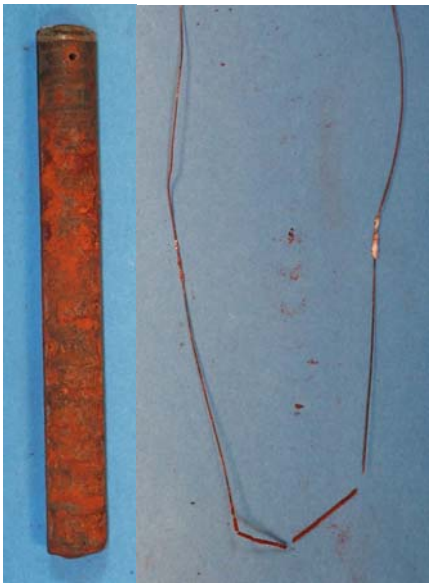

Figure D.6 Bar #10,
No. 26 Gauge Wire

Figure D.7 Bar #11,
No. 24 Gauge Wire

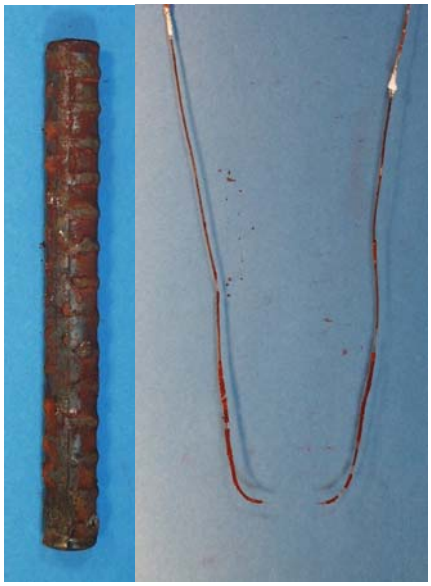

Figure D.8 Bar #12,
No. 22 Gauge Wire

Figure D.9 Bar #14,
No. 26 Gauge Wire

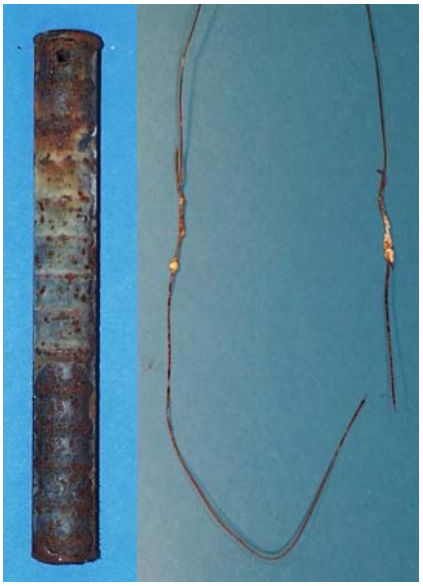

Figure D.10 Bar #15,
No. 24 Gauge Wire

Figure D.11 Bar #17, No. 21 Gauge Wire

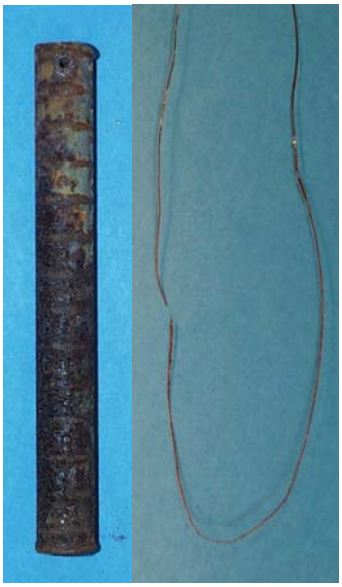

Figure D.12 Bar #18, No. 26 Gauge Wire

Figure D.13 Bar #19, No. 24 Gauge Wire

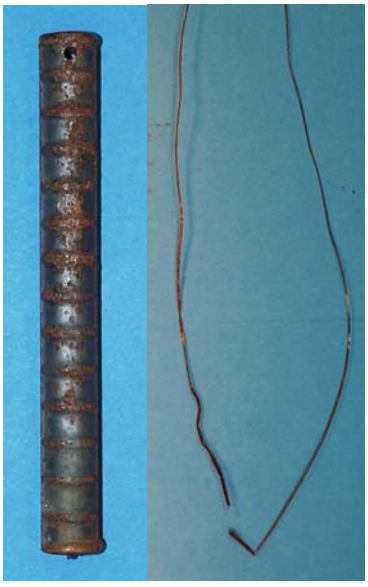

Figure D.14 Bar #22, No. 26 Gauge Wire

Figure D.15 Bar #23, No. 24 Gauge Wire

Figure D.16 Bar #24, No. 22 Gauge Wire

D.2 PHOTOGRAPHS OF REBAR AND WIRE EMBEDDED IN PETRI DISHES FILLED WITH POTTING COMPOUND AT CONCLUSION OF ACCELERATED CORROSION TESTS

Figure D.17 Bar #25, No. 26 Gauge Wire, Exposed Loop

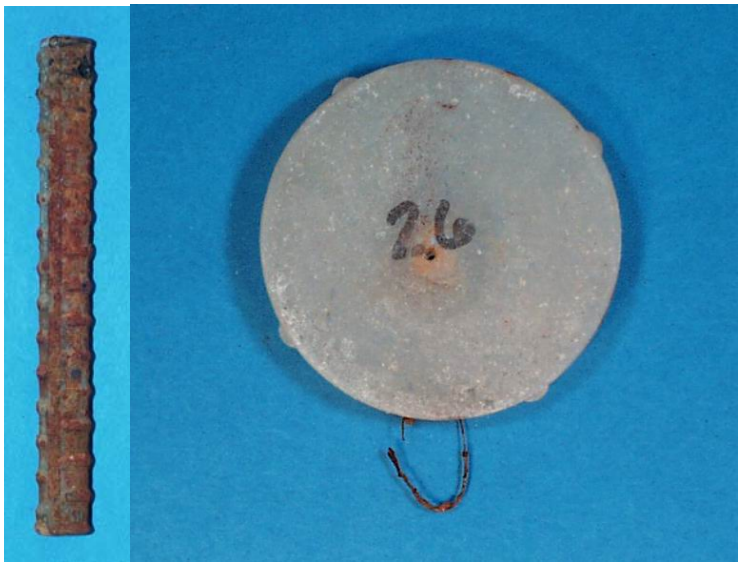

Figure D.18 Bar #26, No. 26 Gauge Wire, Exposed Loop

APPENDIX E

Sensors Exposed to Construction Process

E.1 SENSOR FREQUENCIES

Characteristic frequencies of the sensors were noted before embedment into concrete and are listed in Table E.1. *CL* denotes the circumferential loop configuration, and *EL* denotes the exposed loop configuration.

Table E.1 Measured Characteristic Frequencies of Sensors Exposed to Construction Process

	Frequency *(MHz)*		**Frequency** *(MHz)*
CL-26-10	6.29	**EL-26-10**	5.98
CL-26-11	6.38	**EL-26-11**	6.00
CL-26-12	6.44	**EL-26-12**	6.09
CL-26-13	6.32	**EL-26-13**	6.06
CL-26-14	6.38	**EL-26-14**	6.09
CL-26-15	6.14	**EL-26-15**	6.06

E.2 LOCATION OF SENSORS IN BEAMS

The measured locations of the sensors are listed in Table E.2. Locations were measured from the northwest corner of each beam. All sensors were attached to the outermost layer of reinforcement on the top side of the beam.

Table E.2 Coordinates of Sensor Placement

	Sensor	x *(in)*	y *(in)*
BEAM 1	**CL-26-13**	144	26
	CL-26-14	78	26
	CL-26-15	121	26
	EL-26-14	30	4.5
	EL-26-15	115	6.5
BEAM 2	**CL-26-10**	12.5	24
	CL-26-11	73	26
	CL-26-12	120	23.5
	EL-26-10	18	6.5
	EL-26-11	61	4.5
	EL-26-12	84	4.5
	EL-26-13	132	4

E.3 FREQUENCY SCANS

The frequency scans of two embedded prototype sensors are plotted in Figures E.1 and E.2.

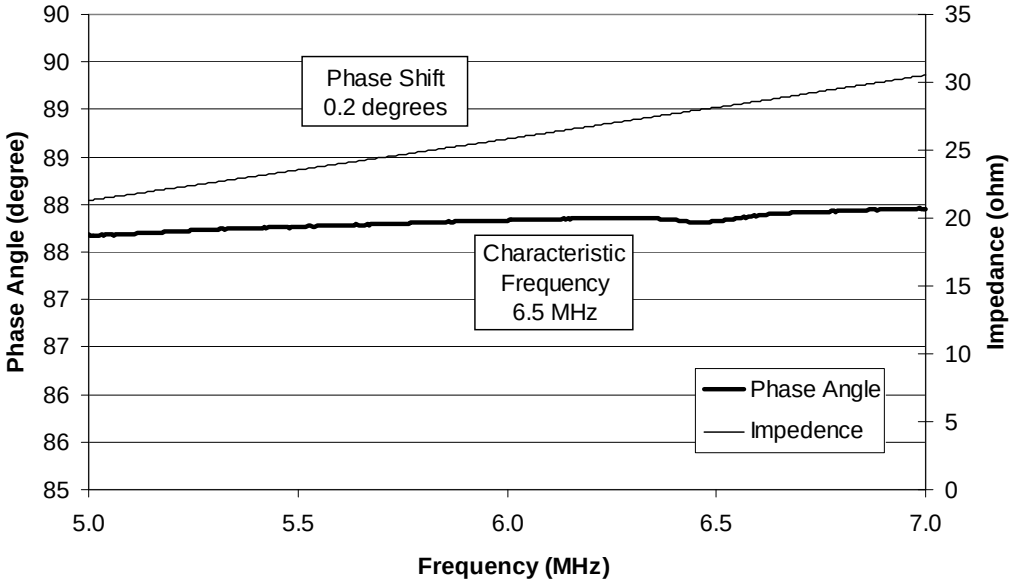

Figure E.1 Variation of Phase Angle and Impedance for CL-26-14

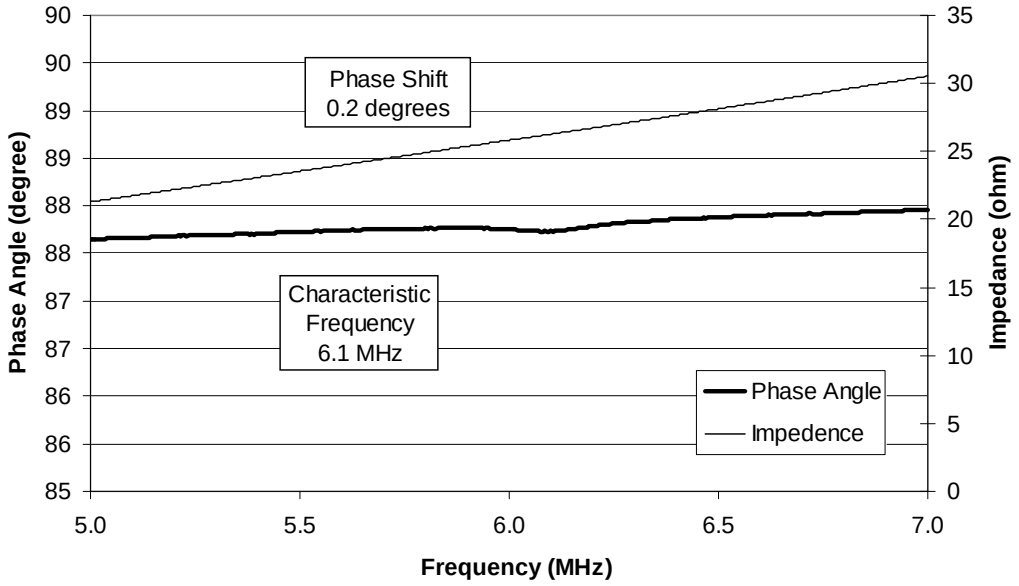

Figure E.2 Variation of Phase Angle and Impedance for EL-26-14

APPENDIX F

Data for Prototype Sensor Testing in Concrete Prisms

F.1 Reinforcing Steel Data

Initial measurements of the rebar specimen are listed in Table F.1. The diameter listed is an average of three diameters taken along the length. The prism that each rebar is embedded in is also listed. This data should be used in conjunction with the final measurements taken during the autopsies to determine corrosion rates and reductions in cross-sectional area.

Table F.1 Initial Length, Weight, and Diameter of Rebar Specimen

Prism	**1**		**2**		**4**		**6**		**5**		**3**	
Rebar	***1***	***2***	***3***	***4***	***5***	***6***	***7***	***8***	***9***	***10***	***11***	***12***
Length *(cm)*	60.48	60.64	60.96	60.64	60.64	61.12	60.01	60.80	59.85	60.96	61.91	60.64
Initial Weight *(g)*	910.8	913.0	912.4	913.6	910.2	923.0	899.0	914.1	900.2	912.9	928.8	911.8
Initial Diameter *(cm)*	1.481	1.483	1.483	1.474	1.480	1.476	1.477	1.477	1.475	1.472	1.472	1.476
Prism	**7**		**9**		**10**		**11**		**12**		**8**	
Rebar	***13***	***14***	***15***	***16***	***17***	***18***	***19***	***20***	***21***	***22***	***23***	***24***
Length *(cm)*	60.96	60.96	60.64	60.33	60.17	60.33	60.33	61.44	60.64	61.28	60.17	60.48
Initial Weight *(g)*	917.6	910.8	905.9	906.5	904.2	909.5	911.5	923.4	903.8	919.2	907.9	907.0
Initial Diameter *(cm)*	1.477	1.481	1.484	1.482	1.479	1.470	1.477	1.477	1.483	1.479	1.471	1.480

References

3M™ (2003). "3M™ Electronic Disc Marker System," http://www.3m.com/

AASHTO T 260-97 (2001). "Standard Method of Test for Sampling and Testing for Chloride Ion in Concrete Raw Materials." American Association of State Highway and Transportation Officials, Washington, D.C.

ACI 222 (1996). "Corrosion of Metals in Concrete." ACI 222R-96, American Concrete Institute, Detroit, Michigan.

ACI 318 (2002). "Building Code and Commentary for Structural Concrete (ACI 318-02) and Commentary (ACI 318R-02)." Committee 318, American Concrete Institute, Farmington Hills, MI.

ASTM C876 (1999). "Standard Test Method for Half-Cell Potentials of Uncoated Reinforcing Steel in Concrete." American Society for Testing and Materials, Philadelphia, PA.

ASTM G1 (1999). "Standard Practice for Preparing, Cleaning, and Evaluating Corrosion Test Specimens." American Society for Testing and Materials, West Conshohocken, PA.

ASTM G44 (1994). "Standard Practice for Evaluating Stress Corrosion Cracking Resistance of Metals and Alloys by Alternate Immersion in 3.5% Sodium Chloride Solution." American Society of Testing and Materials, West Conshohocken, PA.

Fuentes, Laura Alexandra (1999). "Implementation of Composite Wrapping Systems on Reinforced Concrete Structures Exposed to a Corrosive Laboratory

Environment." M.S. Thesis, Dept. of Civil Engineering, University of Texas at Austin.

Jones, Denny A. (1996). Principles and Prevention of Corrosion, 2nd Edition. Prentice Hall, Inc., Upper Saddle River, NJ.

Kitowski, Charles Jason (1993). "An Investigation of the Effect of Chloride on Reinforcing Steel Exposed to Simulated Concrete Solutions." M.S. Thesis, University of Texas at Austin.

Koch, G.H., Brongers, M.P., Thompson, N.G., Payer, J.H., and Virmani, Y.P. (1999). "Corrosion Costs and Preventive Strategies in the United States." Supplement to Materials Performance, U.S. Department of Transportation, Federal Highway Administration, July.

Lee, Youbok (1998). "microID™ 125 kHz RFID System Design Guide." Microchip Technology Inc., Mountain View, CA.

Manning, D.G. (1988). "Durability of Prestressed Concrete Highway Structures." Transportation Research Board, Washington, D.C.

Mietz, J. and Isecke, B. 1996. "Monitoring of Concrete Structures with Respect to Rebar Corrosion." Construction and Building Materials, Great Britain, Vol. 10, No. 5, 367-373.

Novak, Lisa J. (2002). "Development of a Wireless Sensor to Detect Cracks in Welded Steel Connections." M.S. Thesis, Dept. of Civil Engineering, University of Texas at Austin.